INFORMATION TO USERS

This manuscript has been reproduced from the microfilm master. UMI films the text directly from the original or copy submitted. Thus, some thesis and dissertation copies are in typewriter face, while others may be from any type of computer printer.

The quality of this reproduction is dependent upon the quality of the copy submitted. Broken or indistinct print, colored or poor quality illustrations and photographs, print bleedthrough, substandard margins, and improper alignment can adversely affect reproduction.

In the unlikely event that the author did not send UMI a complete manuscript and there are missing pages, these will be noted. Also, if unauthorized copyright material had to be removed, a note will indicate the deletion.

Oversize materials (e.g., maps, drawings, charts) are reproduced by sectioning the original, beginning at the upper left-hand corner and continuing from left to right in equal sections with small overlaps.

ProQuest Information and Learning
300 North Zeeb Road, Ann Arbor, MI 48106-1346 USA
800-521-0600

Identification of Molecular Determinants of Substrate Specificity and Activity for Biphenyl Dioxygenase from *Comamonas testosteroni* B-356

Nathalie Yvonne Rachel Agar

A Thesis

in

The Department

of

Chemistry and Biochemistry

Presented in Partial Fulfillment of the Requirements

For the Degree of Doctor of Philosophy at

Concordia University

Montreal, Quebec, Canada

June 2002

ABSTRACT

Identification of Molecular Determinants of Substrate Specificity and Activity of Biphenyl Dioxygenase from *Comamonas testosteroni* B-356

Nathalie Y.R. Agar, Ph.D.
Concordia University, 2002

The oxygenase component of biphenyl dioxygenase (BPDO) from *Comamonas testosteroni* B-356 dihydroxylates biphenyl and some polychlorinated biphenyls (PCBs), thereby initiating their degradation. Identification of molecular determinants for BPDO substrate selectivity and activity should allow engineering it to accept a range of chlorinated biphenyls for bioremediation.

Highly active BPDO has been purified, and crystallized under anaerobic conditions. The first crystal structures of BPDO, and its substrate-bound and product-bound binary complexes, have been solved. Steady-state kinetics assays monitoring O_2 consumption demonstrated that BPDO transformed biphenyl and dichlorobiphenyls with the following order of apparent specificities: biphenyl > 3,3'- > 2,2'- > 4,4'-dichlorobiphenyl, but with specificity constants all within a factor of 3. The ability of the enzyme to utilize O_2 depended strongly on the biphenyl substrate, with specificity constants for oxygen over one order of magnitude smaller in the presence of the dichlorinated biphenyls compared to biphenyl. Moreover, the selected dichlorobiphenyls were found to be partial uncouplers of the reaction, reducing O_2 to H_2O_2. Based on the high-resolution crystal structure of BPDO and its binary complexes, the roles of some specific residues were investigated by site-directed mutagenesis. Moreover, three BPDOs sharing between 70-95 % sequence identity were overexpressed, purified in

highly active forms, and compared in terms of steady-state kinetic parameters for biphenyls, as well as uncoupling behaviour.

BPDO comprises two metal centers required for enzymatic activity: a catalytic mononuclear iron and a [2Fe-2S] Rieske-type cluster for electron transfer. To overexpress holo-BPDOs, the iron-sulfur cluster (*isc*) assembly genes from *Pseudomonas aeruginosa* PA01 were cloned and used for coexpression. The Fe-S cluster of BPDO was shown to be sensitive to reactive oxygen species such as superoxide, but the *isc* gene products appeared to have the ability to repair damaged clusters in crude extract reconstitution assays.

The experimental approaches and results described in this thesis contribute to the identification of structural features important for substrate selectivity, and ultimately may be useful for construction of modified BPDOs with enhanced activity on chlorinated biphenyls.

ACKNOWLEDGEMENTS

I wish to express my most sincere gratitude to my major Professor, Dr. Justin B. Powlowski, for his trust, guidance, and support.

I am also grateful to Dr. Lindsay D. Eltis for introducing me to research with such enthusiasm, and for his devotion as a mentor.

I wish to extend my gratitude to Dr. Michael K. Johnson for hosting me repeatedly into his laboratory, and giving me the opportunity to meet with many great scientists. I also wish to express my gratitude to Dr. Dennis R. Dean for welcoming me to his research field, and for his warm hospitality.

I am very grateful to my examining committee members, Dr. Ann M. English, and Dr. Joanne L. Turnbull for their time, support, and advices.

I am also very grateful to Dr. Donald M. Kurtz Jr. from The University of Georgia, and Dr. Sushil K. Misra from our Physics Department for examining my thesis.

I also wish to thank NSERC, FCAR, and Concordia University (J.W. McConnell and External Grant Holder Fellowships) for their financial support.

I wish to express my deepest gratitude to Dr. Jeffrey N. Agar for unconditional contributions to my research, and constant support.

To Jeffrey, my soul mate. To our loved daughters Alexandrine, Noémie, and Chloé, and to future babies.

To my parents Reine, and Jean. To my sisters Brigitte, and Geneviève, and brother in law Christian. To Aunt Marthe and Geno. To Aunt Gemma and my cousin Stéphane. To my beloved godparents Yvonne, and Hyacinthe.

TABLE OF CONTENTS

LIST OF FIGURES..... xi

LIST OF TABLES..... xiv

LIST OF ABBREVIATIONS..... xvi

CONTRIBUTIONS OF AUTHORS..... xix

CHAPTER 1: INTRODUCTION

1.1 Polychlorinated Biphenyl Degradation..... 2

1.2 Biphenyl Dioxygenase..... 3

1.3 Molecular Insights from Related Oxygenases..... 7

1.3.1 Phthalate Dioxygenase..... 8

1.3.2 Naphthalene Dioxygenase..... 11

1.3.3 4-Methoxybenzoate Monooxygenase..... 20

1.3.4 Cytochrome P-450..... 21

1.3.5 Proposed Pathways of O_2 Activation by Rieske Nonheme Iron Dioxygenases..... 25

1.4 Biological Iron-Sulfur Cluster Assembly..... 28

1.4.1 Iron-Sulfur Center Assembly Gene Cluster..... 28

1.4.2 Proposed Mechanisms and Roles for Biological Iron-Sulfur Assembly..... 33

1.4.3 Significance to Biphenyl Dioxygenase Studies..... 38

1.5 Objectives of this Thesis..... 38

REFERENCES..... 41

CHAPTER 2: Steady-State Kinetic Characterization and Crystallization of a PCB-Transforming Dioxygenase

ABSTRACT..... 50

INTRODUCTION..... 51

MATERIALS AND METHODS..... 56

RESULTS..... 64

DISCUSSION..... 77

ACKNOWLEDGEMENTS..... 82

REFERENCES..... 83

CHAPTER 3: Crystal Structure of BPDO and its Substrate-Bound and Product-Bound Complexes

ABSTRACT..... 88

INTRODUCTION..... 89

EXPERIMENTAL PROCEDURES..... 90

RESULTS AND DISCUSSION..... 92

REFERENCES..... 112

CHAPTER 4: Site-Directed Mutagenesis at the Mononuclear Iron Active Site of BPDO

ABSTRACT..... 115

INTRODUCTION..... 116

EXPERIMENTAL PROCEDURES..... 123

RESULTS..... 128

DISCUSSION..... 137

REFERENCES..... 139

CHAPTER 5: A Comparison of the Specificities of BPDO from Psychrotolerant and Mesophilic PCB-Degrading Bacteria

ABSTRACT..... 143

INTRODUCTION..... 144

MATERIALS AND METHODS..... 149

RESULTS..... 154

DISCUSSION..... 163

ACKNOWLEDGEMENTS..... 170

REFERENCES..... 171

CHAPTER 6: Iron-Sulfur Cluster Assembly and Reassembly in Biphenyl Dioxygenase Mediated by the Iron-Sulfur Cluster Assembly Gene Products from *Pseudomonas aeruginosa* PA01

ABSTRACT..... 177

INTRODUCTION..... 178

EXPERIMENTAL PROCEDURES..... 183

RESULTS.....192

DISCUSSION.....215

ACKNOWLEDGEMENTS.....220

REFERENCES.....221

CHAPTER 7: Summary.....226

REFERENCES.....231

APPENDIX A.....232

LIST OF FIGURES

PAGE

Figure 1.1 Biphenyl and polychlorinated biphenyl (PCB) degradation pathway..... 4

Figure 1.2 Phthalate binding to the active site of PDO..... 9

Figure 1.3 Naphthalene dioxygenase reaction..... 12

Figure 1.4 Crystal structure of NDO to 2.24 Å resolution..... 15

Figure 1.5 Hypothesis for the NDOS reaction cycle..... 18

Figure 1.6 Cytochrome P-450 substrate hydroxylation cycle and the uncoupling alternative pathways..... 23

Figure 1.7 Alternative pathways of O_2 activation for Rieske nonheme iron dioxygenases..... 26

Figure 1.8 Crystal structure of the Rieske-type iron-sulfur cluster of BPDO... 29

Figure 1.9 Organization of iron-sulfur cluster assembly genes in *Azotobacter vinelandii* and *Escherichia coli* along with the corresponding characterized genes from the *Saccharomyces cerevisiae*..... 31

Figure 1.10 Proposed mechanisms for iron-sulfur cluster assembly..... 35

Figure 2.1 Representation of BPDO from *Comamonas testosteroni* B-356..... 52

Figure 2.2 The steady-state dihydroxylation of biphenyl by $BPDO_{B356}$..... 67

Figure 2.3 High resolution diffraction pattern obtained from a single crystal of BPDO..... 74

Figure 3.1 Two orthogonal views of the BPDO $\alpha_3\beta_3$ hexamer..... 93

Figure 3.2 The $\alpha\beta$ dimer of BPDO..... 95

Figure 3.3 Electron density showing the coordination geometry of the mononuclear Fe(II)..... 98

Figure 3.4 Electron density map revealing the location of biphenyl at the active site..... 101

Figure 3.5 Comparison of BPDO and BPDO-biphenyl complex showing conformational changes occurring within the active site upon substrate binding..... 104

Figure 3.6 Electron density map showing the change in coordination geometry in presence of the product..... 106

Figure 3.7 Comparison of the Fe(II) ligands in BPDO and BPDO-product complex..... 108

Figure 4.1 Crystal structure views of BPDO active site to depict the potential role of specific residues selected for site-directed mutagenesis studies..... 118

Figure 4.2 Diagram of the hypothetical internal electron transfer pathway in BPDO..... 120

Figure 4.3 UV-Visible absorbance spectra of BPDO_wild type and BPDO_Q226 variants..... 132

Figure 4.4 Visible circular dichroism of BPDO_wild type and BPDO_Q226 variants..... 135

Figure 5.1 The reaction catalyzed by BPDO..... 145

Figure 5.2 The effect of increasing temperature on the activities of $BPDO_{Cam1}$ and $BPDO_{LB400}$..... 159

Figure 5.3 Alignment of amino acid sequences of terminal oxygenase subunits BphA and BphE from $BPDO_{Cam1}$ and $BPDO_{LB400}$..... 168

Figure 6.1 *Isc* gene cluster map from *Pseudomonas aeruginosa* PA01..... 181

Figure 6.2 BPDO of *Comamonas testosteroni* B-356..... 193

Figure 6.3 SDS-PAGE of $BPDO_{Cam1}$ expression in the presence and absence of the *isc* genes..... 197

Figure 6.4 UV-visible absorbance spectrum of $BPDO_{B356}$ to identify the Rieske type iron-sulfur cluster, and visible CD spectrum..... 200

Figure 6. 5 Far UV CD spectroscopy to compare secondary structure of holo- and apo-oxygenases..... 203

Figure 6.6 Oxidative stress on the oxygenase [2Fe-2S] cluster..... 206

Figure 6.7 *In vitro* reconstitution of iron-sulfur cluster using crude extracts of *E. coli* C41[DE3] pRKNMC and pRKISC, as monitored by UV-vis absorbance spectroscopy..... 208

Figure 6.8 *In vitro* reconstitution of iron-sulfur cluster using crude extracts of *E.coli* C41[DE3] pRKNMC and pRKISC, as monitored by visible circular dichroism spectroscopy..... 212

LIST OF TABLES

PAGE

Table 2.1 Purification of the oxygenase component of the biphenyl dioxygenase system from *C. testosteroni* B-356..... 65

Table 2.2 Apparent steady-state kinetic and coupling parameters of BPDO from *C. testosteroni* B-356 for selected biphenyl substrates..... 70

Table 2.3 The apparent steady-state kinetic utilization of O_2 by BPDO from *C. testosteroni* B-356 in the presence of selected biphenyl substrates..... 71

Table 2.4 Statistics pertaining to diffraction data acquired from one crystal of *C. testosteroni* B-356 BPDO..... 76

Table 4.1 Oligonucleotides for site-directed mutagenesis of BPDO..... 124

Table 4.2 Yields and specific activities of purified BPDO variants..... 129

Table 4.3 Steady-state kinetic parameters of BPDO variants for biphenyl..... 131

Table 5.1 Apparent steady state kinetic and coupling parameters of different BPDOs for selected biphenyl substrates..... 145

Table 5.2 Apparent steady-state kinetic parameters of BPDOs for biphenyl at various temperatures..... 159

Table 5.3 Thermodynamic parameters of ISP_{Cam} and ISP_{LB400} at 25°C with biphenyl..... 168

Table 6.1 Plasmids, strains, and oligonucleotides..... 184

Table 6.2 Molar CD absorptivities of BPDO and BPDO Fe-S cluster

reassembly assays..... 214

LIST OF ABBREVIATIONS

Ala (A), alanine

Asn (N), asparagine

Asp (D), aspartate

ATP, adenosine triphosphate

AUC, analytical ultracentrifuge

BCA, bicinchoninic acid

BPDO, biphenyl dioxygenase

CD, circular dichroism

DHBD, 2,3-dihydroxybiphenyl dioxygenase

diClB, dichlorobiphenyl

DNA, deoxyribonucleic acid

dNTP, deoxynucleoside triphosphate; the letter N refers to any or all of the common bases

ddNTP, dideoxynucleoside triphosphate; the letter N refers to any or all of the common bases

DTT, dithiothreitol

EDTA, ethylenediamine-tetraacetic acid

EPR, electron paramagnetic resonance

FAD, flavin adenine dinucleotide

$Fe(SO_4)_2(NH_4)_2$, ferrous ammonium sulfate

FPLC, fast protein liquid chromatography

Gln (Q), glutamine

Glu (E), glutamate

H_2O, water molecule

H_2O_2, hydrogen peroxide

HEPES, 4-(2-(hydroxyethyl)-1-piperazineethanesulfonic acid

HPLC, high performance liquid chromatography

IPTG, isopropyl-1-thio-β-D-galactopyranoside

ISC, iron sulfur cluster assembly

LMW, low molecular weight

MCD, magnetic circular dichroism

MES, 2-(N-morpholino)ethanesulfonic acid

Met (M), methionine

NADH, nicotinamide adenine dinucleotide

NDO, naphthalene dioxygenase

NMR, nuclear magnetic resonance

NO, nitric oxide

O_2, molecular oxygen

PCB, polychlorinated biphenyl

PCR, polymerase chain reaction

PDO, phthalate dioxygenase

PEG, polyethylene glycol

PAGE, polyacrylamide gel electrophoresis

SDS, sodium dodecyl sulfate

TCA, trichloroacetic acid

Thr (T), threonine

UV, ultra violet

VDW, van der Waal

CONTRIBUTIONS OF AUTHORS

Chapter 2 is published in *Journal of Biological Chemistry* (2000) **275**. 12430-12437 with Justin B. Powlowski. Christopher L. Colbert. Jeffrey T. Bolin. and Lindsay D. Eltis. I performed all of the experiments except protein crystallization and x-ray diffraction. and wrote the first version of the manuscript.

Chapter 3 is part of a manuscript in preparation with the following authors: Christopher L. Colbert. Nathalie Y.R. Agar. Justin B. Powlowski. Lindsay D. Eltis. and Jeffrey T. Bolin. Christopher L. Colbert did the crystallographic characterization of BPDO. I prepared BPDO for crystallization. and performed all other biochemical characterization experiments. This chapter provides results and discussion from the crystal structure of BPDO in light of the work presented in this thesis. I wrote chapter 3 based on results presented in Christopher L. Colbert's Ph.D. thesis (Purdue University. IN. USA).

Chapter 4 is a manuscript in preparation with the following authors: Nathalie Y.R. Agar. Christopher L. Colbert. Bernard F. Gibbs. Jeffrey T. Bolin. and Justin B. Powlowski. I produced. purified. characterized the six BPDO variants. and wrote the first version of the manuscript.

Chapter 5 is a manuscript submitted for publication in *Journal of Bacteriology* with the following authors: Emma R. Master. Nathalie Y.R. Agar. Justin B. Powlowski. William W. Mohn and Lindsay D. Eltis. I overexpressed and purified BPDOs for this manuscript. and carried out the initial kinetic characterization using techniques developed

for Chapter 2. Dr. Master assisted in the enzyme purifications, extended the kinetic and biochemical characterizations, and wrote the first version of this manuscript.

Chapter 6 is a manuscript with the following authors: Nathalie, Y.R. Agar, Pascal D. Fortin, Yong Ge, Lindsay D. Eltis, and Justin B. Powlowski. I performed all the experiments reported in this manuscript except for the cloning of the *isc* genes from *Pseudomonas aeruginosa* PA01, which was done by Pascal D. Fortin and Yong Ge. I wrote the original version of this manuscript.

I wrote Chapters 1 and 7, respectively the Introduction and Discussion, of this thesis.

Chapter 1

Introduction

1.1 Polychlorinated Biphenyl (PCB) Degradation

Considerable effort has been directed to harnessing the tremendous catabolic capacity of microorganisms to destroy toxic persistent pollutants in a technology known as bioremediation. An important limitation in the development of effective bioremediation strategies is the inability of existing microbial catabolic activities to degrade highly chlorinated, structurally diverse, xenobiotics such as polychlorinated biphenyls (PCBs). The resistance of certain PCBs to biodegradation is related to the degree of substitution, and position of the chlorines. Depending on their substitution pattern, polychlorinated biphenyls can exist as 209 different congeners. Problematic environmental samples mainly consist of penta-, hexa-, and hepta-chlorinated biphenyls, and coplanar polychlorinated biphenyls (1).

The toxicological evaluation of PCBs is complex since they are found as mixtures of many congeners and often are mixed with other toxic contaminants. Exposure to PCBs in the general population is mainly through contaminated food, which accounts for approximately 14 μg per person every day in most industrialised countries (1). However, exposure via this route has not been conclusively linked to disease. In contrast, continuous exposure to high concentrations of PCB mixtures for people working with PCB may result in effects mainly on skin and liver. Moreover, data from documented episodes of intoxication have shown skin, liver, respiratory, and central nervous problems, and revealed the carcinogenic potential of PCB to humans (1).

Bacterial catabolic pathways for aromatic compounds represent promising potential resources for degradation of these thermally and chemically stable pollutants. Understanding the overall biotransformation process requires characterization of key

enzymes catalyzing the reactions of the degradative pathway. Such information can be useful for the manipulation of existing pathways, and the rational design of novel routes for particularly recalcitrant xenobiotics (2;3). The four-step catabolic pathway for the degradation of biphenyl and certain polychlorinated biphenyls to benzoate and 2-ketopent-4-dienoate is encoded by the *bph* operon of *Comamonas testosteroni* B-356 (4), and other biphenyl-degrading bacteria (5;6) (Fig. 1.1). Each of the four enzymes from the *bph*-encoded pathway has been isolated from several different bacterial strains, and characterized biochemically to various extents. Structures have been published for three of the four pathway enzymes, BphB, BphC and BphD (7-9), as well as the ferredoxin component (BphF) of biphenyl dioxygenase (10).

1.2 Biphenyl Dioxygenase

Biphenyl dioxygenase comprises an FAD-containing reductase (BphG), a Rieske-type ferredoxin (BphF), and an $\alpha_3\beta_3$ terminal oxygenase (BphAE) which contains a Rieske-type iron-sulfur cluster and a mononuclear nonheme iron catalytic center (Fig. 1.1). The enzyme catalyses ring *cis*-dihydroxylation at positions 2 and 3 of biphenyl using molecular oxygen, and uses NAD(P)H as a source of electrons (11). Purifications of biphenyl dioxygenases from *Comamonas testosteroni* B-356 (12), and *Pseudomonas cepacia* LB400 (13) have previously been reported.

The oxygenase component is mainly responsible for biphenyl dioxygenase selectivity towards polychlorinated substrates. Sharing over 70 % sequence identity for the two subunits of their oxygenase component, dioxygenases from *C. testosteroni* B-356 ($BPDO_{B356}$), *P. cepacia* LB400 ($BPDO_{LB400}$), and *Pseudomonas pseudoalcaligenes*

Figure 1.1 Biphenyl and polychlorinated biphenyl (PCB) degradation pathway.

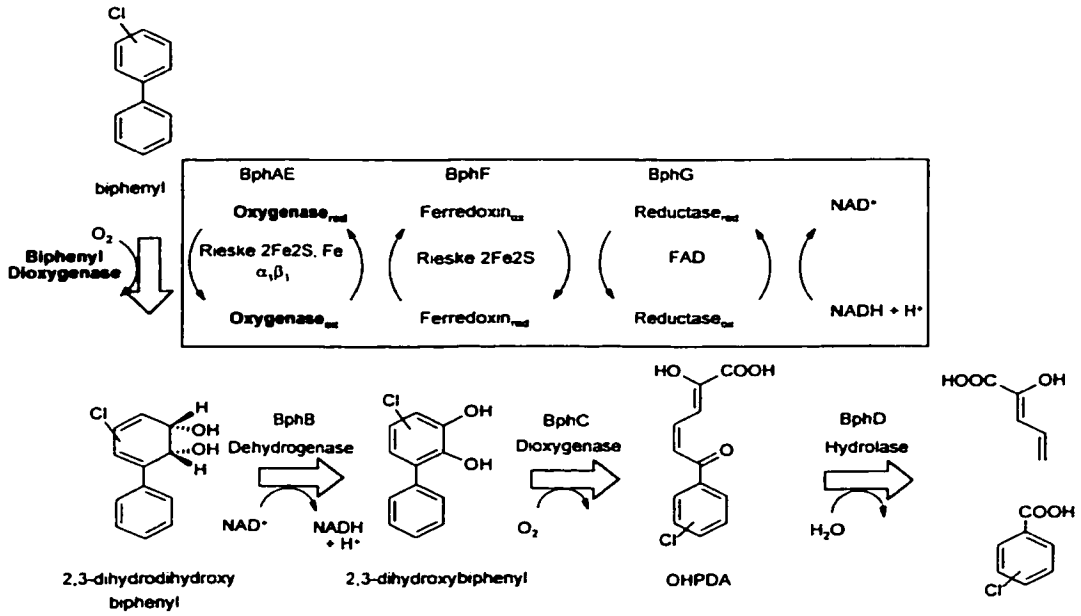
Cl
biphenyl
O_2
Biphenyl Dioxygenase
BphAE
Oxygenase$_{red}$
Rieske 2Fe2S, Fe
$\alpha_1\beta_1$
Oxygenase$_{ox}$
BphF
Ferredoxin$_{ox}$
Rieske 2Fe2S
Ferredoxin$_{red}$
BphG
Reductase$_{red}$
FAD
Reductase$_{ox}$
NAD+
NADH + H+
Cl
H
OH
OH
H
2,3-dihydrodihydroxy biphenyl
BphB
Dehydrogenase
NAD+
NADH + H+
Cl
OH
OH
2,3-dihydroxybiphenyl
BphC
Dioxygenase
O_2
HO
COOH
O
Cl
OHPDA
BphD
Hydrolase
H_2O
HOOC
OH
COOH
Cl

KF707 ($BPDO_{KF707}$) display different reactivity patterns for the dihydroxylation of biphenyl and its chlorinated derivatives. While $BPDO_{B-356}$ and $BPDO_{KF707}$ introduce hydroxyl groups solely at positions 2 and 3 (12;14), the homologue from LB400 can catalyse dihydroxylation both at the 2, 3- and the 3, 4- positions (15).

Different experimental approaches have been used to elucidate the factors regulating these dioxygenase reactivity patterns. Hybrid proteins consisting of the α and β subunits from different oxygenases have been produced and used to identify the involvement of each subunit in determining substrate preference. Even though the α subunit is the major determinant of substrate specificity, these studies indicated that both the α and β subunits of the oxygenase are determinants of substrate specificity (16-19), although both the [2Fe-2S] and mononuclear iron centers reside on the α subunit (20) (Chapter 3).

Site-directed mutagenesis based on BphA sequence alignments for a set of 15 PCB-degrading bacterial strains, and on their ability to degrade 17 PCB congeners, has revealed the identity of certain residues, and combinations of residues, involved in substrate selectivity (14). Two categories of PCB-degrading abilities were identified, and correspond to a broad substrate specificity similar to strain LB400, and a narrow substrate specificity similar to strain KF707. The LB400-type specificity involves the ability of biphenyl dioxygenase to dihydroxylate in positions 3 and 4, in addition to the usual 2 and 3 positions, but with a poor activity on *para* substituted biphenyls. In contrast, the KF707-type specificity reveals superior activity on di-*para*-substituted congeners, with exclusively 2,3-*cis*-dihydroxylation activity. Comparison of BphA amino acid sequences from the 15 different strains identified four distinct regions of one to four residues related

to the two characteristic substrate specificity types. Based on this, individual mutations in regions I, II, and IV to convert an LB400-type activity to a KF707-type did not substantially change substrate specificity, whereas significant differences in substrate specificity were observed from combinations of mutations in regions III and IV, and from individual mutations in region III (14).

Recently, a pseudomonad that can use biphenyl as a carbon source was isolated from Arctic soil by Mohn and co-workers (21). The oxygenase component of this biphenyl dioxygenase system is referred to as $BPDO_{Cam1}$. This novel BPDO shares 95% sequence identity with $BPDO_{LB400}$ and $BPDO_{KF707}$, and 70% sequence identity with $BPDO_{B356}$. Measurements of dichlorinated biphenyl consumption by whole cells expressing $BPDO_{Cam1}$ indicate that, as with $BPDO_{KF707}$, $BPDO_{Cam1}$ exhibits a preference for *para*-substituted biphenyls, and only hydroxylates at the 2,3-positions of the biphenyl substrate (21).

Efforts have also been invested in directed evolution for production of BPDOs with improved activity. This approach has rendered some evolved oxygenases with broader substrate specificity, and a different mode of oxygenation (22), but as a random-based process it also has inherent limitations (22-24). This suggests that efforts to combine features from different BPDOs will pay off in terms of creating enzymes with novel degradative properties for bioremediation, and that it will involve rational design as well as directed evolution approaches.

1.3 Molecular Insights from Related Oxygenases

Since BPDO has not previously been extensively studied at the molecular level, better-characterized oxygenase systems provide some useful biochemical and mechanistic insights. These include the phthalate and naphthalene dioxygenase systems, as well as the 4-methoxybenzoate and cytochrome P-450 monooxygenases.

1.3.1 Phthalate Dioxygenase

The phthalate dioxygenase system (PDOS) catalyzes the first step in the bacterial degradation of phthalate, converting it to *cis*-4,5-dihydroxydihydrophthalate (Fig. 1.2). PDOS is a two-component enzyme composed of a 36 kDa monomeric reductase (PDR), and a 200 kDa tetrameric terminal oxygenase (PDO). PDR comprises a flavin (FMN) cofactor, and a ferredoxin-type [2Fe-2S] cluster, both required to transfer electrons from NADH to the oxygenase component, PDO. Each PDO subunit contains a Rieske-type [2Fe-2S] cluster involved in electron transfer as well as a mononuclear iron required for catalysis (25;26): each subunit shares over 30 % sequence identity with the corresponding subunit from BPDO.

Magnetic circular dichroism studies of phthalate and azide binding to the mononuclear iron active site of phthalate dioxygenase have shown that the resting enzyme contains a six-coordinate Fe(II) site which changes upon aromatic substrate binding to a mixture of two different five-coordinate substrate-bound species. The empty coordination position can then bind the O_2 analogue, azide. In the absence of aromatic substrate, azide binding involves exchange of one of the Fe(II) ligands, producing a different six-coordinate species, with a binding constant for azide approximately two orders of magnitude higher than for the PDO-phthalate complex (27;28).

Figure 1.2 Phthalate binding to the active site of PDO (29).

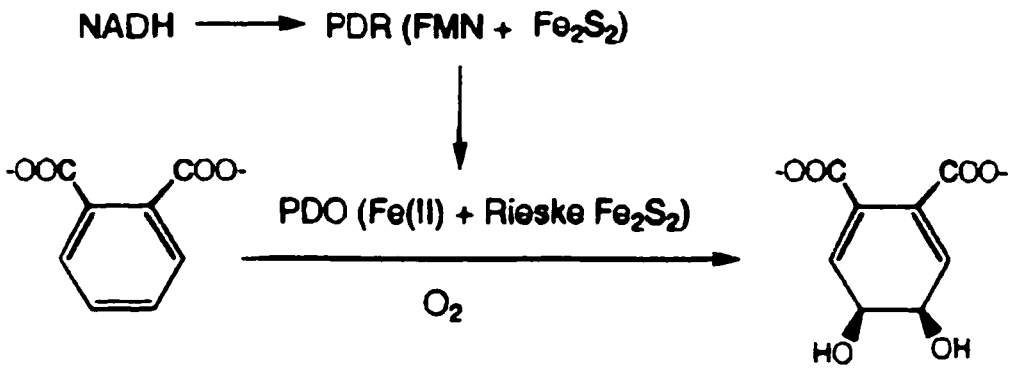
NADH
PDR (FMN + Fe_2S_2)
-OOC
COO-
PDO (Fe(II) + Rieske Fe_2S_2)
O_2
-OOC
COO-
HO
OH

1.3.2 Naphthalene Dioxygenase

The naphthalene dioxygenase system (NDOS) is a three component enzyme that catalyzes the dihydroxylation of naphthalene using O_2, and NAD(P)H as a source of electrons, producing *cis*-(1*R*,2*S*)-dihydroxy-1,2-dihydronaphthalene (30). NDOS consists of three protein components: a 36 kDa reductase (NDR) that contains FAD and a plant-type [2Fe-2S] cluster; a 14 kDa ferredoxin (NDF) that contains a Rieske-type [2Fe-2S] cluster involved in electron transfer; and a 210 kDa oxygenase (NDO) of $\alpha_3\beta_3$ constitution that contains a Rieske-type [2Fe-2S] cluster and a mononuclear iron required for catalysis (Fig. 1.3) (31-33).

The crystal structure of NDO, with which BPDO shares 30% overall sequence identity and approximately 50% similarity, suggests a route for electron transfer between the two metal centers of the enzyme. The quaternary structure of NDO has a mushroom-like shape (Fig. 1.4.A) with a trimer of α subunits forming the head of the mushroom, and a trimer of β subunits arranged as the stem. The distance between the [2Fe-2S] cluster and the mononuclear iron in a single α subunit is 43.5 Å, whereas the distance between the [2Fe-2S] cluster of one α subunit and the mononuclear iron on an adjacent one is 12 Å, suggesting inter-subunit electron transfer to the active site (20;34;35).

The union of the three α subunits of NDO is not fully formed at the top of the mushroom, leaving an entrance to a cavity formed by the α subunit trimer (Fig. 1.4.B). Since the active site is exposed to this cavity (Fig. 1.4.C), the broad entrance may be the access route for the aromatic substrate. However, others have suggested that a separate entrance exists (Fig. 1.4.A). The structure also indicates that some β subunit residues at the interface of the two trimers (Fig. 1.4.C), near the proposed active site, could influence

Figure 1.3 Naphthalene dioxygenase reaction (36).

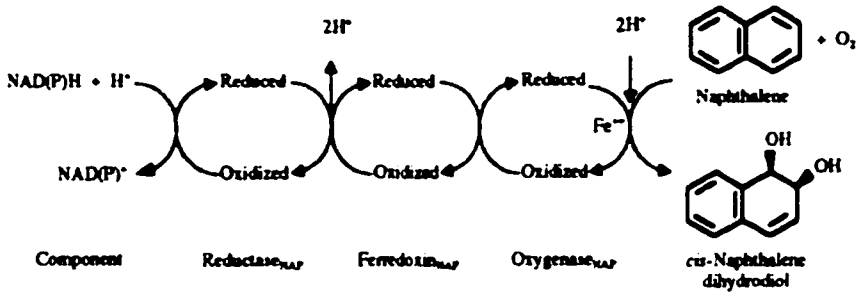
2H+
2H+
+ O2
NAD(P)H + H+
Reduced
Reduced
Reduced
Naphthalene
Fe++
OH
OH
NAD(P)+
Oxidized
Oxidized
Oxidized
Component
Reductase
Ferredoxin
Oxygenase
cis-Naphthalene dihydrodiol

enzyme activity. Studies of hybrids of naphthalene and 2,4-dinitrotoluene dioxygenases indicated that the replacement of the β subunit affected the rate of substrate oxidation, but did not alter the substrate range or regiospecificity of the enzymes on the selected substrates (37).

Additional valuable information has recently emerged from functional studies of naphthalene dioxygenase. In one such study (38), reaction of naphthalene dioxygenase with benzene in place of naphthalene resulted in uncoupling of the dihydroxylation reaction from oxygen consumption. Part of the excess O_2 consumed by the enzyme was detected as H_2O_2, and since NADH and O_2 consumption were tightly coupled, the possibility of H_2O release was ruled out. The H_2O_2 that was released acted both as an inhibitor of benzene-dependent O_2 consumption, and as an inactivator of NDO. It was proposed that the inactivation of NDO occurs by a Fenton-type reaction (Eq.1.1) from the reaction of H_2O_2 with the reduced mononuclear iron, releasing a strong oxidizing agent, hydroxyl radical (38).

Equation 1.1

$$Fe^{2+} + H_2O_2 \rightarrow \quad OH + Fe^{3+} + {}^{\cdot}OH$$

Site-directed mutagenesis studies to elucidate the roles of specific amino acid residues in NDO have also been reported. Results derived from substitution of an aspartate residue at position 205, which is at the interface of adjacent subunits, with alanine, glutamate, asparagine, or glutamine have led to the proposal that Asp205 is involved in a major pathway of electron transfer from the Fe-S cluster to the mononuclear iron site (39). NDO catalyses the dihydroxylation of naphthalene, but can also catalyse

Figure 1.4 Crystal structure of NDO to 2.24 Å resolution (20). The α-subunits are depicted in yellow, the β-subunits in blue, the mononuclear iron center in red, and the [2Fe-2S] cluster in orange. The residues in green represent the N-terminal methionine of each α-subunit as a reference point. A) Side view of the hexamer. Residues depicted in purple and pink are suggested to form the substrate entrance (20); B) Top view of the hexamer; C) Side view of one αβ-subunit. Figure prepared from (PDB Id 1NDO) using RasMol version 2.5.

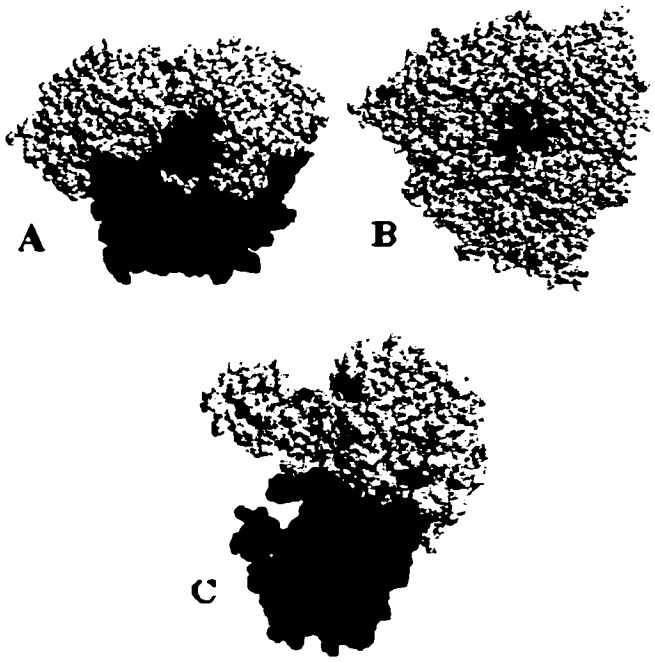
A
B
C

the oxygenation of a wide variety of other aromatic compounds (40;41). From the crystal structure of NDO, a number of hydrophobic residues located at the active site have been identified, and subjected to site-directed mutagenesis to identify some that could be responsible for the substrate specificity of NDO (36). Most of the selected amino acid substitutions did not significantly affect the enzyme's substrate preference, but substitution of Phe352 by valine, leucine, or threonine resulted in alterations to NDO's regioselectivity and enantioselectivity with selected substrates (42;43).

A recent study of single turnover chemistry and regulation of O_2 activation by the oxygenase component of naphthalene dioxygenase has added considerably to our understanding of dihydroxylation of aromatic substrates by nonheme iron dioxygenases (44). This study showed that the fully-reduced oxygenase component itself is capable of efficiently catalyzing the *cis*-dihydroxylation of an aromatic substrate without the participation of the ferredoxin (NDF) and reductase (NDR) components. Since both substrate hydroxylation and rapid reaction with oxygen were shown to occur only in the presence of aromatic substrate when both the Rieske and mononuclear iron centers were reduced, the mechanism of regulation appears to be based within the oxygenase. Therefore, both the ferredoxin and reductase components appear to be responsible only for providing the oxygenase component with electrons, rather than for playing an effector role in oxygen activation and substrate hydroxylation as is the case with some other oxygenases (44).

The overall interplay of components necessary for catalysis by NDOS is illustrated in Figure 1.5. It is believed that reduced NDF interacts with NDO to reduce both the [2Fe-2S] and mononuclear iron centers, but electrons may also be accepted by

Figure 1.5 Hypothesis for the NDOS reaction cycle (44).

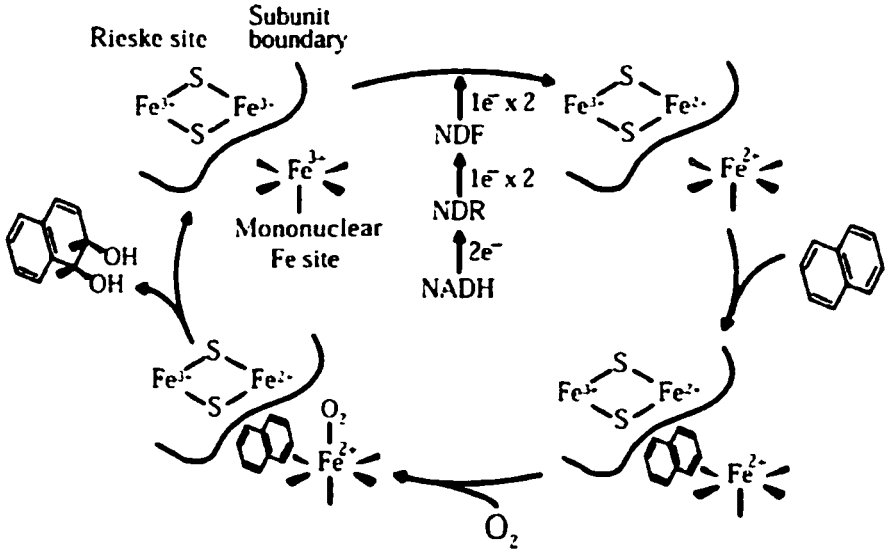
Rieske site
Subunit boundary
1e⁻ x 2
NDF
1e⁻ x 2
NDR
2e⁻
NADH
Mononuclear Fe site
OH
OH
O₂
O₂

NDO from other sources (e.g. dithionite). The fully reduced NDO component binds naphthalene, and the reduced NDO-naphthalene complex then becomes competent to bind O_2, reductively activate it by two electrons, and proceed with *cis*-dihydroxylation of naphthalene. After dissociation of the product, re-reduction of both NDO metal cofactors by reduced NDF allows the enzyme to initiate a new catalytic cycle (44).

1.3.3 4-Methoxybenzoate Monooxygenase

Another relatively well-characterized oxygenase related to BPDO is 4-methoxybenzoate monooxygenase, which consists of two components with an FMN / [2Fe-2S] containing reductase and a Rieske-type [2Fe-2S] / mononuclear Fe(II) containing oxygenase. The enzyme is fairly nonspecific for aromatic substrates, including 4-methylmercaptobenzoate, 4-aminobenzoate, 3-hydroxybenzoate, in addition to 4-methoxybenzoate (45). Depending on the substrate analogue present, the enzyme system can act as either a monooxygenase, a dioxygenase, an oxidase (releasing the activated oxygen molecule as hydrogen peroxide), or reduce the oxygen molecule to water.

Uncoupling, i.e. production of reduced oxygen species rather than hydroxylated aromatic product, has been well-studied in 4-methoxybenzoate monooxygenase compared to most other oxygenases (except cytochrome P-450). Kinetic and stoichiometric studies of this system indicate that the iron-peroxo complex attacks an aromatic ring system according to the empiric rules of electrophilic substitution. Therefore, electron-withdrawing substituents decreased the reactivity of the aromatic system, and consequently decreased product formation, resulting in increased uncoupling.

Thus, the electron density of the aromatic ring, which depends on the nature and position of the substituents, influences the course of the oxygen activation reaction (45).

Studies of the 4-methoxybenzoate monooxygenase iron center, which is the dioxygen-binding site, involved replacement of dioxygen by a nitrosyl ligand, leading to the formation of a rather stable Fe(III)-NO^- complex with characteristic EPR signals. The results of these studies indicate that binding of different substrates to the active site modulates the microenvironment of both the oxidized and the nitrosylated iron, changing the distortion of the iron center. However, although there is evidence for the modulating effects of the aromatic substrate analogues, it is still not possible to correlate enzymatic function to these effects (46).

1.3.4 Cytochrome P-450

Cytochrome P-450 enzymes constitute a large family of multicomponent heme-containing monooxygenases, which are capable of catalyzing a range of oxidative transformations such as carbon hydroxylation, heteroatom oxidation, and double-bond epoxidation. The catalytic versatility of these enzymes allows them to play vital roles in the synthesis and degradation of a wide array of physiologically important compounds and xenobiotics (reviewed in (47)). The pivotal biological roles of cytochrome P-450s have attracted a lot of attention over the past 25 years, rendering an unprecendented level of insight into the reaction chemistry of an oxygenase.

Briefly, the reaction cycle of cytochrome P-450 (Fig. 1.6) is initiated by binding of the organic substrate, resulting in an increase in the reduction potential of the heme iron atom, allowing reduction of the ferric iron to its ferrous state. In the case of

cytochrome P-450$_{cam}$, which catalyses the hydroxylation of camphor, electrons are provided from NAD(P)H, via the flavoprotein, putidaredoxin reductase (PdR), and the iron-sulfur protein, putidaredoxin (Pd). Once O_2 binds and the ferrous dioxy (Fe^{II}-O_2) complex is formed, the complex is further reduced to a ferric peroxo (Fe^{III}-OOH) species. Cleavage of the Fe^{III}-OOH dioxygen bond then occurs, leaving the enzyme with a ferryl (formally Fe^{V}=O) species. The highly oxidative ferryl oxygen is then inserted into a carbon-hydrogen bond of the substrate, followed by product dissociation (47;48).

According to structural studies of camphor-free P-450$_{cam}$, its substrate binding pocket is occupied by six water molecules, which are expelled upon organic substrate binding, thereby converting the heme iron from six-coordinate, water-ligated, to the five-coordinate form (49). Upon binding of organic substrates that do not fill tightly the substrate binding pocket, extra solvent water molecules can remain near the O-O bond undergoing cleavage, thereby promoting uncoupling of the hydroxylation reaction. The two modes of uncoupling found in cytochrome P-450 involve either transfer of two electrons to O_2, with the production of hydrogen peroxide, or four electrons, with the production of water (50-52).

These and other studies provide a useful complement of information that can guide our attempts to understand substrate specificity determinants, enzyme mechanism, and other factors regulating the initial step in the degradation of recalcitrant polychlorinated biphenyls (53). This in turn, should allow the possibility of engineering BPDO to cope with a wide variety of PCB substrates.

Figure 1.6 Cytochrome P-450 substrate hydroxylation cycle (full arrows) and the uncoupling alternative pathways (dashed arrows) (47).

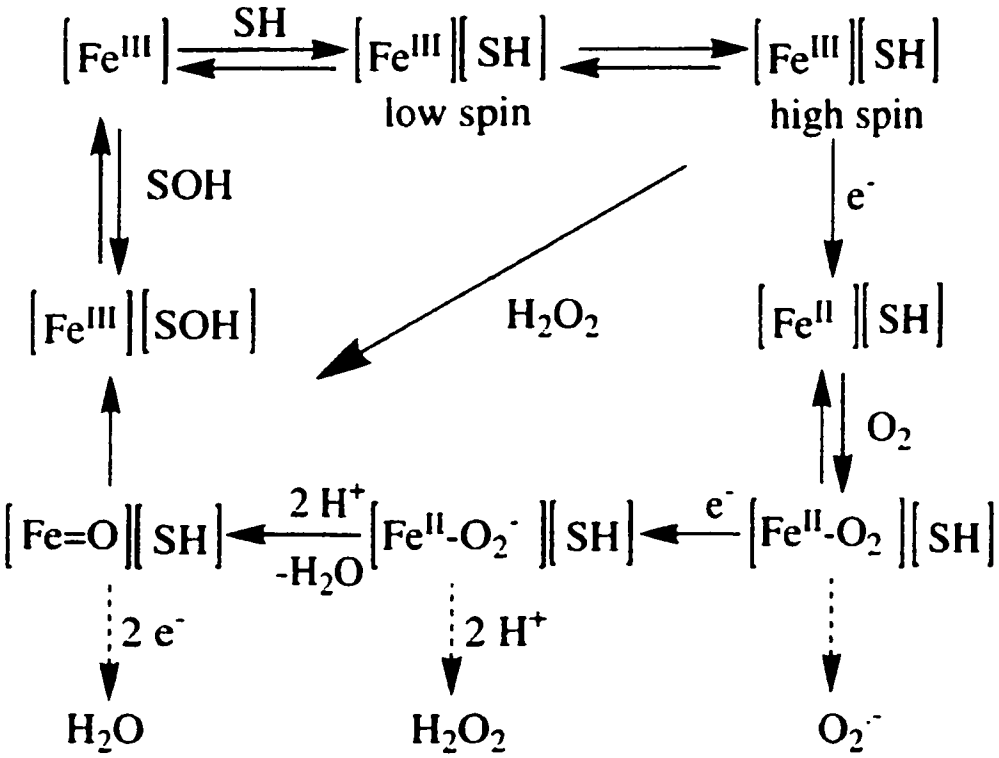
[Fe^III] SH [Fe^III][SH] [Fe^III][SH]
low spin
high spin
SOH
e-
[Fe^III][SOH]
H2O2
[Fe^II][SH]
O2
[Fe=O][SH] 2 H+ -H2O [Fe^II-O2-][SH] e- [Fe^II-O2][SH]
2 e-
2 H+
H2O
H2O2
O2-

1.3.5 Proposed Pathways of O_2 Activation by Rieske Nonheme Iron Dioxygenases

A very limited amount of experimental evidence is available to support proposals for a chemical mechanism of *cis*-dihydroxylation at the mononuclear iron site of the Rieske nonheme iron dioxygenases. One early proposal derived from studies on 4-methoxybenzoate monooxygenase, and was recently supported by work on NDO (44). In this model, an Fe^{3+}-(hydro)peroxo species attacks the substrate (Fig. 1.7, scheme A), or is at least an intermediate in the pathway of naphthalene catalyzed *cis*-dihydroxylation. Based on studies of cytochrome P-450 chemistry, a second proposed mechanism invokes O-O bond cleavage as part of oxygen activation, providing the oxygenase with a high-valent (formally Fe^{5+}) iron-oxo species for dihydroxylation of the organic substrate (Fig. 1.7, scheme B). In a third hypothesis, the ferredoxin or reductase components supply another electron to the oxygen-bound complex to generate a Fe^{4+} species, therefore facilitating O-O bond cleavage, and returning the mononuclear iron to an Fe^{2+} resting-state (Fig. 1.7, scheme C). Even though the work presented by Lipscomb and coworkers on NDO (44) does not define a chemical mechanism unambiguously, their results clearly rule out the pathway involving electron transfer from a second protein component after formation of the reactive tertiary complex (Fig. 1.7, scheme C).

Figure 1.7 Alternative pathways of O_2 activation for Rieske nonheme iron dioxygenases (44).

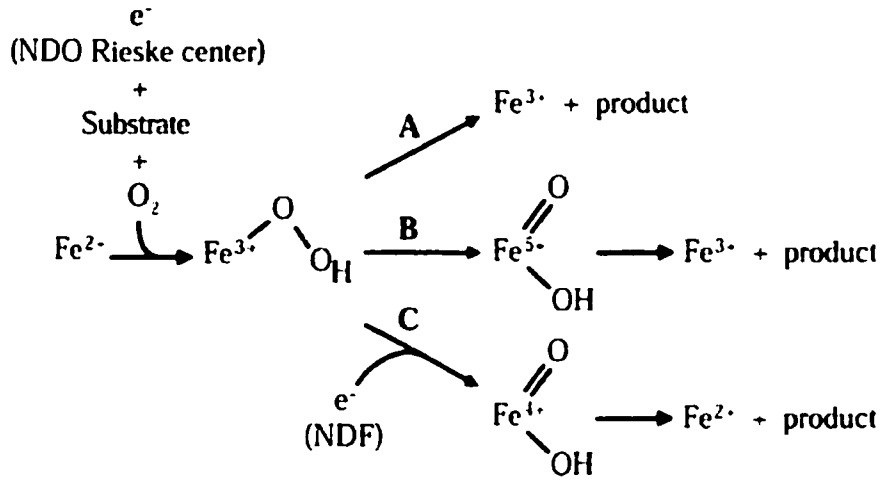
e-
(NDO Rieske center)
+
Substrate
+
O2
Fe2+
Fe3+
O
OH
A
Fe3+ + product
B
Fe5+
O
OH
Fe3+ + product
C
e-
(NDF)
Fe4+
O
OH
Fe2+ + product

1.4 Biological Iron-Sulfur Cluster Assembly

The oxygenase component of biphenyl dioxygenase (BPDO) comprises two distinct metal centers that are required for dihydroxylation of biphenyl and polychlorinated biphenyls: a non-heme mononuclear iron and a Rieske-type [2Fe-2S] cluster. The latter cofactor is composed of two iron atoms, and two inorganic sulfides, attached to the protein via two histidinyl residues on one iron and two cysteinyl residues on the other (Fig. 1.8). Although Fe-S clusters may assemble spontaneously into apo-protein *in vitro* in the presence of iron and inorganic sulfide, the toxicity of free iron and sulfide likely precludes this as a major mechanism *in vivo*. In fact, the *in vivo* biological assembly of iron-sulfur cluster cores has been shown to be a highly organized, and tightly regulated protein-assisted process.

1.4.1 Iron-Sulfur Center Assembly Gene Clusters

The initial observations leading to the discovery of genes responsible for iron-sulfur cluster core assembly arose from phenotypic studies on *Azotobacter vinelandii*, a nitrogen fixing bacterium (54-57). These studies revealed the requirement for a cysteine desulfurase enzyme, NifS, in maturation of the nitrogenase component's Fe-Mo cofactor, and led to a proposal for NifU to be required for concomitant iron mobilisation (55-57). NifS and NifU were also proposed to have specific roles in the repair of nitrogenase metalloclusters (reviewed in 54). Further functional and primary sequence investigations of *Azotobacter vinelandii* and *Escherichia coli* revealed the existence of homologues of NifS and NifU (Fig. 1.9), suggesting that these proteins have a more

Figure 1.8 Crystal structure of the Rieske-type iron-sulfur cluster of $BPDO_{B\text{-}356}$ (Chapter 3).

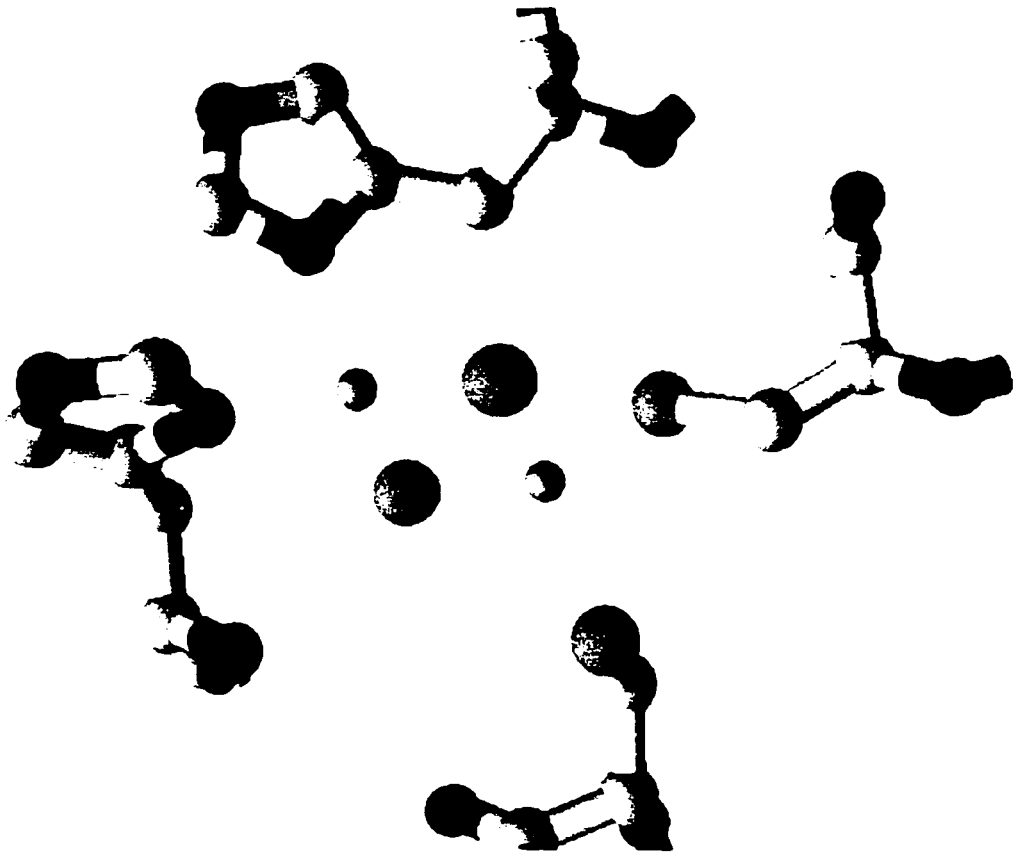

Figure 1.9 Organization of iron-sulfur cluster assembly genes in *Azotobacter vinelandii* and *Escherichia coli* along with the corresponding characterized genes from the *Saccharomyces cerevisiae*. The eukaryotic genes are not clustered in the yeast's chromosomal DNA, so their order on this figure is only for the clarity of representation (J.N. Agar, Ph.D. thesis, 2000, University of Georgia, GA, USA).

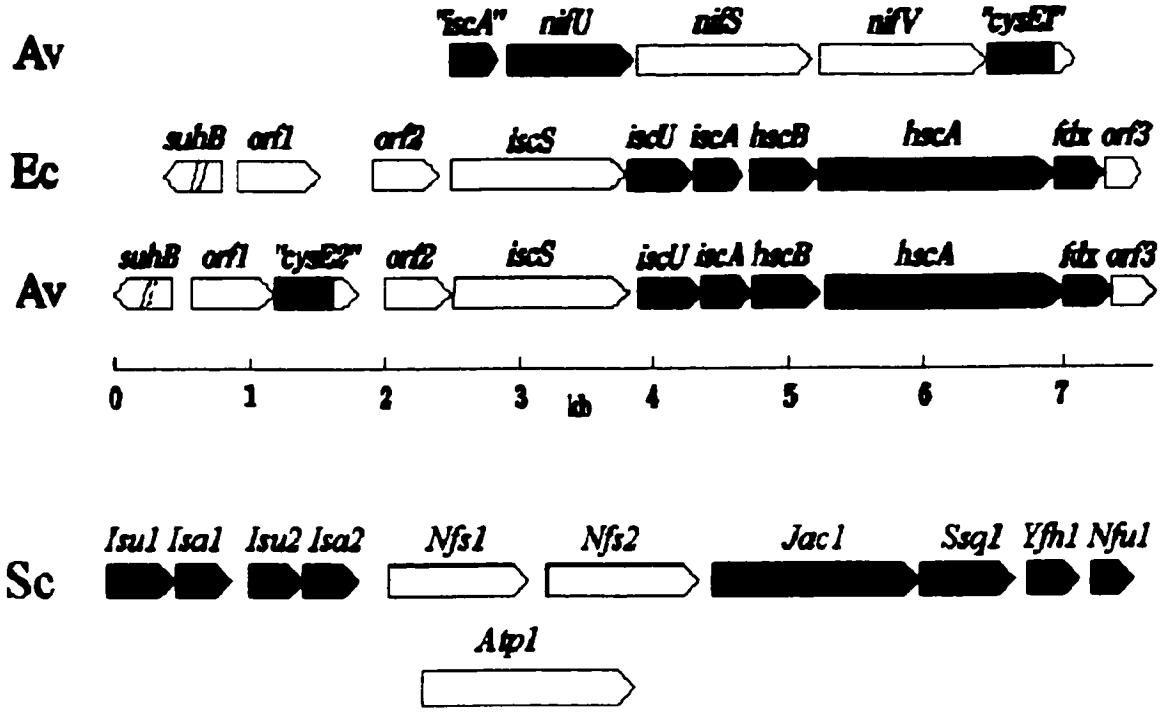
Av
"iscA" nifU nifS nifV "cysET"
Ec
suhB orf1 orf2 iscS iscU iscA hscB hscA fdx orf3
Av
suhB orf1 "cysE2" orf2 iscS iscU iscA hscB hscA fdx orf3
0 1 2 3 kb 4 5 6 7
Sc
Isu1 Isa1 Isu2 Isa2 Nfs1 Nfs2 Jac1 Ssq1 Yfh1 Nfu1
Atp1

general housekeeping role in the maturation of cellular Fe-S proteins. The housekeeping homologues of NifS and NifU were designated IscS and IscU, respectively, for iron-sulfur cluster assembly. The *iscS* and *iscU* genes were found to be located in a gene cluster that includes *iscA*, a homologue of another gene (previously termed *orf6*) contained within the major *nif* cluster of *Azotobacter vinelandii*. Moreover, analysis of available genome sequences revealed the conservation of *iscSUA* in *Escherichia coli*, *Hemophilus influenzae*, and *Saccharomyces cerevisiae*, as well as humans (54). A search of thirty-four complete genomes revealed twenty-eight that contain at least one iron-sulfur cluster assembly gene (J.N. Agar, 2000, Ph.D. thesis, University of Georgia, GA, USA).

The complete *isc* gene cluster of *A. vinelandii*, *E. coli*, and *S. cerevisiae* are illustrated in Fig. 1.9, and the functions of the corresponding gene products are described in the following section. Interestingly, the *isc* gene product homologues in yeast have been shown to be exclusively localised in the mitochondria (review (58)). A search of the genome sequence of *Pseudomonas aeruginosa* PA01 also revealed the presence of an iron-sulfur cluster assembly gene cluster, located between 4265497 and 4274027 bp (59).

1.4.2 Proposed Mechanism and Roles for Biological Iron-Sulfur Cluster Assembly

Following the landmark discoveries by Dean and coworkers of the existence of a conserved mechanism of iron-sulfur cluster biogenesis, a number of groups have extended the biochemical and genetic characterisation of biological iron-sulfur cluster assembly systems. This work has led to two proposed pathways for iron-sulfur cluster

biosynthesis (60), and is summarized below. One of the two proposed pathways is presented in Figure 1.10.

NifS, IscS, and their yeast homologue, Nfsp 1, are all pyridoxal phosphate (PLP)-dependent enzymes with cysteine desulfurase activity, and have been shown to be the source of sulfur for iron-sulfur cluster biosynthesis (step1, Fig. 1.10) (54:56:57:61). In addition to this role, Nfsp 1 has been shown to regulate cellular and mitochondrial iron homeostasis in *Saccharomyces cerevisiae* (61). A number of studies have demonstrated that NifS and IscS direct the assembly of transient clusters into NifU and IscU, which then become scaffolds for the synthesis of mature clusters (steps 2-4, Fig. 1.10) (62-65). The mechanism of IscS-directed Fe-S cluster assembly appears to initially involve direct transfer of sulfane sulfur (S^0) from a cysteine persulfide on IscS to a cysteine residue on IscU (step1, Fig. 1.10) (66:67).

IscA had originally been proposed to be a specific metallochaperone for the delivery of ferrous iron to other Fe-S cluster assembly proteins, but its low binding affinity for iron argues against this proposal (60). IscA is currently believed to provide an alternate scaffold for cluster biosynthesis (step 1-4, Fig. 1.10), and to have the ability to couple the delivery of iron and sulfur by using ferrous ion to reduce sulfane sulfur. Such a mechanism would minimize the cellular concentrations of the toxic iron and sulfur entities (60:68).

In addition to the direct involvment of IscSUA in Fe-S cluster synthesis, other proteins encoded in the *isc* gene cluster (Fig. 1.9) assist in this process. Thus, the molecular chaperones, Hsc66 and Hsc20 (respectively encoded by the *hscA* and *hscB* genes) appear to interact with IscU, resulting in significant stimulation of Hsc66's

Figure 1.10 Proposed mechanism for iron-sulfur cluster assembly (60).

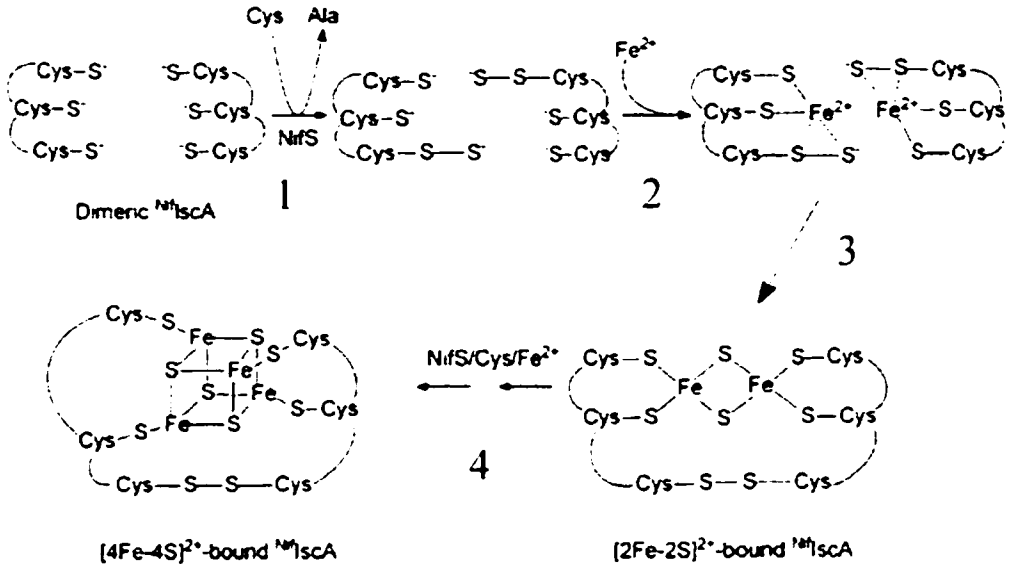
Cys
Ala
NifS
Fe2+
Dimeric NifIscA
1
2
3
4
NifS/Cys/Fe2+
[4Fe-4S]2+-bound NifIscA
[2Fe-2S]2+-bound NifIscA

ATPase activity (69-72). Hsc66, as part of the hsp70 class of molecular chaperones, requires ATP binding and hydrolysis to control peptide substrate affinity. Its presence in the *isc* gene cluster suggests that it may play a role in folding of Fe-S cluster containing proteins. The crystal structure of the ferredoxin, Fdx, suggests that it might be involved in binding and reduction of S^0 and/or Fe^{3+}, but its precise role remains to be determined (73;74). The concerted process of iron-sulfur cluster biosynthesis appears to be elegantly auto-regulated by the [2Fe-2S] cluster-containing IscR transcription factor, encoded by the gene previously designated as *orf2* (75). Once an iron-sulfur cluster is assembled in mature form into one of the scaffold proteins, it is proposed to be reductively transferred intact to a target apo-protein (76;77).

In addition to the increasingly well-established roles of the iron-sulfur cluster assembly gene products in *de novo* biogenesis, it has been proposed they are also capable of repairing damaged clusters (54;78). A number of physiological processes, such as the production of reactive oxygen species or nitrosyl radicals, have the potential to induce fatal modifications to iron-sulfur clusters (79-82). The two possible responses of the cell are degradation of the apo-protein together with *de novo* synthesis of its holo-form, or repair/reassembly of the cluster to regenerate the holo form (54). Some experimental evidence for the involvement of *isc* cluster gene products in repair functions has appeared in the literature. The cysteine desulfurase, IscS, has recently been shown to repair a nitric oxide-modified ferredoxin [2Fe-2S] cluster *in vitro* (83). Moreover, efficient repair of Fe-S clusters has been shown in aerobically growing *E.coli* cells, even in the presence of a protein synthesis inhibitor (79;82).

1.4.3 Significance to Biphenyl Dioxygenase Studies

In this thesis, biological iron-sulfur cluster assembly is addressed in light of limitations previously reported and encountered in the overproduction of BPDO. An additional consideration relates to the engineering of bacterial strains for improved PCB bioremediation. Polychlorinated biphenyls (PCB) are generally found as mixtures of 209 possible congeners. Substrates that do not fit tightly in the substrate binding pocket of a number of oxygenases, including BPDO, have been shown to induce uncoupling of the reaction, releasing reactive oxygen species. Some of these species are capable of destroying Fe-S clusters. Since the Fe-S cluster is required for BPDO to dihydroxylate aromatic substrates, it is of interest to examine whether regeneration of Fe-S cluster by the *isc* gene products is feasible. Such a repair mechanism might then be exploited to improve the efficiency of BPDO in a stressed bioremediation system.

1.5 Objectives of this Thesis

Considerable limitations in the development of effective bioremediation strategies for diversely and highly chlorinated biphenyls arise from the inefficiency of existing microbial strains in degrading them. The study of the structure and function of key catabolic enzymes is critical to expanding existing microbial catabolic activities, as it facilitates the modification of enzyme specificity and the design of novel metabolic pathways. BPDO is a key enzyme in the aerobic degradation of biphenyl and some PCBs, utilizing O_2 to catalyse the *cis*-dihydroxylation of these compounds. It is therefore a prime target for engineering to alter or improve its PCB-hydroxylating ability.

The work in this thesis describes kinetic, structural, and spectroscopic characterization of BPDO undertaken to strengthen our understanding of how this enzyme works, and to reveal some of the molecular factors regulating its substrate selectivity. BPDO was characterized with respect to kinetic parameters of the system for selected biphenyl substrates, for molecular oxygen in presence of those substrates, and for reaction stoichiometry to account for uncoupling (Chapter 2). This approach was further exploited in Chapters 4 and 5 to investigate substrate preference as a function of enzyme structure. Structural insights of BPDO were provided by X-ray crystallography, and studies of structural details of the active site in BPDO, and BPDO binary substrate-bound and product-bound complexes, enable the identification of residues potentially limiting the accommodation of highly chlorinated substrates, and molecular oxygen (Chapter 3). Complementary information emerging from similar studies with site-directed BPDO variants (Chapter 4), and structurally similar BPDOs from biphenyl degrading strains *Pseudomonas cepacia* LB400, and a pseudomonad isolated from Arctic soil (Chapter 5), should enhance our understanding of aromatic ring dihydroxylation systems. Finally, the co-expression of the *isc* gene cluster for improved production of the oxygenase component of BPDO overcomes previous limitations to its extended biochemical characterization. Moreover, it may lead to the engineering of bioremediation systems that not only allow more efficient expression of key degradative oxygenases, but that also maintain the levels of active proteins during time of localized oxidative stress.

The availability of this information should contribute to the rational design of a biphenyl dioxygenase with broadened substrate selectivity, and improved catalytic

activity. Most importantly, the methodology developed to investigate the oxygenase reactivity can further be applied to broaden the initial study, and expand the study of similar systems. In parallel with this thesis, information derived from directed evolution (Roch Aumont, 2002, M.Sc. Thesis, Concordia University) should also contribute to the identification of some molecular determinants for substrate selectivity of biphenyl dioxygenase. Moreover, directed evolution may directly provide us with a collection of BPDOs with complementary substrate preference that could be exploited for bioremediation of polychlorinated biphenyls.

REFERENCES

1. Dobson, S. and van Esch G.J. (1993) *Polychlorinated biphenyls and terphenyls.* World Health Organization, Geneva

2. Focht, D. D. (1995) *Curr.Opin.Biotechnol.* **6**, 341-346

3. Timmis, K. N., Steffan, R. J., and Unterman, R. (1994) *Annual Review in Microbioloby* **48**, 525-557

4. Bergeron, J., Ahmad, D., Barriault, D., Larose, A., Sylvestre, M., and Powlowski, J. (1994) *Can.J.Microbiol.* **40**, 743-753

5. Haddock, J. D., Nadim, L. M., and Gibson, D. T. (1993) *J.Bacteriol.* **175**, 395-400

6. Taira, K., Hirose, J., Hayashida, S., and Furukawa, K. (1992) *J.Biol.Chem.* **267**, 4844-4853

7. Hulsmeyer, M., Hecht, H. J., Niefind, K., Hofer, B., Eltis, L. D., Timmis, K. N., and Schomburg, D. (1998) *Protein Sci.* **7**, 1286-1293

8. Han, S., Eltis, L. D., Timmis, K. N., Muchmore, S. W., and Bolin, J. T. (1995) *Science* **270**, 976-980

9. Nandhagopal, N., Yamada, A., Hatta, T., Masai, E., Fukuda, M., Mitsui, Y., and Senda, T. (2001) *J.Mol.Biol.* **309**, 1139-1151

10. Colbert, C. L., Couture, M. M., Eltis, L. D., and Bolin, J. T. (2000) *Structure.Fold.Des* **8**, 1267-1278

11. Hurtubise, Y., Barriault, D., Powlowski, J., and Sylvestre, M. (1995) *J.Bacteriol.* **177,** 6610-6618

12. Hurtubise, Y., Barriault, D., and Sylvestre, M. (1996) *J.Biol.Chem.* **271,** 8152-8156

13. Haddock, J. D. and Gibson, D. T. (1995) *J.Bacteriol.* **177,** 5834-5839

14. Mondello, F. J., Turcich, M. P., Lobos, J. H., and Erickson, B. D. (1997) *Appl.Environ.Microbiol.* **63,** 3096-3103

15. Haddock, J. D., Horton, J. R., and Gibson, D. T. (1995) *J.Bacteriol.* **177,** 20-26

16. Hirose, J., Suyama, A., Hayashida, S., and Furukawa, K. (1994) *Gene* **138,** 27-33

17. Tan, H. M. and Cheong, C. M. (1994) *Biochem.Biophys.Res.Commun.* **204,** 912-917

18. Kimura, N., Nishi, A., Goto, M., and Furukawa, K. (1997) *J.Bacteriol.* **179,** 3936-3943

19. Hurtubise, Y., Barriault, D., and Sylvestre, M. (1998) *J.Bacteriol.* **180,** 5828-5835

20. Kauppi, B., Lee, K., Carredano, E., Parales, R. E., Gibson, D. T., Eklund, H., and Ramaswamy, S. (1998) *Structure.* **6,** 571-586

21. Master, E. R. and Mohn, W. W. (1998) *Appl.Environ.Microbiol.* **64,** 4823-4829

22. Kumamaru, T., Suenaga, H., Mitsuoka, M., Watanabe, T., and Furukawa, K. (1998) *Nat.Biotechnol.* **16,** 663-666

23. Suenaga H. Mitsuoka M. Ura Y. Watanabe T. and Furukawa K (2001) *J. Bacteriol.* **183,** 5441-5444

24. Suenaga, H., Goto, M., and Furukawa, K. (2001) *J.Biol.Chem.* **276,** 22500-22506

25. Batie, C. J., LaHaie, E., and Ballou, D. P. (1987) *J.Biol.Chem.* **262,** 1510-1518

26. Gassner, G. T., Ludwig, M. L., Gatti, D. L., Correll, C. C., and Ballou, D. P. (1995) *FASEB J.* **9,** 1411-1418

27. Gassner, G. T., Ballou, D. P., Landrum, G. A., and Whittaker, J. W. (1993) *Biochemistry* **32,** 4820-4825

28. Pavel, E. G., Martins, L. J., Ellis, W. R., Jr., and Solomon, E. I. (1994) *Chem.Biol.* **1,** 173-183

29. Coulter, E. D., Moon, N., Batie, C. J., Dunham, W. R., and Ballou, D. P. (1999) *Biochemistry* **38,** 11062-11072

30. Ensley, B. D., Gibson, D. T., and Laborde, A. L. (1982) *J.Bacteriol.* **149,** 948-954

31. Ensley, B. D. and Gibson, D. T. (1983) *J.Bacteriol.* **155,** 505-511

32. Haigler, B. E. and Gibson, D. T. (1990) *J.Bacteriol.* **172,** 465-468

33. Haigler, B. E. and Gibson, D. T. (1990) *J.Bacteriol.* **172,** 457-464

34. Carredano, E., Karlsson, A., Kauppi, B., Choudhury, D., Parales, R. E., Parales, J. V., Lee, K., Gibson, D. T., Eklund, H., and Ramaswamy, S. (2000) *J.Mol.Biol.* **296,** 701-712

35. Carredano, E., Kauppi, B., Choudhury, D., and Ramaswamy, S. (2000) *Acta Crystallogr.D.Biol.Crystallogr.* **56,** 313-321

36. Parales, R. E., Lee, K., Resnick, S. M., Jiang, H., Lessner, D. J., and Gibson, D. T. (2000) *J.Bacteriol.* **182,** 1641-1649

37. Parales, R. E., Emig, M. D., Lynch, N. A., and Gibson, D. T. (1998) *J.Bacteriol.* **180,** 2337-2344

38. Lee, K. (1999) *J.Bacteriol.* **181,** 2719-2725

39. Parales, R. E., Parales, J. V., and Gibson, D. T. (1999) *J.Bacteriol.* **181,** 1831-1837

40. Gibson, D. T., Resnick, S. M., Lee, K., Brand, J. M., Torok, D. S., Wackett, L. P., Schocken, M. J., and Haigler, B. E. (1995) *J.Bacteriol.* **177,** 2615-2621

41. Resnick, S. M. and Gibson, D. T. (1996) *Appl.Environ.Microbiol.* **62,** 4073-4080

42. Parales, R. E., Resnick, S. M., Yu, C. L., Boyd, D. R., Sharma, N. D., and Gibson, D. T. (2000) *J.Bacteriol.* **182,** 5495-5504

43. Yu, C. L., Parales, R. E., and Gibson, D. T. (2001) *J.Ind.Microbiol.Biotechnol.* **27,** 94-103

44. Wolfe, M. D., Parales, J. V., Gibson, D. T., and Lipscomb, J. D. (2001) *J.Biol.Chem.* **276,** 1945-1953

45. Wende, P., Bernhardt, F. H., and Pfleger, K. (1989) *Eur.J.Biochem.* **181,** 189-197

46. Twilfer, H., Bernhardt, F. H., and Gersonde, K. (1985) *Eur.J.Biochem.* **147,** 171-176

47. Auclair, K., Moenne-Loccoz, P., and Ortiz De Montellano, P. R. (2001) *J.Am.Chem.Soc.* **123,** 4877-4885

48. Ortiz De Montellano, P. R. (1995) *Cytochrome P-450 : Structure, Mechanism, and Biochemistry*, 2nd edition, Plenum, New York

49. Kadkhodayan, S., Coulter, E. D., Maryniak, D. M., Bryson, T. A., and Dawson, J. H. (1995) *J.Biol.Chem.* **270,** 28042-28048

50. Atkins, W. M. and Sligar, S. G. (1987) *J.Am.Chem.Soc.* **109,** 3754-3760

51. Loida, P. J. and Sligar, S. G. (1993) *Biochemistry* **32,** 11530-11538

52. Gorsky, L. D., Koop, D. R., and Coon, M. J. (1984) *J.Biol.Chem.* **259,** 6812-6817

53. Reineke, W. (1998) *Annu.Rev.Microbiol.* **52,** 287-331

54. Zheng, L., Cash, V. L., Flint, D. H., and Dean, D. R. (1998) *J.Biol.Chem.* **273,** 13264-13272

55. Fu, W., Jack, R. F., Morgan, T. V., Dean, D. R., and Johnson, M. K. (1994) *Biochemistry* **33,** 13455-13463

56. Zheng, L., White, R. H., Cash, V. L., and Dean, D. R. (1994) *Biochemistry* **33,** 4714-4720

57. Zheng, L., White, R. H., Cash, V. L., Jack, R. F., and Dean, D. R. (1993) *Proc.Natl.Acad.Sci.U.S.A* **90,** 2754-2758

58. Muhlenhoff, U. and Lill, R. (2000) *Biochim.Biophys.Acta* **1459,** 370-382

59. Stover, C. K., Pham, X. Q., Erwin, A. L., Mizoguchi, S. D., Warrener, P., Hickey, M. J., Brinkman, F. S., Hufnagle, W. O., Kowalik, D. J., Lagrou, M., Garber, R. L., Goltry, L., Tolentino, E., Westbrock-Wadman, S., Yuan, Y., Brody, L. L., Coulter, S. N., Folger, K. R., Kas, A., Larbig, K., Lim, R., Smith, K., Spencer, D.,

Wong, G. K., Wu, Z., Paulsen, I. T., Reizer, J., Saier, M. H., Hancock, R. E., Lory, S., and Olson, M. V. (2000) *Nature* **406,** 959-964

60. Krebs, C., Agar, J. N., Smith, A. D., Frazzon, J., Dean, D. R., Huynh, B. H., and Johnson, M. K. (2001) *Biochemistry* **40,** 14069-14080

61. Li, J., Kogan, M., Knight, S. A., Pain, D., and Dancis, A. (1999) *J.Biol.Chem.* **274,** 33025-33034

62. Agar, J. N., Zheng, L. M., Cash, V. L., Dean, D. R., and Johnson, M. K. (2000) *J. Am. Chem. Soc.* **122,** 2136-2137

63. Agar, J. N., Krebs, C., Frazzon, J., Huynh, B. H., Dean, D. R., and Johnson, M. K. (2000) *Biochemistry* **39,** 7856-7862

64. Yuvaniyama, P., Agar, J. N., Cash, V. L., Johnson, M. K., and Dean, D. R. (2000) *Proc.Natl.Acad.Sci.U.S.A* **97,** 599-604

65. Agar, J. N., Yuvaniyama, P., Jack, R. F., Cash, V. L., Smith, A. D., Dean, D. R., and Johnson, M. K. (2000) *J.Biol.Inorg.Chem.* **5,** 167-177

66. Smith, A. D., Agar, J. N., Johnson, K. A., Frazzon, J., Amster, I. J., Dean, D. R., and Johnson, M. K. (2001) *J.Am.Chem.Soc.* **123,** 11103-11104

67. Urbina, H. D., Silberg, J. J., Hoff, K. G., and Vickery, L. E. (2001) *J.Biol.Chem.* **276,** 44521-44526

68. Ollagnier-de-Choudens, S., Mattioli, T., Takahashi, Y., and Fontecave, M. (2001) *J.Biol.Chem.* **276,** 22604-22607

69. Hoff, K. G., Silberg, J. J., and Vickery, L. E. (2000) *Proc.Natl.Acad.Sci.U.S.A* **97,** 7790-7795

70. Silberg, J. J. and Vickery, L. E. (2000) *J.Biol.Chem.* **275,** 7779-7786

71. Silberg, J. J., Hoff, K. G., Tapley, T. L., and Vickery, L. E. (2001) *J.Biol.Chem.* **276,** 1696-1700

72. Hoff, K. G., Ta, D. T., Tapley, T. L., Silberg, J. J., and Vickery, L. E. (2002) *J.Biol.Chem., ahead of print*

73. Kakuta, Y., Horio, T., Takahashi, Y., and Fukuyama, K. (2001) *Biochemistry* **40,** 11007-11012

74. Jung, Y. S., Gao-Sheridan, H. S., Christiansen, J., Dean, D. R., and Burgess, B. K. (1999) *J.Biol.Chem.* **274,** 32402-32410

75. Schwartz, C. J., Giel, J. L., Patschkowski, T., Luther, C., Ruzicka, F. J., Beinert, H., and Kiley, P. J. (2001) *Proc.Natl.Acad.Sci.U.S.A* **98,** 14895-14900

76. Nishio, K. and Nakai, M. (2000) *J.Biol.Chem.* **275,** 22615-22618

77. Wu, G., Mansy, S. S., Wu Sp, S. P., Surerus, K. K., Foster, M. W., and Cowan, J. A. (2002) *Biochemistry* **41,** 5024-5032

78. Zheng, L. and Dean, D. R. (1994) *J.Biol.Chem.* **269,** 18723-18726

79. Rogers, P. A. and Ding, H. (2001) *J.Biol.Chem.* **276,** 30980-30986

80. Kuo, C. F., Mashino, T., and Fridovich, I. (1987) *J.Biol.Chem.* **262,** 4724-4727

81. Ding, H. and Demple, B. (2000) *Proc.Natl.Acad.Sci.U.S.A* **97,** 5146-5150

82. Flint, D. H., Smyk-Randall, E., Tuminello, J. F., Draczynska-Lusiak, B., and Brown, O. R. (1993) *J.Biol.Chem.* **268,** 25547-25552

83. Yang, W., Rogers, P. A., and Ding, H. (2002) *J.Biol.Chem.* **277,** 12868-12873

Chapter 2

Steady-State Kinetic Characterization and Crystallization of a PCB-Transforming Dioxygenase

ABSTRACT

The oxygenase component of biphenyl dioxygenase (BPDO) of *Comamonas testosteroni* B-356 dihydroxylates biphenyl and some polychlorinated biphenyls (PCBs), thereby initiating their degradation. The enzyme was overexpressed in a pseudomonad and purified anaerobically. Reconstituted, purified BPDO had a specific activity of 4.9 U/mg, and its oxygenase component appeared to contain a full complement of the Rieske [2Fe-2S] center and catalytic iron. Crystals of the oxygenase in space group *R*3 were obtained under anaerobic conditions using polyethylene glycol as the precipitant. X-ray diffraction was measured to 1.6 Å. Steady-state kinetics assays monitoring O_2 consumption demonstrated that BPDO had an apparent specificity for biphenyl of 1.2 ± 0.1 x 10^6 $M^{-1}s^{-1}$ in air-saturated buffer (50 mM MES, pH 6.0, 25 °C). Moreover, BPDO transformed dichlorobiphenyls (diClBs) in the following order of apparent specificities: 3,3'- > 2,2'- > 4,4'-diClB. Strikingly, the ability of the enzyme to utilize O_2 depended strongly on the biphenyl substrate: the k_{cat}/K_mO_2 was 3.6 ± 0.3, 0.06 ± 0.02, and 0.4 ± 0.07 x 10^5 $M^{-1}s^{-1}$ in the presence of biphenyl, 2,2'-diClB, and 3,3'-diClB, respectively. Moreover, the ratio of biphenyl to O_2 consumed was 0.97, 0.44, 0.63 and 0.48, in the presence of biphenyl, 2,2'-, 3,3'-, and 4,4'-diClB, respectively. Within experimental error, the balance of consumed O_2 was detected as hydrogen peroxide. Thus, PCB congeners such as 2,2'-diClB that bind to and uncouple BPDO exact a high energetic cost, produce a cytotoxic compound, and can inhibit the degradation of other congeners. Each of these effects would be predicted to inhibit the aerobic microbial catabolism of PCBs.

INTRODUCTION

The microbial catabolic activities responsible for the degradation of aromatic compounds constitute an essential link in the global carbon cycle. These activities are of considerable practical interest due to their potential to destroy toxic, persistent pollutants, a strategy known as bioremediation (1). In the case of highly chlorinated, structurally diverse xenobiotics such as PCBs[1], the development of a practical bioremediation technology has been limited in part by the failure of existing microbial catabolic activities to effectively degrade these compounds (1,2). This failure may arise because these activities have not yet evolved to degrade compounds that have only recently been introduced into the biosphere. An important aspect of the adaptation of catabolic activities for bioremediation is the study of the structure and function of key catabolic enzymes. Such studies provide insight into the molecular basis of an important biological process, thereby facilitating the modification of enzyme specificity and the design of novel metabolic pathways.

BPDO catalyzes the initial reaction in the aerobic degradation of biphenyl and some PCBs. BPDO is a typical aromatic ring-hydroxylating dioxygenase, utilizing O_2 and electrons originating from NADH to transform biphenyl to *cis*-(2*R*,3*S*)-dihydroxy-1-phenylcyclohexa-4,6-diene (3,4; Fig. 2.1). This dihydroxylation prepares the ring for subsequent degradation by ring-cleavage enzymes. The enzyme comprises an FAD-containing reductase (BphG), a Rieske-type ferredoxin (BphF), and a two-subunit

---

[1] Abbreviations: BPDO, biphenyl dioxygenase; DHBD, 2,3-dihydroxybiphenyl dioxygenase; diClB, dichlorobiphenyl; HEPES, 4-(2-(hydroxyethyl)-1-piperazineethanesulfonic acid; MES, 2-(N-morpholino)ethanesulfonic acid; PCB, polychlorinated biphenyl; PCR, polymerase chain reaction; PEG, polyethylene glycol; PAGE, polyacrylamide gel electrophoresis; SDS, sodium dodecyl sulfate.

Figure 2.1 BPDO of *Comamonas testosteroni* B-356. The enzyme comprises an FAD-containing reductase (BphG), a Rieske-type ferredoxin (BphF), and an oxygenase, which contains a Rieske-type [2Fe-2S] cluster and a catalytic mononuclear iron center. Biphenyl is stereospecifically hydroxylated at positions 2 and 3, yielding *cis*-(2*R*,3*S*)-dihydroxy-2,3-dihydrobiphenyl.

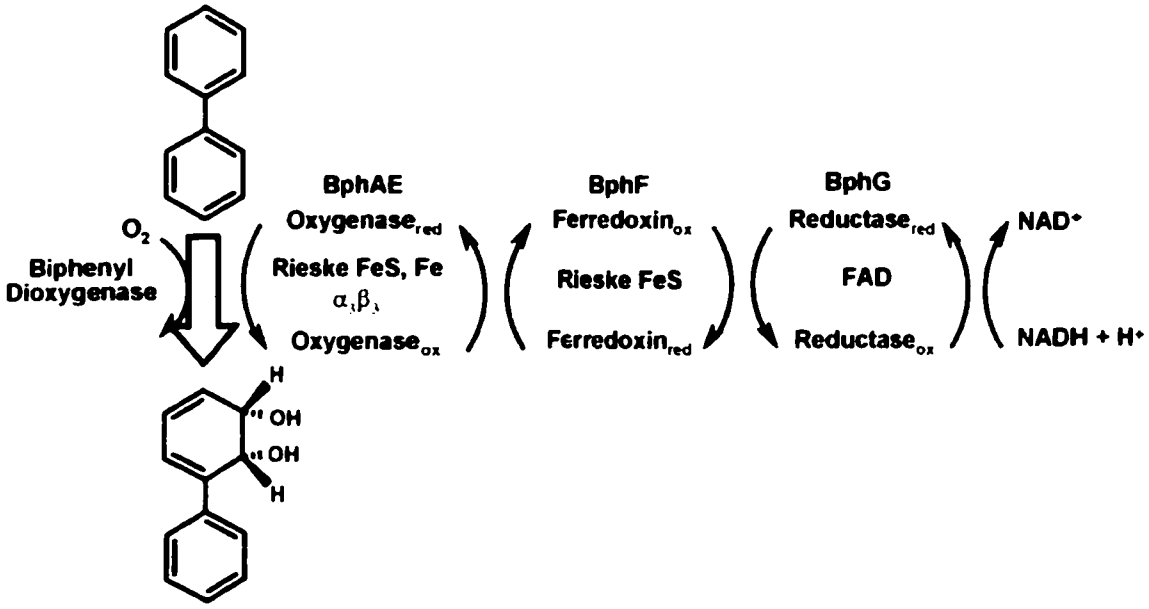
O2
Biphenyl
Dioxygenase
BphAE
Oxygenase red
Rieske FeS, Fe
α3β3
Oxygenase ox
BphF
Ferredoxin ox
Rieske FeS
Ferredoxin red
BphG
Reductase red
FAD
Reductase ox
NAD+
NADH + H+
H
OH
OH
H

oxygenase of $\alpha_3\beta_3$ constitution, which contains a Rieske-type [2Fe-2S] cluster and a mononuclear iron center. Accordingly, BPDO has been classified as a group IIB aromatic ring-hydroxylating dioxygenase together with benzene and toluene dioxygenases (5). Structural and spectroscopic studies of related dioxygenases indicate that the mononuclear Fe center orchestrates substrate transformation (reviewed in 6). BphG, BphF and the oxygenase [2Fe-2S] cluster function to transfer electrons from NADH to this center.

BPDO is a major determinant of the PCB-catabolizing capabilities of biphenyl-degrading strains, and the enzymes from different strains possess significantly different congener-transforming abilities. For example, $BPDO_{LB400}$ from *Burkholderia cepacia* LB400 transforms a much broader range of congeners than $BPDO_{KF707}$ of *Pseudomonas pseudoalcaligenes* KF707, even though they share over 95% sequence identity. Interestingly, $BPDO_{KF707}$ transforms 4,4'- diClB much more effectively than $BPDO_{LB400}$ (7). $BPDO_{B356}$ of *Comamonas testosteroni* B-356, which shares 70% sequence identity with $BPDO_{LB400}$ and $BPDO_{KF707}$, transforms a more limited range of congeners than $BPDO_{LB400}$ but also transforms 4,4'-diClB poorly (8). Moreover, $BPDO_{B356}$ and $BPDO_{KF707}$ exclusively catalyze the 2,3-dihydroxylation of biphenyl substrates (7, 9), while the LB400 homologue catalyzes the 3,4-dihydroxylation of certain PCB congeners (10). Finally $BPDO_{LB400}$ has been shown to catalyze the dehalogenation of certain *ortho* chlorinated congeners (10). Significantly, no BPDO has been found to effectively transform highly chlorinated biphenyls.

Several investigators have attempted to elucidate the structural determinants of congener preference in BPDO with the ultimate objective of enhancing this enzyme's PCB-transforming ability. Studies of variant $BPDO_{LB400}$ and $BPDO_{KF707}$ implicate a relatively small number of residues in the carboxy terminus of the oxygenase α subunit in determining congener preference (11, 12). Moreover, chimeric oxygenases obtained by

shuffling the genes encoding $BPDO_{LB400}$ and $BPDO_{KF707}$ possess enhanced PCB-degrading abilities with respect to the parental enzymes (13, 14). This is consistent with studies of related enzymes, such as naphthalene dioxygenase, in which the determinants of substrate specificity appear to reside in the carboxyl terminus of the α subunit (15). However, the substrate preferences of hybrid oxygenases in which the α and β subunits originate from more divergent enzymes, such as $BPDO_{LB400}$, $BPDO_{B356}$, and $BPDOp_6$, clearly indicate that the β subunit contributes to determining substrate preference (9,16).

Detailed structural and biochemical information on BPDO would greatly facilitate ongoing efforts to enhance this enzyme's PCB-degrading capabilities and contribute to our understanding of ring-hydroxylating dioxygenases. The ability to obtain such information has been limited by the propensity of the BPDO oxygenase to form inclusion bodies in *Escherichia coli*, its O_2-lability, and the lack of a continuous activity assay. We report here the improved expression and purification of recombinant $BPDO_{B356}$. An oxygraph assay was established to investigate the specificity of the enzyme and its steady-state utilization of O_2 in the presence of different biphenyls. Conditions for crystallization of the BPDO oxygenase were established, and analysis of preliminary X-ray diffraction data from these crystals is reported.

MATERIALS AND METHODS

Materials - Biphenyl was purchased from Aldrich (Mississauga, Ontario, Canada) and Anachemia (Quebec, Canada). Catechol was purchased from Fisher Scientific (Quebec, Canada). 2,3-Dihydroxybiphenyl was a kind gift from Professor Victor Snieckus. 2,2'-DiClB was purchased from Analabs, Inc. (North Haven, CT). 3,3'-DiClB and 4,4'-diClB were purchased from ULTRA Scientific (North Kingstown, RI). Restriction enzymes and *Pfu*I polymerase were purchased from Promega and Stratagene, respectively. Synthetic oligonucleotides with the sequences

5'-CCGGATTAATTAGAGCTCCCGACACGTGC-3'

and

5'-CAGGTGAAGGCCTTTGCGTTGCCA-3'

were purchased from the Sheldon Biotechnology Center (McGill University, Montreal, Canada). The *Sac*I restriction site introduced by the former is underlined. Kits used to screen for potential crystallization conditions were from Hampton Research (Laguna Niguel, CA), whereas PEGs used in crystallization protocols were from Fluka (Milwaukee,WI). Ferene-S was purchased from ICN Biomedicals Inc. (Aurora, OH). All other chemicals were of analytical or HPLC grade.

Bacterial Strains and Plasmids - Strains used for protein expression or DNA propagation included *E. coli* DH5α (17), *E. coli* JM109 (18), and *P. putida* KT2442 (19). *E. coli* and *P. putida* were grown at 37 °C and 30 °C, respectively. Plasmids used were pVLT31 (20) and pUCBPHA-C, a derivative of pUC18 that contains a 6.3-kb *Sma*I-*Sma*I fragment of *C. testosteroni* B-356 DNA that includes *bphAEXFBC* (21). Strains harbouring pVLT31 and its derivatives were grown in the presence of tetracycline (10 μg/ml). For BPDO expression, strains were grown in Luria-Bertani broth containing a phosphate buffer originally described for Terrific Broth (22) and supplemented (10 ml/l) with an HCl-solubilized solution of minerals (23). One liter of medium in a 2.8-liter Fernbach

flask was inoculated with 9 ml of an overnight culture. When the OD_{600} of the culture reached 0.7, isopropyl-1-thio-β-D-galactopyranoside was added to a final concentration of 1 mM and the culture was incubated for an additional 18 h before harvesting by centrifugation. The harvested cell pellet was washed 2 times with 500 ml of 25 mM HEPES pH 7.3, containing 10% glycerol and frozen until use.

DNA manipulation and amplification - DNA was purified using the Wizard Plus Minipreps Kit (Promega, Madison, WI). DNA was digested, ligated and transformed into *E. coli* using standard protocols (24). DNA was amplified using PCR reactions containing 0.3 μg of the template DNA, 2.5 U of *Pfu* polymerase, 0.4 mM of each dNTP, and 20 pmol of each oligonucleotide primer in a final volume of 25 μl. Twenty temperature cycles were performed using a DNA Thermal Cycler from Perkin Elmer (Norwalk, USA) as follows: 94 °C for 1 min, 55 °C for 2 min, and 72 °C for 45 s. Plasmids were introduced into *P. putida* KT2442 by electroporation using the Pulse Controller and Gene Pulser from BioRad with 1-mm cuvettes (BTX, Inc., San Diego, CA) (25). DNA sequencing was performed at the Sheldon Biotechnology Center using a Perkin-Elmer 373A sequencer and the ABI sequencing strategy.

Protein purification - Chromatography was performed on an ÄKTA Explorer (Amersham Pharmacia Biotech, Quebec, Canada). This system was installed next to a Labmaster Model 100 glovebox (M.Braun, Peabody, MA), so that anaerobic buffers could be delivered to the former, and the column eluate could be directed to a fraction collector in the glovebox (23). Buffers were prepared using water purified on a Barnstead NANOpure UV apparatus to a resistivity of greater than 17.5 MΩcm. Buffer A was 25 mM HEPES, pH 7.3, 10% glycerol, 2 mM dithiothreitol, and 0.5 mM ferrous ammonium sulfate. Buffer B was buffer A containing 1 M NaCl, and buffer PS was buffer A containing 5% (saturation) ammonium sulfate. Buffers HA and HB were, respectively, 5 mM and 400 mM sodium phosphate, pH 6.3, 10% glycerol, and 2 mM dithiothreitol.

Warmed buffers were degassed with N_2 and equilibrated in the glovebox for 24 hours before adding dithiothreitol and ferrous ammonium sulfate.

The washed cell pellet from 10 l of culture was resuspended in 80 ml of 25 mM HEPES, pH 7.3, 10% glycerol, containing 1 mM phenylmethylsulfonyl fluoride, 0.1 mg/ml DnaseI, 1 mM $MgCl_2$, and 2 mM $CaCl_2$. Cell suspensions were sonicated in 45 ml batches using a Virsonic 475 (Virtis, NY) apparatus with 10 x 12 s pulses at level 6. The cell debris was removed by ultracentrifugation for 60 min at 300,000 x g. The clear supernatant was carefully decanted, passed through a 0.45 μm filter, and diluted with 80 ml of buffer A. This fraction, identified as crude extract, was degassed. All subsequent procedures were performed under an inert atmosphere unless otherwise specified.

The crude extract was divided into five portions, each of which was loaded onto a Source 15Q (Amersham Pharmacia Biotech) anion exchange column (2 X 9 cm), which had been equilibrated with buffer A. The column was operated at a flow rate of 15 ml/min. Bound proteins were eluted with a linear gradient of NaCl from 0 to 0.15 M over 10 column volumes. Fractions with absorbance at 323 and 455 nm, characteristic of the Rieske-type [2Fe-2S] center, and that contained the expected polypeptides, as judged from SDS-PAGE, were concentrated to 20 ml by ultrafiltration using a stirred cell equipped with a YM30 membrane (Amicon, Ontario, Canada), and filtered. The preparation was brought to 5% saturation with ammonium sulfate, divided into two equal portions, filtered, and loaded onto a phenyl-Sepharose (Amersham Pharmacia Biotech) column (1 X 9 cm) pre-equilibrated with buffer PS. The column was operated at a flow rate of 0.75 ml/min. The oxygenase eluted at 0% saturated ammonium sulfate in a decreasing ammonium sulfate concentration gradient (5% to 0% over 2 column volumes). Reddish-colored fractions were concentrated by ultrafiltration, and equilibrated with buffer HA by gel filtration on a 0.7 X 12.5-cm column of Bio-Gel P6 DG (Bio-Rad, Ontario, Canada). The sample was then loaded onto a hydroxyapatite type II resin, 20

μm diameter. (BioRad) column (2 X 5 cm). and the protein eluted with a linear gradient from 60 mM to 120 mM sodium phosphate over 3 column volumes. Fractions of characteristic absorbance were concentrated to 15-20 mg/ml by ultrafiltration. and flash frozen as beads in liquid N_2.

Analytical Methods - SDS-PAGE with a 12% resolving gel was performed using a Bio-Rad MiniPROTEAN II apparatus. and gels were stained with Coomassie Blue according to established procedures (26). Protein concentrations were estimated using the bicinchoninic acid protein assay reagent kit (Pierce Chemical Co.. Rockford. USA) after removal of interfering substances (27). Bovine serum albumin was used as a standard. Iron content was determined colorimetrically using Ferene-S (28). Sulfur content was determined colorimetrically with N.N-dimethyl-*p*-phenylenediamine. and Na_2S as a standard (29). Concentrations of recombinant $BphF_{LB400}$ and $BphG_{B356}$ were determined spectrophotometrically using $\varepsilon_{326} = 9\ mM^{-1}cm^{-1}$ (30) and $\varepsilon_{450} = 11.8\ mM^{-1}cm^{-1}$ (R. Aumont. personal communication). respectively. 2.3-Dihydroxybiphenyl dioxygenase (DHBD) and catechol 2.3-dioxygenase were prepared as described previously (23. 31).

Steady-State Kinetic Measurements - Enzymatic activity was measured by following O_2 consumption using a computer-interfaced Clarke-type polarographic O_2 electrode (Yellow Springs Instruments Model 5301 (Yellow Springs. OH)) (23). or a Hansatech DW1 O_2 electrode (Norfolk. England) with a similar interface. Data were recorded every 0.1 s. Initial velocities were determined from progress curves by analyzing the data using Microsoft Excel (Redmond. WA). The slope of the progress curve and the correlation coefficient of the slope were calculated for all consecutive 6 s intervals using the full set of 61 data points (23).

The standard activity assay contained 70 μM $Fe(SO_4)_2(NH_4)_2$, 288 μM biphenyl, 123 μM NADH, 1.2 μM $BphG_{B356}$, 2.8 μM $BphF_{LB400}$ and 0.36 μM oxygenase. The reaction was initiated by adding oxygenase after equilibrating the assay with all other components for 20 s. The assay was performed in a total volume of 1.3 ml of air-saturated 50 mM MES (I = 0.05 M), pH 6.0, 25.0 ± 0.1 °C (Michel Sylvestre, personal communication). Buffers and stock solutions were prepared fresh daily. Stock solutions and protein samples were prepared anaerobically, stored under argon on ice, and withdrawn using a gas-tight syringe. The O_2 electrode was zeroed and calibrated on each day kinetic assays were performed using either DHBD or, at O_2 concentrations lower than 75 μM, catechol 2,3-dioxygenase as described previously (23). Activity determinations were corrected for the O_2 consumption observed in the presence of NADH, biphenyl, reductase and ferredoxin only. One unit of enzyme activity is defined as the quantity of enzyme required to consume 1 μmol of O_2 /min under the standard assay conditions.

Apparent steady-state kinetic parameters for biphenyls were determined by measuring rates of oxygen uptake in the presence of quantities of biphenyls up to and exceeding their respective solubility limits. In this respect, the solubilities of biphenyl, 2,2'-, 3,3'- and 4,4'-diClB were taken to be 45 μM, 4.5 μM, 1.6 μM and 0.27 μM, respectively (32). These values, reported in water, are similar to those in 50 mM MES, pH 6.0, 25 °C, as determined by titrating buffer with stock solutions of biphenyls in ethanol and monitoring UV-visible spectra for the appearance of turbidity at 400 nm, as well as the absorbance of the biphenyl at 250 nm.

For reactions performed using dissolved O_2 concentrations other than that of air-saturated buffer, reaction buffers were bubbled with appropriate mixtures of humidified O_2 and N_2 gases for 15-30 min prior to the experiment, as described previously (23). The equilibrated buffer was transferred to the reaction chamber using a gas-tight syringe

and the stopper was inserted into the reaction chamber. The reaction chamber was flushed continuously with the humidified gas mixture during this operation, as well as during the assay. For reactions performed using O_2 concentrations lower than 2.5%, the reaction chamber was blanketed with argon. Standard curves were established for the ranges 0-5%, 5-20%, and 20-100% O_2. Initial velocities determined at different substrate concentrations were fitted to the Michaelis-Menten equation using the least-squares fitting and dynamic weighting options of LEONORA (33). Data from experiments with varying biphenyl and O_2 concentrations were analyzed using the non-linear least-squares fitting routines supplied with Grafit 4 (Erithacus Software Ltd., Middlesex, England).

Coupling measurements - Coupling experiments were carried out in 50 mM MES, pH 6.0, 25.0 ± 0.1 °C using excess biphenyl substrate, 350 μM NADH, and the same concentrations of BPDO components that were used in the standard activity assay. Reactions were initiated by adding oxygenase and were quenched 1-3 min later by diluting 300 μl of reaction mixture with 600 μl methanol. Oxygen consumption was monitored using the O_2 electrode. The consumption of biphenyl substrate was determined by HPLC measurements using a Hewlett Packard SERIES 1050 system (Waldronn, West Germany) equipped with a C-18 reverse-phase column (0.46 x 15-cm) from Higgins Analytical, Inc. (Mountain View, CA). The instrument was operated with solvents under a constant helium purge and at a flow rate of 1 ml/min. Biphenyl was eluted with a 20 ml gradient of 50% H_2O: 50% acetonitrile to 10% H_2O: 90% acetonitrile. Samples of 100 μl were injected and the amount of biphenyl was determined from the area of the absorbance peak at 203 nm using a standard curve. Standard curves having correlation factors greater than 0.95 were established by determining the peak areas of known amounts of biphenyls. Samples for the standard curve were treated in the same way as reaction mixtures to account for any losses of biphenyl incurred during sample manipulation.

The amount of hydrogen peroxide produced during biphenyl transformation was estimated using catalase, 650 U of which was added to the reaction mixture at the time corresponding to the methanol quench. The amount of O_2 that was detected upon the addition of catalase was taken to represent 50% of the hydrogen peroxide produced during biphenyl transformation.

Crystallization of BPDO oxygenase - All crystallization experiments were performed under anaerobic conditions in a N_2 atmosphere glove box (Innovative Technologies, Newburyport, MA) maintained at ≤ 2 ppm O_2. Samples of BPDO were prepared and stored under liquid N_2 as described above. A typical sample contained 20 mg/ml enzyme, 80 mM sodium phosphate pH 6.3, 10% v/v glycerol, and 2 mM DTT. The sitting-drop vapor-diffusion technique was used for all experiments. At initial conditions the sitting drop had a volume of 4 µl and contained the protein sample and the well solution in a 1:1 ratio. The well volume was 1 ml. The sparse matrix method (34), as incorporated within the Hampton Research Crystal Screen I kit, was used at 20° and 10° C to search for preliminary crystallization parameters. Improvement of promising conditions was pursued by variation of two parameters over a 24 cell grid. Crystals used in the diffraction experiments described below grew at 20° C. The well solution initially contained 100 mM sodium citrate, pH 5.8, 10% v/v 2-propanol, and 24% w/v PEG4000.

X-ray Data Collection and Analysis - All diffraction patterns were recorded from frozen crystals by the rotation/oscillation method. The patterns were analyzed and reduced to average intensities by the use of the HKL program suite (35); intensities were converted to structure factor amplitudes using programs from the CCP4 package (36). Crystals were prepared for diffraction experiments by soaking them for 1 min in 400 µl of a solution containing 100 mM sodium citrate, pH 5.8, 10% (v/v) 2-propanol, 24% (w/v) PEG4000, and 20% (v/v) glycerol before flash-freezing by direct immersion in liquid N_2. Initial, partial diffraction patterns were obtained by the use of Cu-Kα

radiation from a Rigaku rotating anode X-ray generator operated at approximately 50 kV and 100 mA and equipped with focusing mirror optics and an R-axis IV imaging plate area detector (Molecular Structures Corp.). A cryogenic crystal cooling device (Oxford Cryosystems, Oxford, UK) was used to maintain a nominal sample temperature of 110 K. Crystals were recovered after the initial experiments and stored under liquid N_2 until diffraction studies were again initiated at the Advanced Photon Source synchrotron (APS) using BioCARS beamline BM14D. At BM14D, diffraction patterns were measured at a nominal sample temperature of 108 K (Cryojet cooling device by Oxford Instruments USA, Boston, MA) using monochromatic X-rays of 1 Å wavelength, a crystal-to-detector distance of 74 mm, and a Quantum-1 CCD detector (Area Detector Systems Corporation, Poway, CA).

RESULTS

Construction and testing of the Expression Vector - Digestion of pUCBPHA-C (21) with *Kpn*I yielded a 3178 bp fragment which, according to the sequence (37), contains the genes encoding $BPDO_{B356}$ oxygenase (*bphAE*) together with 1 kb of flanking upstream DNA. This fragment was purified and ligated with *Kpn*I-digested and dephosphorylated pVLT31, a broad host range expression vector (20). The construct containing the cloned fragment in the correct orientation, as verified by restriction digestion using *Sma*I, was designated pVLT31AE7. *P. putida* KT2442 containing pVLT31AE7 failed to express significant levels of BPDO when induced (results not shown).

A second construct, designated pVLT31AE7-3, was derived from pVLT31AE7 by removing approximately 1 kb between the Ptac promoter of pVLT31 and the ribosome binding site of *bphA*. Briefly, a 411 bp fragment of DNA containing the 5' end of *bphA* and its ribosome binding site was amplified by PCR using the oligonucleotides described in *Materials and Methods*, purified from an agarose gel, and digested with *Sac*I and *Sac*II. This fragment was ligated into pVLT31AE7 digested with *Sac*I and *Sac*II, thereby replacing the 1400 bp *Sac*I/*Sac*II fragment of pVLT31AE7 with a 351 bp *Sac*I/*Sac*II fragment. In pVLT31AE7-3, the Ptac promoter is located 71 bp upstream of the ATG start codon of *bphA*. This construct was partially sequenced to ensure the absence of PCR-induced errors. *P. putida* KT2442 containing pVLT31AE7-3 expressed high levels of soluble recombinant BPDO under appropriate induction conditions (55 mg of BPDO from 10 l of cell culture). Attempts to improve this expression by modifying the ribosome binding site upstream of *bphA* were not successful (results not shown).

Purification of BPDO - Relevant details of the anaerobic purification of BPDO from *P. putida* KT2442(pVLT31AE7-3), which was completed over a 20 hour period, are summarized in Table 2.1. SDS-polyacrylamide gel electrophoresis followed by

Table 2.1

Purification of the oxygenase component of the biphenyl dioxygenase system from *C. testosteroni* B-356

Purification step	Total protein	Total activity	Specific activity	Yield
	mg	U	U/mg	%
Crude extract	5480	1470	0.3	100
SourceQ	766	807	1.1	54.8
Phenyl-Sepharose	128	482	3.8	32.7
Hydroxyapatite	55.6	274	4.9	18.6

Activity units (U) are defined in Materials and Methods.

Coomassie Blue staining revealed that the oxygenase was of comparable purity to the aerobically purified preparation (3). The specific activity of purified BPDO was 4.9 U/mg. The iron content of the purified oxygenase was estimated to be from 8.5-12.0 mol per mol of BPDO by the chemical Ferene-S iron assay, for different preparations. The sulfur content was estimated to be 5.3 mole of S per mole of oxygenase hexamer. Under aerobic conditions, the absorbance spectrum was similar to that of BPDO purified aerobically from *C. testosteroni* strain B-356 (3), and was characteristic of a Rieske-type [2Fe-2S] cluster with maxima at 323 and 455 nm and a shoulder at about 575 nm. In the oxidized form of BDPO oxygenase, the ratio of the absorbance maxima at 280 nm and 323 nm was 9.2.

Oxygen Uptake Assays - In the presence of biphenyl, O_2-uptake rates were dependent on the concentrations of $BphF_{LB400}$ and $BphG_{B356}$. In the presence of 0.36 μM oxygenase, the initial rate of O_2-uptake was similar at ratios of 3 and 6 BphG per $\alpha_3\beta_3$ hexamer but in the latter case, the background rate of O_2-uptake was considerably higher. With respect to BphF, the initial rate of O_2-uptake was not saturated even at 20 BphF per oxygenase αβ subunit, the highest ratio tested. Significantly, BPDO activities obtained using $BphF_{LB400}$ and histidine-tagged $BphF_{B356}$ were identical within experimental error. To standardize the activity assay, the concentrations of each dioxygenase component were 0.36 μM oxygenase αβ subunit, 2.8 μM $BphF_{LB400}$, and 1.2 μM $BphG_{B356}$ in all subsequent experiments. Under these conditions, the reductase concentration was close to saturating, and the background rate of O_2-uptake was less than 10% of that in the presence of saturating concentrations of biphenyl.

Steady-state kinetic analysis - Under the standard assay conditions, BPDO exhibited Michaelis-Menten kinetics for the dependence of the initial rate of O_2-uptake on the concentration of biphenyl (Fig. 2.2A). The biphenyl concentration could be varied sufficiently within its solubility range to allow reliable estimates of the apparent k_{cat} and

Figure 2.2 The steady-state dihydroxylation of biphenyl by $BPDO_{B356}$. (A) The dependence of the initial velocity of O_2-uptake on biphenyl concentration in air-saturated buffer. The fitted parameters were K_m = 6.2 ± 0.5 μM and V_{max} = 141 ± 3 μM/min. (B) The dependence of the initial velocity of O_2-uptake on O_2 concentration in the presence of a nominal biphenyl concentration of 288 μM. The fitted parameters were K_{mO_2} = 28 ± 2 μM and V_{max} = 227 ± 9 μM/min. All experiments were performed using 50 mM MES, pH 6.0, 25 °C. Solid lines represent fits of the data to the Michaelis-Menten equation obtained using the least squares, dynamic weighting options of LEONORA. The data are from a single representative experiment. Similar results were obtained for several different enzyme preparations (data not shown). The two highest concentrations of biphenyl in **A** are above the published aqueous solubility limit.

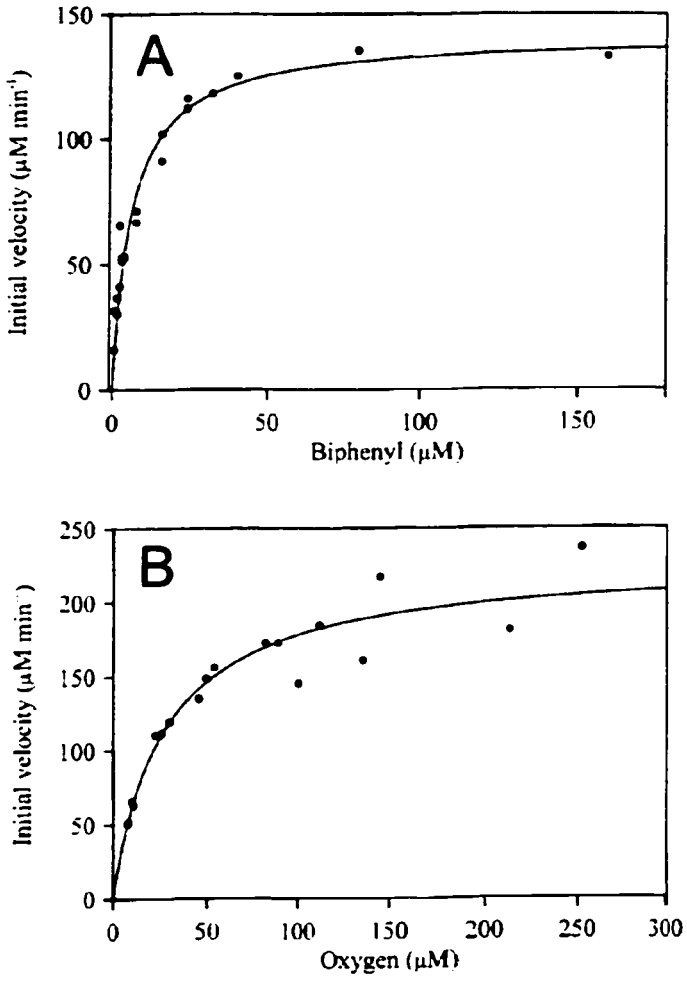
A
Initial velocity (μM min⁻¹)
150
100
50
0
0
50
100
150
Biphenyl (μM)
B
Initial velocity (μM min⁻¹)
250
200
150
100
50
0
0
50
100
150
200
250
300
Oxygen (μM)

K_m (Table 2.2). The initial rates of O_2-uptake by BPDO in the presence of 2,2'- and 3,3'-diClBs, respectively, also fit the Michaelis-Menten equation very well and random trends in the residuals were observed (data not shown). Interestingly, the V_{max} values observed in the presence of these compounds apparently exceeded their respective solubility limits. This is particularly striking for 3,3'-diClB, for which the apparent K_m is approximately twice its solubility limit (Table 2.2). The steady-state parameters of BPDO for 4,4'-diClB could not be estimated due to the extremely limited aqueous solubility of this compound (0.27 μM) and the low initial rates of O_2-uptake. Thus, for this diClB, only the maximum initial rate of O_2-uptake observed is reported in Table 2.2.

BPDO also exhibited Michaelis-Menten behavior for the dependence of the initial rate of O_2-uptake on the concentration of O_2 in the presence of saturating amounts of biphenyl (Fig. 2.2B), as well as 2,2'-diClB and 3,3'-diClB (results not shown). Interestingly, the apparent specificity of BPDO for O_2 in the presence of biphenyl was ten-fold and 50-fold higher than in the presence of 3,3'-diClB and 2,2'-diClB, respectively (Table 2.3). In the presence of 4,4'-diClB, the initial rate of O_2-uptake increased linearly with the concentration of O_2, indicative of a very high K_m.

Rate data with varying concentrations of both biphenyl (5-100 μM) and O_2 (15-250 μM) were obtained in order to elucidate the kinetic mechanism of BPDO. These data were fitted using non-linear regression with robust weighting to either a two substrate sequential or ping-pong Michaelis-Menten mechanism using Grafit 4 (data not shown). Both fits yielded kinetic parameters consistent with those reported above, and with standard errors ranging from 4-15%. Comparison of both fits using the F test yielded a high probability value (0.52), indicating that neither fit was significantly better than the other. Therefore, the kinetic mechanism could not be unambiguously assigned from this data.

Table 2.2

Apparent steady-state kinetic and coupling parameters of BPDO from *C. testosteroni* B-356 for selected biphenyl substrates

Substrate	K_m	k_{cat}	k_{cat}/K_m	*Biphenyl:O_2*	*H_2O_2:O_2*
	μM	s^{-1}	x 10^6 $M^{-1}s^{-1}$		
Biphenyl	6.2 (0.5)	7.3 (0.2)	1.2 (0.1)	0.97 (0.10)	N.D.
2,2'-diClB	2.6 (0.9)	1.2 (0.1)[a]	0.5 (0.4)	0.44 (0.11)	0.7 (0.2)
3,3'-diClB	3.3 (0.5)	4.2 (0.1)[a]	1.3 (0.2)	0.63 (0.13)	0.33 (0.05)
4,4'-diClB	-	1.98 (0.04)[b]	-	0.48 (0.11)	0.4 (0.1)

Experiments were performed using air-saturated 50 mM MES, pH 6.0, 25 ^{0}C. The reported ratios represent mean values obtained from 3-5 determinations. Standard deviations are given in parentheses. Additional experimental details are provided in "Materials and Methods". [a]The values reported for 2,2'- and 3,3'-diClBs were obtained using quantities of these compounds that apparently exceeded their respective aqueous solubility limits. [b]The value reported for 4,4'-diClB was calculated from the maximum initial rate of O_2–uptake.

Table 2.3

The apparent steady-state kinetic utilization of O_2 by BPDO from *C. testosteroni* B-356 in the presence of selected biphenyl substrates

Substrate	K_{mO_2}	k_{cat}	k_{cat}/K_{mO_2}
	μM	s^{-1}	x 10^5 $M^{-1}s^{-1}$
Biphenyl	28 (2)	10.2 (0.4)	3.6 (0.3)
2,2'-diClB	750 (200)	4.6 (0.7)	0.06 (0.02)
3,3'-diClB	190 (30)	7.0 (0.5)	0.40 (0.07)
4,4'-diClB	-[a]	-	-

Experiments were performed in 50 mM MES, pH 6.0, 25 ^{0}C. Additional experimental details are provided in "Materials and Methods". Values in parentheses represent standard deviations of the calculated parameters. [a]In the presence of 4,4'-diClB, the initial rate of O_2-uptake increased linearly with the concentration of O_2.

To determine whether substrate utilization by BPDO is coupled, the stoichiometry of biphenyl substrate and O_2 consumed in the enzyme-catalyzed reaction was investigated. In the presence of a saturating concentration of biphenyl (125 μM), the amount of O_2 consumed corresponded to the amount of biphenyl utilized, within experimental error (Table 2.2). Furthermore, no hydrogen peroxide, a possible uncoupling product, was detected upon the addition of catalase to the O_2 electrode chamber. In contrast, the utilization of diClB and O_2 by BPDO was significantly uncoupled: the amounts of 2,2'-, 3,3'-, and 4,4'-diClB transformed corresponded to approximately 50% of the O_2 consumed. Within experimental error, the balance of consumed O_2 was detected as hydrogen peroxide (Table 2.2).

Crystallization trials - Several experiments in the initial crystallization screens produced brown crystallites. The productive precipitants included PEG4000, PEG8000, ammonium sulfate, and 2-propanol. Variation of the buffer and pH as well as the concentrations of 2-propanol and PEG4000 rapidly yielded crystals suitable for diffraction experiments. Characteristically brown crystals with a rhombic morphology grew in one to two weeks to a typical size of 0.3 mm x 0.1 mm x 0.1 mm.

Diffraction studies - Analysis of diffraction patterns established that the crystals belonged to the space group *R*3 with unit cell parameters for the triply primitive hexagonal setting of $a=b=136.35$ Å and $c=106.07$ Å. Test images collected by the use of a rotating anode source showed diffraction to 2.2 Å resolution and a nominal mosaicity of 0.60°. The complete diffraction pattern was subsequently measured using synchrotron radiation to 1.6 Å resolution with a refined mosaicity of 0.46°. Scaling yielded an overall *R*sym=8.7%; statistics as a function of resolution are presented in Table 2.4. Analysis of the cumulative intensity distribution with the CCP4 program TRUNCATE (38) revealed that the crystal was twinned. Further evaluation of the data by the use of a web-based twinning analysis package (www.doe-mbi.ucla.edu, 38) revealed merohedral twinning

about the hexagonal *a.b* axes and a twinning fraction of 0.34. The data used to prepare Table 2.4 were not corrected for twinning.

Figure 2.3 High resolution diffraction pattern obtained from a single crystal of BPDO oxygenase. The x-ray source was synchrotron radiation as described in "Materials and Methods". The image was recorded for 45 s over an oscillation angle of 1° at a crystal-to-detector distance of 73.8 mm. The edge of the image corresponds to a resolution of 1.75 Å.

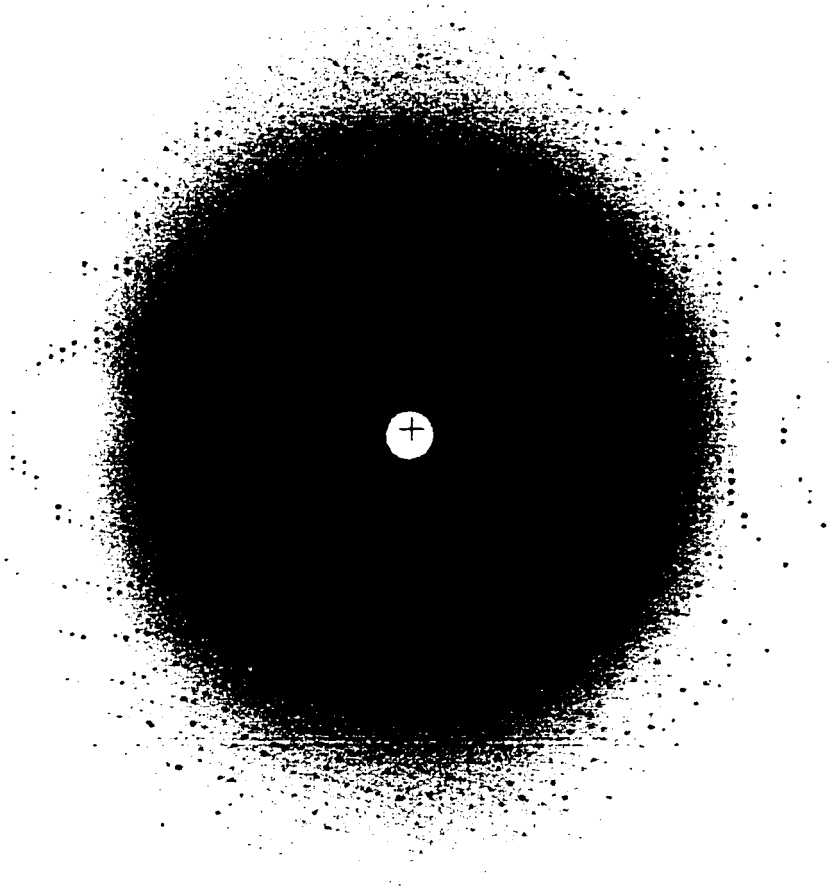

Table 2.4

Statistics[1] pertaining to diffraction data acquired from one crystal of *C. testosteroni* B-356 BPDO

Resolution limits	Fraction measured	Redundancy	I/σ	$R_{sym}(I)$
50.0 – 3.45 Å	.965	4.2	19.5	.075
3.45 - 2.74 Å	.983	4.1	20.1	.076
2.74 - 2.39 Å	.988	4.1	18.8	.083
2.39 - 2.17 Å	.993	4.1	16.4	.094
2.17 - 2.02 Å	.995	4.0	13.2	.107
2.02 - 1.90 Å	.997	3.9	10.3	.134
1.90 - 1.80 Å	.997	3.8	7.8	.164
1.80 - 1.72 Å	.995	3.5	5.4	.213
1.72 - 1.66 Å	.946	2.6	3.6	.250
1.66 - 1.60 Å	.841	2.1	2.6	.284
50.0 - 1.60 Å	.970	3.7	15.6	.087

1. Redundancy reports a lower estimate of the number of observations per unique reflection. $I/\bar{\sigma}$ is the average intensity divided by the average error as defined by the HKL programs. $R_{sym}(I) = \sum_{hkl}\sum_{j}\left|I_{hkl,j} - \bar{I}_{hkl}\right| \Big/ \sum_{hkl}\sum_{j} I_{hkl,j}$, where $\bar{I}_{hkl}$ is the mean intensity of the j observations of a reflection with reduced Miller indices $h.k.l$.

DISCUSSION

The described overexpression and rapid, anaerobic purification of $BPDO_{B356}$ oxygenase reproducibly yielded 55 mg of highly active enzyme from 10 l of cell culture. The specific activity of the preparation was significantly greater than that reported for aerobic preparations of the enzyme (4,40), although direct comparisons are difficult as the activity assay in the current study was optimized. Nevertheless, iron and sulfur analyses are consistent with the presence of a full complement of Rieske-type [2Fe-2S] cluster and mononuclear iron in the purified oxygenase based on theoretical values of 3 Fe and 2 S per α subunit. In contrast, aerobically purified preparations of BPDO oxygenase contained less than a full complement of iron (3, 4). Moreover, stability problems have been noted in a His-tagged form of the oxygenase expressed in *E. coli* (40). The improved overexpression and purification described herein overcome some significant shortcomings of previously reported procedures, facilitating careful biochemical study of the enzyme.

Although BPDO is a major determinant of the aerobic microbial degradation of PCBs, many aspects of its reactivity with different congeners remain unknown. Most studies of the ability of BPDO to transform different PCBs are based on single time point assays and have focussed on the identity of the dioxygenation products (*e.g.*, 41). Many of these were performed using whole cells and/or mixtures of PCB congeners. Activity assays have been limited by the multicomponent nature of BPDO, its O_2-lability, and the limited solubilities of chlorinated biphenyls. The continuous activity assay described herein overcomes many of these limitations, enabling a more thorough characterization of the reactivity of BPDO towards chlorinated biphenyls. Significantly, BPDO activity could not be saturated with the ferredoxin. Similarly, the oxygenase of phthalate dioxygenase, a related two component enzyme, could not be saturated with its reductase

(42). The determined apparent kinetic parameters nevertheless provide valuable insights into the specificity of BPDO.

The steady state kinetic parameters for BPDO indicate that the K_m for biphenyl is well below the solubility limit of this substrate, and that the turnover number is low. The K_{mO_2} of 28 μM indicates that BPDO is close to saturation with O_2 under ambient conditions. In contrast, DHBD, the extradiol dioxygenase of the *bph* pathway, has a K_{mO_2} of 1.3 mM (20 mM HEPPS, 80 mM NaCl, pH 8, 25 °C; 23), although these two dioxygenases presumably function under similar cytoplasmic conditions, including O_2 concentrations. However the k_{cat}/K_{mO_2} of DHBD is an order of magnitude greater than that of BPDO and even in air-saturated buffer, the apparent specificity of DHBD for its aromatic substrate is an order of magnitude greater than that of BPDO. Ongoing studies in our laboratories indicate that these differences can not be attributed to the different experimental conditions. Moreover, the apparent physiological k_{cat}/K_{mO_2} of BPDO is probably even lower as the ratio of BphF to oxygenase is much lower *in vivo* than in the current assay.

The kinetic mechanism of BPDO could not be determined unambiguously from our data, which could be fit equally well with either two substrate sequential or ping-pong mechanisms. Rates at the lowest biphenyl and O_2 concentrations pushed the limits of detection of the oxygen electrode based assay since k_{cat} for BPDO is low. In addition, product inhibition was not available as a kinetic tool, since oxygen consumption was observed in the presence of *cis*-(2*R*,3*S*)-dihydroxy-1-phenylcyclohexa-4,6-diene (data not shown). Nevertheless, it is extremely unlikely that BPDO operates by a ping-pong mechanism, since both atoms of oxygen must be available for insertion into the biphenyl substrate at the active site. Indeed, previous kinetics studies have indicated sequential kinetic mechanisms for other dioxygenases (42a, 42b).

The maximal rates of O_2-utilization by BPDO observed in the presence of different diClBs are consistent with the ability of whole cells of *C. testosteroni* B-356 (8) and purified his-tagged $BPDO_{B356}$ (9) to transform diClBs determined using single time point assays. Accordingly, it was reported that 3,3'-diClB is transformed at rates approximately 5 times faster than either 2,2'- or 4,4'-diClB. In the current study, it was found that the maximal rate of O_2-consumption by BPDO in the presence of 3,3'-diClB was approximately 3.5 times higher than that in the presence of 2,2'-diClB (Table 2.2). Moreover, the consumption of O_2 was 50% better coupled to biphenyl transformation in the presence of 3,3'-diClB than 2,2'-diClB. However, it is not clear why the V_{max} of BPDO in the presence of diClBs was attained at levels of these compounds that exceed their solubility limits or whether the enzyme is saturated with these compounds at the observed V_{max}'s. The attainment of V_{max} at such high levels of diClBs could be due to partitioning of the substrate to the active site of the enzyme from the solid phase. Regardless of these considerations, it is interesting to note that while 2,2'-diClB is more soluble than 3,3'-diClB, it is transformed much less efficiently, suggesting that 3,3'-diClB is a better substrate for BPDO.

The current data demonstrate that chloro substituents not only influence the specificity of BPDO, but also dramatically affect its ability to utilize O_2. The ability of BPDO to utilize O_2 is reflected in two parameters: the k_{cat}/K_mO_2 and the coupling of biphenyl transformation to O_2 consumption. While many details of the catalytic mechanism of ring-hydroxylating dioxygenases have yet to be established, most studies are consistent with a mechanism that follows the cytochrome P450 paradigm (6,43), at least in the early stages. Accordingly, the resting state oxygenase first binds the aromatic substrate, converting the high spin hexacoordinate active site Fe(II) to a pentacoordinate state (44-46). The pentacoordinate Fe(II) then binds O_2 and the catalytic center is reduced to yield an activated oxygen species that, in the case of BPDO, dioxygenates the

aromatic substrate. Chlorinated biphenyls that do not occupy the active site of BPDO in the same manner as biphenyl may not efficiently convert the hexacoordinate center to a pentacoordinate state (this question is addressed further in Chapter 3). This is analogous to the failure of some substrates to convert low spin Fe(III) to high spin Fe(III) in cytochrome P450 (*e.g.*, 47). Alternatively, chloro substituents might occlude the O_2-binding site. Either effect would decrease the $k_{cat}/K_{m}O_2$, as observed. Moreover, if the biphenyl is not positioned to react with the putative activated oxygen species, then the latter can decay to various reduced species, resulting in uncoupling. Although uncoupling in ring-hydroxylating dioxygenases has not been well studied, this is again analogous to the cytochrome P450 paradigm (*e.g.*, 48). The major product of diClB-induced uncoupling in BPDO was H_2O_2, consistent with what has been reported for the benzene-induced uncoupling of naphthalene dioxygenase (49). Further study of uncoupling in BPDO is warranted in light of its ramifications for PCB degradation.

The transformation products of diClBs obtained using $BPDO_{B356}$ were not examined in this study. However, products of diClBs generated using a his-tagged preparation of $BPDO_{B356}$ have been partially characterized by GC-MS (9). In several cases, the low yields of transformation products precluded their unambiguous identification and the determination of their relative amounts. The transformation of 2,2'-diClB yielded two products: a monochlorinated dihydroxybiphenyl and a dichlorinated dihydrodiol (M. Sylvestre, personal communication). The monochlorinated dihydroxybiphenyl had GC-MS spectra that were similar to those of 2,3-dihydroxy-2'-ClB, formed by $BPDO_{LB400}$ (10). The dichlorinated dihydrodiol differed from that formed by $BPDO_{LB400}$, which was also not unambiguously identified (10). The transformation of 3,3'-diClB yielded a single dichlorinated dihydrodiol which can be transformed by the following two enzymes of the biphenyl degradation pathway. This compound was thus identified as 2,3-dihydro-2,3-dihydroxy-3',5-diClB (9). Finally,

$BPDO_{B356}$ transformed 4,4'-diClB to two products, one of which was tentatively identified as 2,3-dihydro-2,3-dihydroxy-4,4'-diClB (M. Sylvestre, personal communication). The more active preparation of BPDO reported herein should facilitate more comprehensive characterization of these transformation products in the future.

The reactivity of BPDO with diClBs has several important implications for the microbial degradation of PCBs, which are generally present in the environment as complex mixtures of congeners. First, congeners such as 2,2'-diClB that bind to the active site of BPDO oxygenase but that are poorly transformed, should competitively inhibit the transformation of other congeners. Second, the uncoupling observed in the presence of diClBs demonstrates that the degradation of some congeners exacts a high energetic cost from the cell. Moreover, reactive oxygen species that result from this uncoupling may be deleterious to the cell. Such uncoupling may explain in part why natural isolates are unable to utilize biphenyls that are chlorinated on both phenyl rings as growth substrates. Further study of the kinetics of PCB transformation combined with the emerging structural data of BPDO oxygenase and mutagenesis studies should provide critical insight into the molecular basis of substrate specificity and substrate coupling in this enzyme.

ACKNOWLEDGMENTS

Nathalie M. Drouin is thanked for skilled technical assistance. Manon M.J. Couture (Biochemistry Department, Université Laval) and Roch Aumont (Chemistry and Biochemistry Department, Concordia University) generously provided purified $BphF_{LB400}$ and $BphG_{B356}$, respectively. Professor Michel Sylvestre (INRS-Sante, Université du Québec) generously provided pUCBPHA-C and his-tagged $BphF_{B-356}$. Frederic H. Vaillancourt and Dr. Stephen Y.K. Seah (Biochemistry Department, Université Laval) generously provided DHBD and catechol 2,3-dioxygenase, respectively. Mathew N. Chakko (Purdue University) is thanked for his assistance in the crystallization experiments. Use of the Advanced Photon Source was supported by the U.S. Department of Energy, Basic Energy Sciences, Office of Energy Research, under Contract W-31-109-Eng-38. BioCARS Sector 14 was supported by the National Institutes of Health, National Center for Research Resources, through grant RR-07707. This work was supported by Natural Sciences and Engineering Research Council of Canada Strategic Grant STP0193182 to LE and JP and by National Institutes of Health Grant GM-52381 to JTB. NI is the recipient of a Natural Sciences and Engineering Research Council of Canada postgraduate scholarship.

REFERENCES

1. Timmis K.N., Steffan R.J., and Unterman R. (1994) *Annu. Rev. Microbiol.*, **48**, 525-557

2. Focht, D.D. (1995) *Curr. Opin. Biotech.*, **6**, 341-346

3. Hurtubise, Y., Barriault, D., Powlowski, J., and Sylvestre, M. (1995) *J. Bacteriol.* **177**, 6610-6618

4. Haddock, J.D., and Gibson, D.T. (1995) *J. Bacteriol.* **177**, 5834-5839

5. Butler, C.S., and Mason, J.R. (1997) *Adv. Microbiol. Physiol.* **38**, 47-84

6. Que Jr., L. and Ho, R.Y.N (1996) *Chem. Rev.* **96**, 2607-2624

7. Gibson, D.T., Cruden, D.L., Haddock, J., Zylstra, G.J., and Brand, J.M. (1993) *J. Bacteriol.* **175**, 4561-4564

8. Barriault, D., Pelletier, C., Hurtubise, Y., and Sylvestre, M. (1997) *Int. Biodeterior. Biodegrad.* **39**, 311-316

9. Hurtubise, Y., Barriault, D., and Sylvestre, M. (1998) *J. Bacteriol.* **180**, 5828-5835

10. Haddock, J., Horton, J.R., and Gibson, D.T. (1995) *J. Bacteriol.* **177**, 20-26

11. Mondello, F.J., Turcich, M.P., Lobos, J.H., and Erickson, B.D. (1997) *Appl. Env. Microbiol.* **63**, 3096-3103

12. Kimura, N., Nishi, A., Goto, M., and Furukawa, K. (1997) *J. Bacteriol.* **179**, 3936-3943

13. Kumamaru, T., Suenaga, H., Mitsuoka, M., Watanabe, T., and Furukawa, K. (1998) *Nature Biotechnology* **16**, 663-666

14. Brühlmann, F., and Chen, W. (1999) *Biotech. Bioengineer.* **63**, 544-551

15. Parales, R.E., Emig, M.D., Lynch, N.A., and Gibson, D.T. (1998) *J. Bacteriol.* **180**, 2337-2344

16. Chebrou, H., Hurtubise, Y., Barriault, D., and Sylvestre, M., (1999) *J. Bacteriol.* **181**, 4805-4811

17. Hanahan, D. (1983) *J. Mol. Biol.* **166**, 557-580

18. Yanisch-Perron, C., Vieira, J., and Messing, J. (1985) *Gene* **33**, 103-119

19. Herrero, M., de Lorenzo, V., and Timmis, K.N. (1990) *J. Bacteriol.* **172**, 6557-6567

20. Lorenzo, V.D., Eltis, L., Kessler, B., and Timmis, K.N. (1993) *Gene*, **123**, 17-24

21. Bergeron, J., Ahmad, D., Barriault, D., Larose, A., and Sylvestre, M. (1994) *Can. J. Microbiol.* **40**, 743-753

22. Ausubel, F.M., Brent, R., Kingston, R.E., Moore, D.D., Seidman, J.G., Smith, J.A., and Struhl, K. (1997) *Current Protocols in MolecularBiology*. J. Wiley & Sons Inc., New York

23. Vaillancourt, F.H., Han, S., Fortin, P.D., Bolin, J.T., and Eltis, L.D. (1998) *J. Biol. Chem.* **273**, 34887-34895

24. Sambrook, J., Fritsch, E.F., and Maniatis, T. (1989) *Molecular Cloning: A Laboratory Manual*, Cold Spring Harbour Laboratory Press, Cold Spring Harbour, New York

25. Cho, J.H., Kim, E.K., and So, J.S. (1995) *Biotechnology Techniques.* **9**, 41-44

26. Laemmli, U.K. (1970) *Nature* **227**, 680-685

27. Brown, R.E., Jarvis, K.L., and Hyland, K.J. (1989) *Anal. Biochem.* **180**, 136-139

28. Haigler, B.E., and Gibson, D.T. (1990) *J. Bacteriol.* **172**, 457-464

29. Chen, J.S., and Mortenson, L.E. (1976) *Anal. Biochem.* **79**, 157-165

30. Couture, M.M.J., Babini, E., Colbert, C.L., Bolin, J.T., and Eltis, L.D. (1999) In preparation.

31. Seah, S.Y.K., Terracina, G., Bolin, J.T., Riebel, P., Snieckus, V., and Eltis, L.D. (1998) *J. Biol. Chem.* **273**, 22943-22949

32. Mackay, D., Shiu, W.Y. and Ma, K.C. (1992) *Illustrated Handbook of Physical-Chemical Properties and Environmental Fate for Organic Chemicals.* Lewis Publishers, Inc., Michigan.

33. Cornish-Bowden, A. (1995) *Analysis of Enzyme Kinetic Data.* Oxford University Press, N.Y.

34. Jancarik, J. and Kim, S.H. (1991) *J. Appl. Crystallogr.* **24**, 409-411

35. Otwinowski, Z. and Minor, W. (1997) *Meth. Enzymol.* **276**, 307-326

36. CCP4 (1994) *Acta. Crystallogr. Sect. D* **50**, 760-763.

37. Sylvestre, M., Sirois, M., Hurtubise, Y., Bergeron, J., Ahmad, D., Shareck, F., Barriault, D., Guillemette, I., and Juteau, J.M. (1996) *Gene* **174**, 195-202

38. French, G.S. and Wilson, K.S. (1978) *Acta Crystallogr.* **A34**, 517-525

39. Yeates, T.O. (1997) *Meth. Enzymol.* **276,** 344-358

40. Hurtubise, Y., Barriault, D., and Sylvestre, M. (1996) *J. Biol. Chem.* **271**, 8152-8156.

41. Seeger, M., Zielinski, M., Timmis, K.N., and Hofer, B. (1999) *Appl. Environ. Microbiol.* **65**, 3614-3621

42. Batie, C.J., LaHaie, E., and Ballou, D.P. (1987) *J. Biol. Chem.* **262**, 1510-1518

42a. Hori, K., Hashimoto, T., and Nozaki, M. (1973) *J. Biochem. (Tokyo)* **74**, 375-384

42b. Wolgel, S. A., Dege, J. E., Perkins-Olson, P. E., Juarez-Garcia, C. H., Crawford, R. L., Münck, E., and Lipscomb, J. D. (1993) *J. Bacteriol.* **175**, 4414-4426

43. Ortiz de Montellano, P.R. (1986) in *Cytochrome P450: Structure, Mechanism and Biochemistry* (Ortiz de Montellano, P.R., ed) Plenum Press, N.Y.

44. Gassner, G.T., Ballou, D.P., Landrum, G.A., and Whittaker, J.W. (1993) *Biochemistry* **32**, 4820-482

45. Pavel, E.G., Martins, L.J., Ellis, W.R.Jr., and Solomon, E.I. (1994) *Chem. Biol.* **1**, 173-183

46. Tsang, H.-T., Batie, C.J., Ballou, D.P., and Penner-Hahn, J.E. (1996) *J. Biol. Inorg. Chem.* **1**, 24-33

47. Fisher, M.T., and Sligar, S.G. (1985) *J. Am. Chem. Soc.* **107**, 5018-5019

48. Loida, P.J., Sligar, S.G., Paulsen, M.D., Arnold, G.E., and Ornstein, R.L. (1995) *J. Biol. Chem.* **270**, 5326-5330

49. Lee, K. (1999) *J. Bacteriol.* **181**, 2719-2725

Chapter 3

Crystal Structure of BPDO and its Substrate-Bound and Product-Bound Complexes

ABSTRACT

The study of the structure-function relationships of biphenyl dioxygenase to identify some of the molecular determinants of enzyme activity requires the availability of a high-resolution crystal structure of its oxygenase component, BPDO. The crystal structures of BPDO, and its substrate-bound and product-bound complexes, were solved in collaboration with Drs. Colbert and Bolin from Purdue University (IN, USA), and Dr. Eltis from University of British Columbia (BC, Canada). The present chapter consists of a brief summary of these results, and a discussion relating structural information to the kinetic characterization presented in Chapters 2 and 4. Taken together, the crystal structure, mutagenesis, and kinetic data provide mechanistic insights on biphenyl dioxygenase activity. A more detailed report of this work is found in Dr. Christopher L. Colbert's Ph.D. thesis (2001, Purdue University, IN, USA), and is part of a manuscript in preparation (Colbert *et al.* in prep.).

INTRODUCTION

Biphenyl dioxygenase catalyses the initial step in the biodegradation of PCBs, and is composed of three components: a reductase, a ferredoxin, and the oxygenase itself (BPDO) (1:2). The enzymatic dihydroxylation of biphenyls involves two-electron uptake from NADH by the reductase component, followed by sequential electron transfers to the ferredoxin, and then to the [2Fe-2S] cluster and mononuclear iron catalytic center of BPDO (Chap. 1).

There is presently no reported crystal structure of any BPDO. The preliminary crystallographic work on the *C. testosteroni* enzyme presented in Chapter 2, and published in 2000 (3), has been extended in collaboration with Professor Lindsay D. Eltis from University of British Columbia (BC, Canada), and Dr. Christopher L. Colbert and Professor Jeffrey T. Bolin from Purdue University (IN, USA). The crystallographic studies provide insights into the mechanism of BPDO, and complement the kinetic characterization of the reactions with different chlorinated biphenyls (Chapter 2). Dr. Christopher L. Colbert was responsible for crystallization of BPDO, data collection, analysis, and model refinement (Ph.D. Thesis, Purdue University, 2001). The author of the present thesis supplied highly active and homogeneous BPDO samples for crystallization.

EXPERIMENTAL PROCEDURES

Purification and Crystallization of BPDO- Overexpression, anaerobic purification, and crystallization details are described in Chapters 2 and 6 of this thesis, and, with the exception of protein crystallization, were performed by Nathalie Agar. Crystallization experiments were all done at Purdue University by Dr. Christopher L. Colbert in the laboratory of Professor Jeffrey T. Bolin.

X-Ray Data Collection and Analysis- The initial data collection and analysis are reported in Chapter 2, and were performed by Dr. Christopher Colbert. The extensive data collection and analysis required to solve the crystal structure of BPDO and its complexes were also carried out by Dr. Christopher L. Colbert (Ph. D. Thesis, Purdue University, 2001). Diffraction data of resting BPDO were obtained to 1.5 Å resolution, while for the substrate and product complexes the resolution was respectively 2.0 Å and 1.8 Å. The statistics for the final refinement of the three BPDO models are presented elsewhere (C. Colbert, Ph.D. Thesis, 2001).

Substrate and Product Bound Complexes Formation- Preparation of substrate- and product-bound complexes is described elsewhere (C. Colbert, Ph.D. Thesis, 2001). Briefly, BPDO was complexed with its substrate, biphenyl, and product, *cis*-(2R,3S)-dihydroxy-1-phenylcyclohexa-4,6-diene, under anaerobic conditions (< 2 ppm O_2). Since the two compounds were poorly soluble in the aqueous crystallization solution, they were added directly to the crystallization drop in solid form. For each complex, a protein crystal was equilibrated with either biphenyl or *cis*-(2R,3S)-dihydroxy-1-

phenylcyclohexa-4,6-diene crystals for 48 hours under anaerobic conditions, and then flash frozen by immersion into liquid N_2.

RESULTS AND DISCUSSION

What follows is a description of the general structural features of the enzyme, and specific details about the active site.

Quaternary Structure of BPDO- BPDO purifies as an $\alpha_3\beta_3$ hexamer (2). Accordingly, the crystal structure of BPDO reveals a quaternary structure of $\alpha_3\beta_3$ hexamer that resembles a mushroom, and is very similar to the previously-reported crystal structure of NDO (4). The BPDO hexamer is illustrated parallel and perpendicular to a three-fold axis in Fig. 3.1. The cap of the mushroom is composed of the three α-subunits, and the stalk of the three β-subunits: the three αβ dimers are related about the three-fold axis, with approximate dimensions of 100 Å x 100 Å x 75 Å. The central cavity formed by the union of the three αβ dimers is 15 Å in diameter and 35 Å in depth, and extends from the α-subunits along the three-fold axis into the β-subunit interface, and is filled with water (Fig. 3.1 B.). The bottom of the cavity is formed by the β-subunit interface, but the base of the β-subunits is open 15 Å along the three-fold axis, allowing solvent to penetrate. The α-subunit consists of a smaller Rieske ferredoxin domain comprising the [2Fe-2S] cluster and a larger mononuclear iron catalytic domain. The interaction between adjacent α-subunits involves an extension of the Rieske domain to clasp the neighboring α-subunit (Fig. 3.1 A). The interface between α- and β-subunits involves a mixture of hydrophobic packing and hydrogen bonds (Fig. 3.2). One of the primary regions of interactions is formed by a web of hydrogen bonds detected between a loop extending from the β-subunit and a disrupted α-helix from the α-subunit in proximity to the mononuclear iron site. The building block of the hexamer appears to be the αβ dimer.

Figure 3.1 Two orthogonal views of the BPDO $\alpha_3\beta_3$ hexamer. On the left, the Rieske domain (green ribbons) from the gold α-subunit interacting with the catalytic Fe(II) of the purple α-subunit. On the right, a rotation of 90° about the *X*-axis gives the view along the three-fold crystallographic axis, shown on the right (C. Colbert, Ph.D. Thesis, 2001).

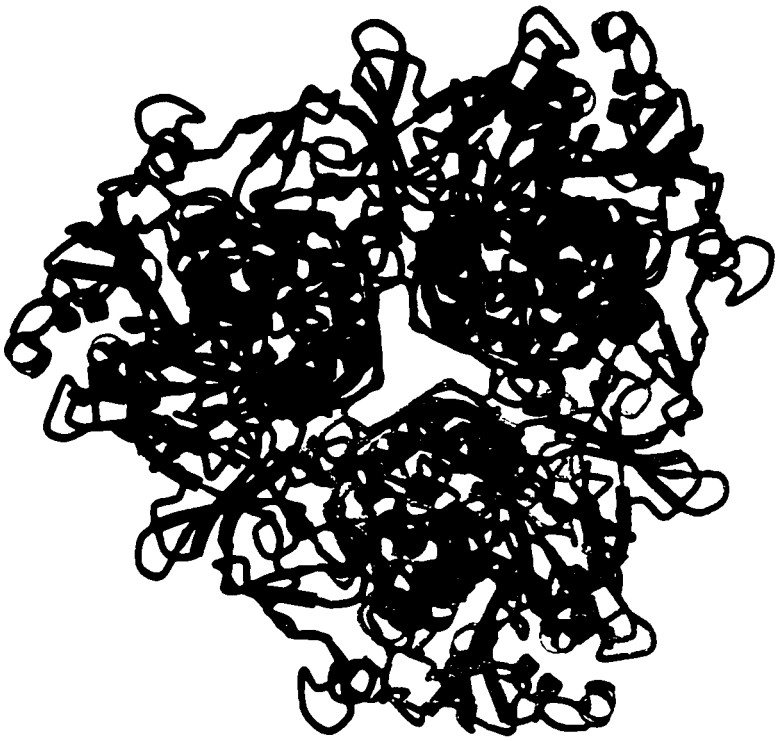

Figure 3.2 The αβ dimer of BPDO. The ribbon diagram above shows the Cα trace of the α (left) and β (right) subunits rendered in rainbow colors from N-terminus (blue) to C-terminus (red). The α-subunit contains an [2Fe-2S] cluster and a mononuclear Fe(II) center separated by 47Å (C. Colbert. Ph.D. Thesis. 2001).

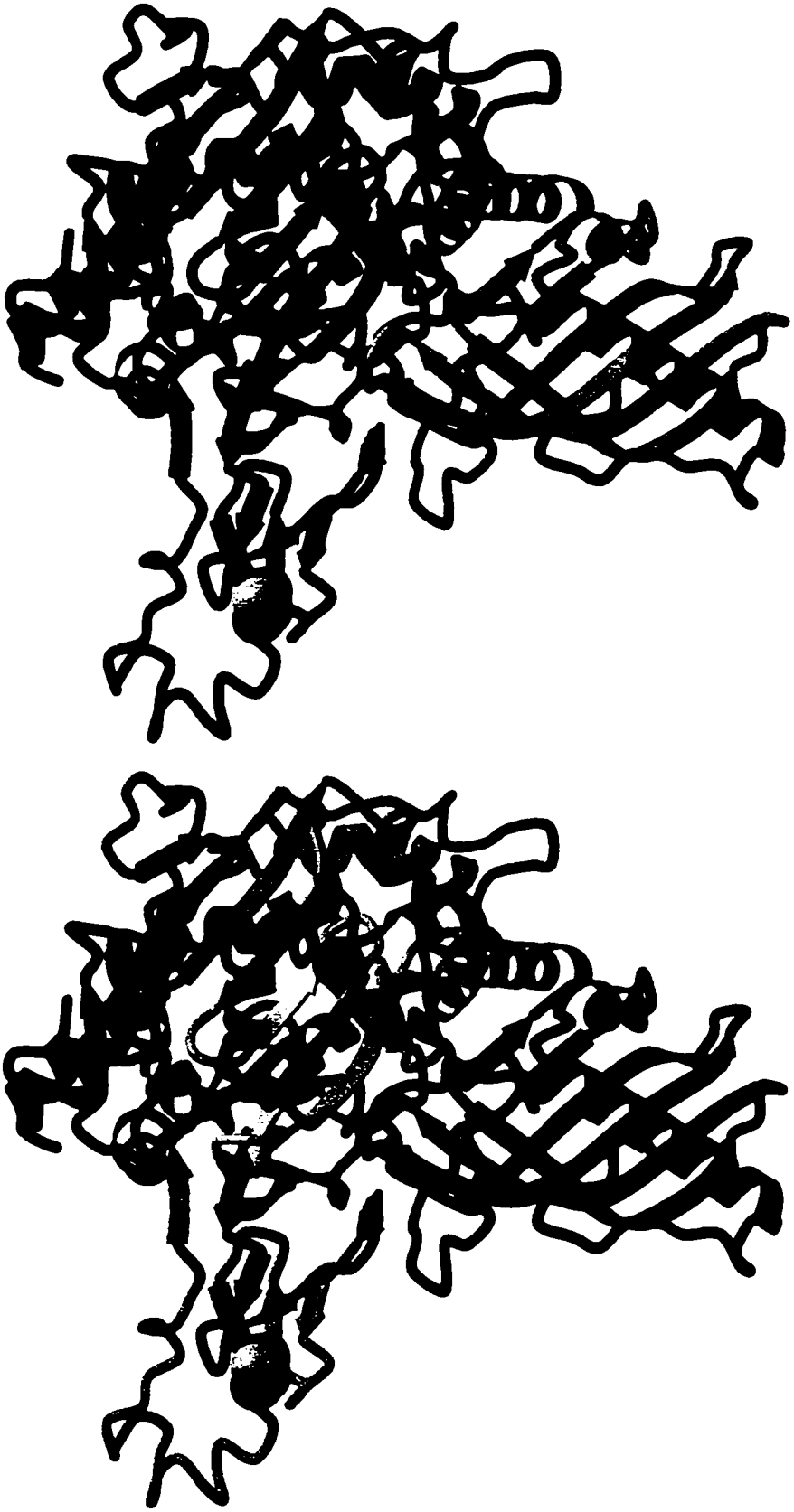

Coordination of the Mononuclear Iron- The substrate binding pocket of BPDO is occupied by a mononuclear Fe(II). Previous studies of the coordination number in free NDO and PDO, and their substrate-bound forms, have revealed discrepancies in the mononuclear iron geometry. The Fe coordination geometry in PDO indicated by magnetic circular dichroism (MCD) studies (5;6) differs from the geometry revealed in the crystal structure of NDO (4). In PDO, the Fe(II) appeared to be hexacoordinate in the absence of substrate, and was transformed into a pentacoordinate form upon substrate binding. This rearrangement would liberate a coordination position for the O_2 molecule required for the dihydroxylation of the organic substrate. The crystal structure of NDO in the absence of substrate, however, revealed a pentacoordinate iron. It is not clear whether the discrepancy results from the two different investigation methods, or whether it reflects an inherent difference in the reactions catalyzed by the two enzymes. In any case, the information provided by the BPDO crystal structure contributes to this debate.

Despite the differences in coordination numbers, experimental evidence for PDO and NDO agrees that the three ligands to the mononuclear Fe contributed by the protein are two histidines and a single aspartate residue (4;7;8). From the crystal structure of BPDO, the equivalent ligands are H233, H239, and D386. In agreement with the NDO structure, in BPDO the histidines are coordinated through their Nε2 atoms, and the aspartate is coordinated in a bidentate manner. The bond distances to the Fe in BPDO are 2.19 Å for the Nε2 histidines, 2.16 Å for the Oδ1 D386, and 2.41 Å for the Oδ2 D386 (Fig. 3.3).

The disagreement between the coordination numbers for NDO and PDO, referred to above, might arise from a differing number of water ligands or ligation by an

Figure 3.3 Electron density showing the coordination geometry of the mononuclear Fe(II). The Fe atom is coordinated by two histidines, one bidentate aspartate, and one water molecule (C. Colbert, Ph.D. Thesis, 2001).

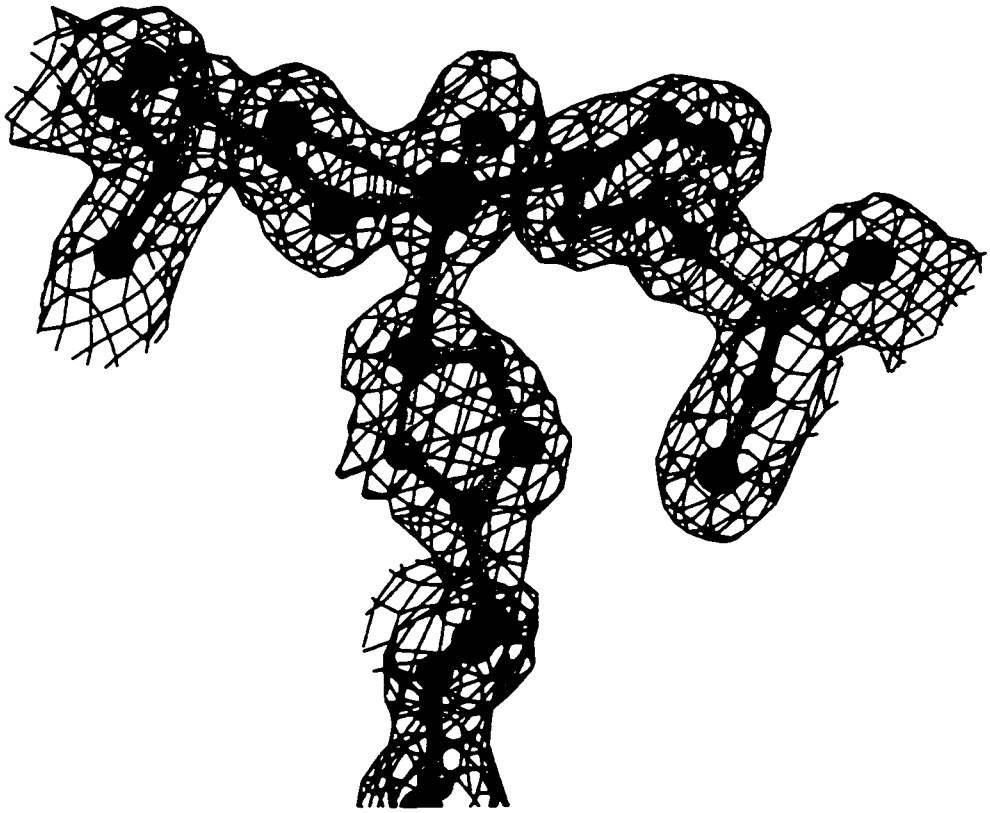

additional amino acid residue. NMR studies of PDO suggested the presence of two labile water ligands (9), whereas the NDO crystal structure revealed a single water ligand (4:10). The structure of BPDO supports the NDO model (Fig. 3.3) since only a single water molecule (S1) was detected in the electron density maps at 1.61 Å from Fe(II). This anomalously short distance reflects the low occupancy of the iron position (0.4), and represents an average for the position of the water ligand in the presence and absence of the iron. To improve the occupancy of the iron site, further crystallization experiments are being done using buffers other than citrate. The sixth ligand to the Fe of NDO has been suggested to be N201, located 3.7 Å above the mononuclear Fe (4:10). The corresponding residue in BPDO is Q226, with its Nε2 located at 3.4 Å from the Fe. It is important to note that the distances of both N201 and Q226 to the respective mononuclear Fe centers are actually too long for a bonding interaction, which is expected to be at a distance of 2.1 ± 0.2 Å.

Biphenyl Complex with BPDO- The protein backbone structure in the BPDO-biphenyl binary complex is very similar to that of native BPDO, although significant changes do occur around the active site (Fig. 3.4). Biphenyl is located near the mononuclear Fe at the active site, but it is at a non-bonding distance. Although the weakly-detected electron density of biphenyl revealed an occupancy of 0.5, it is still probably sufficiently indicative of the fully occupied structure to serve as a reasonable model for substrate binding. The C2 atom of biphenyl is at the closest approach to the Fe, at 4.08 Å, with water S1 nearly directly lined up between the Fe and C2 atom. Local changes in the Fe ligands induced upon substrate binding at the active site of BPDO include a 0.5 Å shift of

Figure 3.4 Electron density map revealing the location of the biphenyl molecule within the active site. The weak density on the proximal ring of biphenyl is indicative of partial occupancy (C. Colbert, Ph.D. Thesis, 2001).

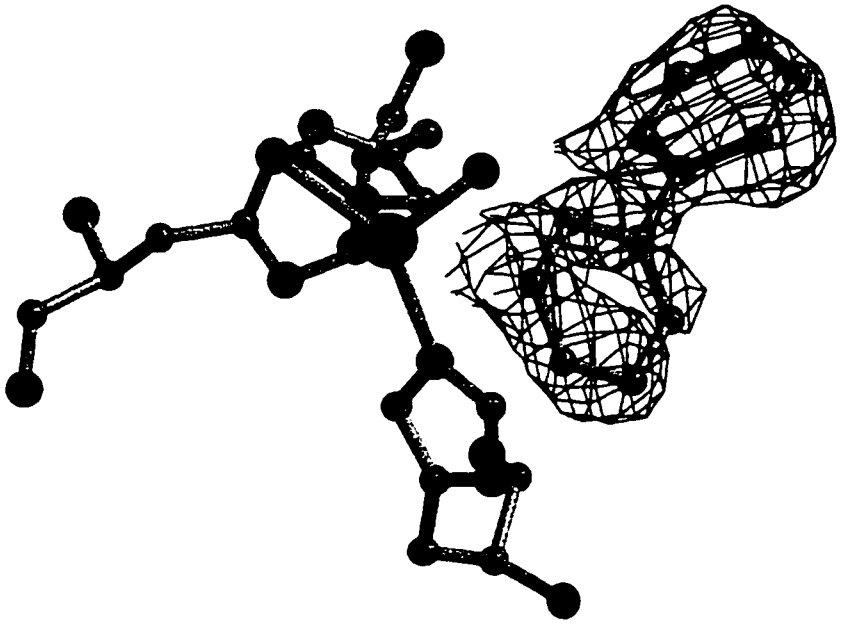

the H239 Cα accompanied by a 135^0 twist of the imidazole ring. Meanwhile, D386 rotates 30^0 to compensate for the proximity of H239 (Fig. 3.5). Despite movements of the Fe ligands induced by biphenyl binding, the Fe geometry remains pentacoordinate. Together with previous studies on PDO and NDO, these results suggest that the resting states of BPDO, NDO, and PDO differ, even though they might still use similar mechanisms for hydroxylation of an aromatic ring.

Product Complex- The crystal structure of BPDO incubated with the product, *cis*-(2R,3S)-dihydroxy-1-phenylcyclohexa-4,6-diene, clearly reveals that it is bound at the active site, and also at a second weak-binding site near the active site entrance (Fig. 3.6). Since the product adopts three alternate orientations at the active site, the reported distances may reflect an ensemble of subtly different structures. Two adopted orientations of the product place the cyclohexadiene ring within the distal pocket while a third orientation places it within the proximal pocket. With the cyclohexadiene ring bound distally, one orientation positions a hydroxyl group of the product within hydrogen bonding distance of M231:Sδ and of the carbonyl of G319, while the other orientation allows hydrogen bonding between the product 2'OH and M231:Sδ, with the product 3'OH in close proximity to F376 and F382 (~3 Å).

As with the BPDO-substrate complex, the BPDO-product complex structure reveals some rearrangements of the Fe ligands. Both H233 and H239 reposition by slight movement and rotation, as represented in Figure 3.7. The most important changes involve a 1.4 Å shift of D386 and the mononuclear Fe, and the Fe geometry changes from pentacoordinate to hexacoordinate with an increase and a decrease, respectively, in

Figure 3.5 Comparison of the substrate-free (light gray bonds) and the BPDO-biphenyl complex (dark gray bonds) showing the conformational changes occurring within the active site upon substrate binding. H239 rotates to avoid a close contact with the substrate resulting in an adjustment of D386. The Fe(II) remains pentacoordinate upon biphenyl binding (C. Colbert, Ph.D. Thesis, 2001).

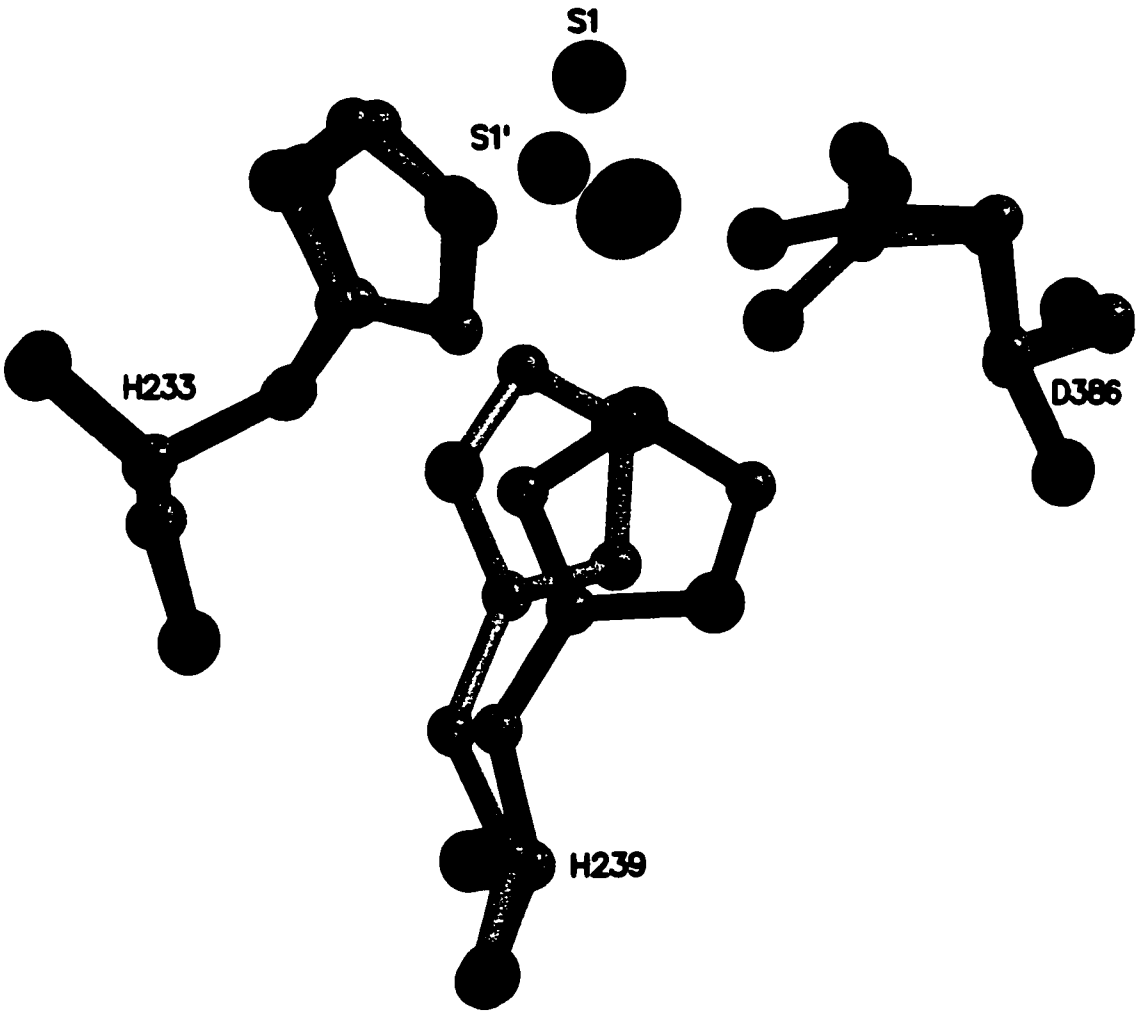
S1
S1'
H233
D386
H239

Figure 3.6 Electron density map showing the change in coordination geometry from pentacoordinate to hexacoordinate of the Fe(II) atom. The additional ligand is a water molecule (C. Colbert, Ph.D. Thesis, 2001).

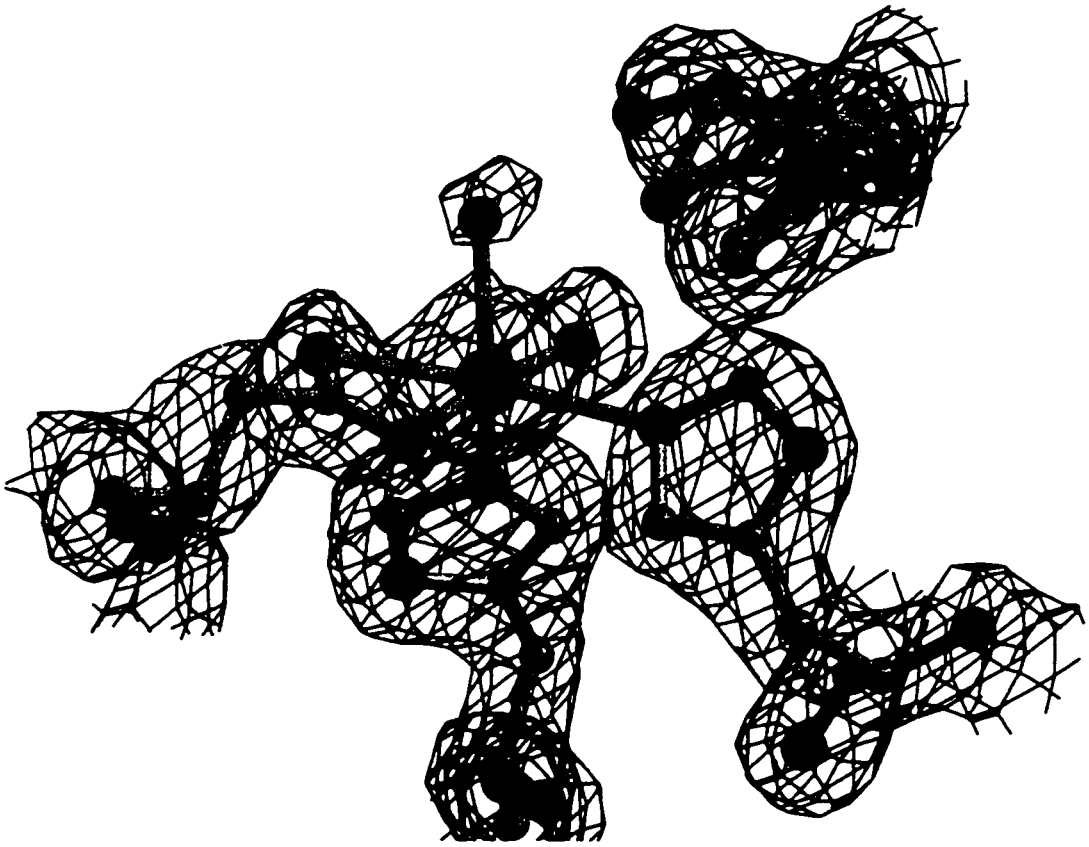

Figure 3.7 Comparison of the Fe(II) ligands in the substrate-free enzyme (light gray bonds) and the BPDO-product complex (dark gray bonds). Similar to the substrate complex, H239 rotates to avoid a close contact with the product, but the major changes are a 1.4 Å shift in the Fe and D386 positions and the addition of the sixth ligand S2 (C. Colbert, Ph.D. Thesis, 2001).

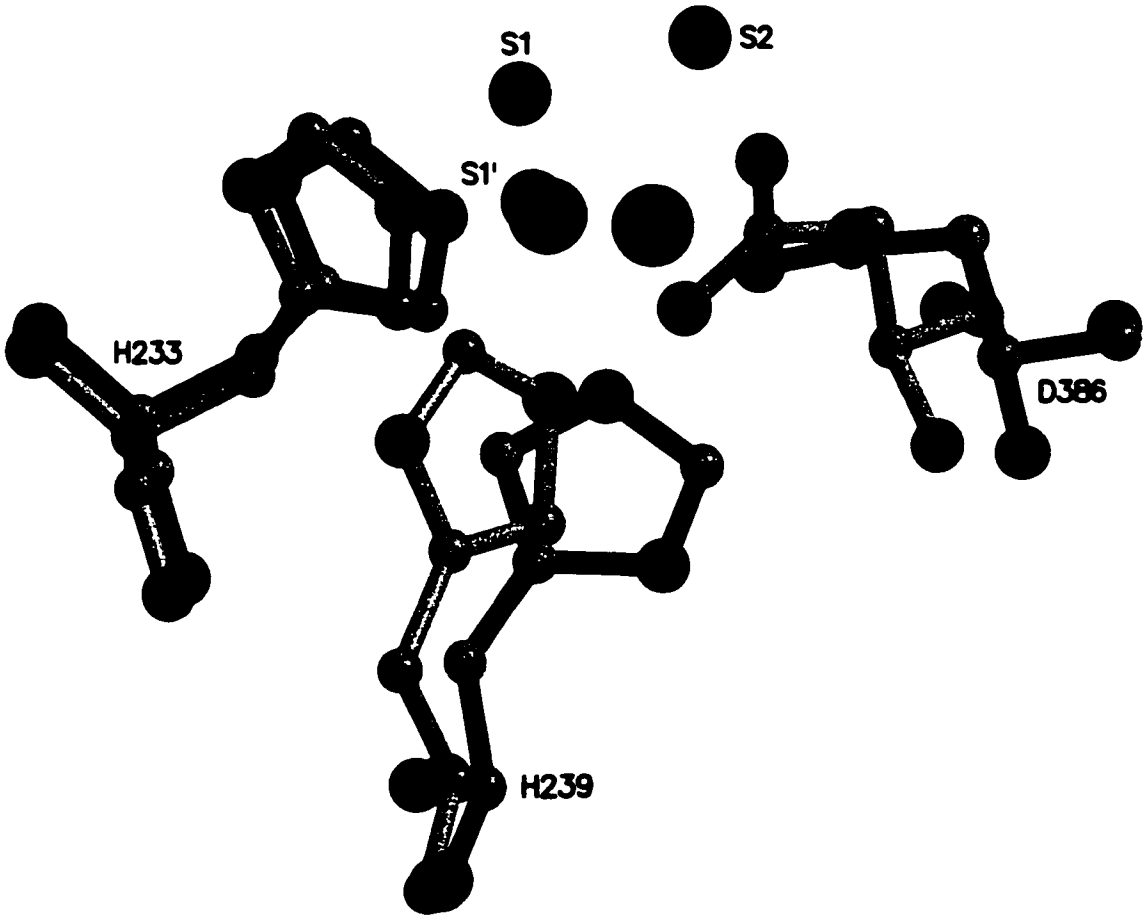
S1
S2
S1'
H233
D386
H239

histidine and aspartate ligand bond distances. The sixth ligand to the Fe is a second water molecule (S2) at 2.3 Å. The Fe bond distances for H233 and H239 increase to 2.46 Å (Δ=0.27 Å) and 2.29 Å (Δ=0.10 Å), respectively, whereas the distances to the bidentate D386 decrease to 2.09 Å (Δ=0.05 Å) and 2.31 Å (Δ=0.10 Å) (Fig. 3.7). The observed shift in the Fe position reduces the distance to Q226 from 3.4 Å to 3.1 Å, with the Nε2 oriented towards the Fe, and Q226 providing a hydrogen bond to the 3-OH group on the product molecule.

The rearrangements of the mononuclear Fe ligands observed in the binary BPDO-product complex suggest that a hexacoordinate Fe may be involved in the catalytic cycle, shedding some light on the discrepancies observed between PDO and NDO. It would appear that the three aromatic ring-hydroxylating dioxygenases, PDO, NDO, and BPDO, undergo a pentacoordinate/hexacoordinate transformation, but with variability in their resting enzyme Fe coordination geometries. The structural changes observed upon product binding to BPDO also may be relevant to the control of internal electron transfer, which will be addressed in Chapter 4. Moreover, the multiple orientations of the product adopted in the binding pocket suggest influential roles for certain residues in the reactivity of BPDO with various chlorinated compounds.

The presence of a sixth ligand in the presence of product may prevent dihydroxylation of the phenyl ring of the product. The mechanism of protection from activating molecular oxygen in the absence of organic substrate appears to differ from the hexacoordinate/pentacoordinate geometry gating found in PDO. In light of BPDO's crystal structure, it is more likely that specific conformational changes at the

mononuclear iron site upon substrate binding may allow subsequent oxygen binding and activation.

Impact of Structural Information on This Thesis- The information provided by these crystal structures allowed the design of experiments to address the roles of specific residues into the reaction cycle of BPDO with biphenyl and chlorinated biphenyls, and in internal electron transfer (Chapter 4).

REFERENCES

1. Hurtubise, Y., Barriault, D., Powlowski, J., and Sylvestre, M. (1995) *J.Bacteriol.* **177,** 6610-6618

2. Haddock, J. D. and Gibson, D. T. (1995) *J.Bacteriol.* **177,** 5834-5839

3. Imbeault, N. Y., Powlowski, J. B., Colbert, C. L., Bolin, J. T., and Eltis, L. D. (2000) *J.Biol.Chem.* **275,** 12430-12437

4. Kauppi, B., Lee, K., Carredano, E., Parales, R. E., Gibson, D. T., Eklund, H., and Ramaswamy, S. (1998) *Structure.* **6,** 571-586

5. Pavel, E. G., Martins, L. J., Ellis, W. R., Jr., and Solomon, E. I. (1994) *Chem.Biol.* **1,** 173-183

6. Gassner, G. T., Ballou, D. P., Landrum, G. A., and Whittaker, J. W. (1993) *Biochemistry* **32,** 4820-4825

7. Coulter, E. D., Moon, N., Batie, C. J., Dunham, W. R., and Ballou, D. P. (1999) *Biochemistry* **38,** 11062-11072

8. Tsang, H. T., Batie, C. J., Ballou, D. P., and Penner-Hahn, J. E. (1996) *Journal of Biological Inorganic Chemistry* **1,** 24-33

9. Bertini, I., Luchinat, C., Mincione, G., Parigi, G., Gassner, G. T., and Ballou, D. T. (1996) *Journal of Biological Inorganic Chemistry* **1,** 468-475

10. Carredano, E., Karlsson, A., Kauppi, B., Choudhury, D., Parales, R. E., Parales, J. V., Lee, K., Gibson, D. T., Eklund, H., and Ramaswamy, S. (2000) *J. Mol. Biol.* **296,** 701-712

Chapter 4

Site-Directed Mutagenesis at the Mononuclear Iron Active Site of BPDO

ABSTRACT

The availability of a high-resolution crystal structure for biphenyl dioxygenase (BPDO) and its binary complexes with substrate and product enables identification of some potential molecular determinants of enzyme activity. Asparagine 221 in the related naphthalene dioxygenase has been proposed to be a ligand to the active site mononuclear iron (1). The equivalent residue in BPDO, glutamine 226, is situated too far from the mononuclear iron to be a ligand in the crystal structures of uncomplexed, substrate-bound or product-bound enzyme. In order to study the importance of this residue, BPDO_Q226A, BPDO_Q226E, and BPDO_Q226N variants were produced and purified to homogeneity under anaerobic conditions. Steady-state kinetic analysis of the variants using biphenyl as substrate indicated that glutamine 226 is not required for coordination of the mononuclear iron. However, spectroscopic investigations reveal an effect of the Q226E substitution on the Fe-S cluster electronic properties and optical activity. Two other amino acid residues were targeted for substitution: methionine 231, which may be involved in determining substrate specificity, and aspartate 230 which may be involved in internal electron transfer. BPDO_M231A, BPDO_M231T, and BPDO_D230N were expressed and purified to homogeneity. Steady-state kinetics results indicated a decrease in k_{cat}/K_m for biphenyl for BPDO_M231A and BPDO_M231T, together with an increase in k_{cat}, and a decrease of uncoupling in the presence of 2,2'-dichlorobiphenyl. BPDO_D230N exhibited very low activity on biphenyl, and incomplete iron occupancy at the mononuclear iron active site.

INTRODUCTION

Biphenyl dioxygenase (BPDO) is a member of a family of multicomponent dioxygenases containing mononuclear iron and Rieske-type [2Fe-2S] prosthetic groups. Spectroscopic studies of the related enzymes, phthalate dioxygenase and naphthalene dioxygenase, have revealed important information about the active sites of these enzymes (2-6). More recently, the structure of naphthalene dioxygenase has been published (1;7), and site-directed mutagenesis has allowed the roles of some active site residues to be investigated (8-10). The availability of a high-resolution crystal structure for native BPDO and its substrate-bound and product-bound complexes (N. Agar, Ph.D. thesis, Chapter 3; Colbert *et al.*, in prep.) enables the design of BPDO site-directed variants. The study of such variants promises to provide insight into the molecular determinants of substrate specificity in this enzyme, and to test hypotheses developed from the study of related dioxygenases.

In the crystal structure of naphthalene dioxygenase, asparagine 221 was proposed to be one of the ligands to the mononuclear iron (1;7). However, the reported distance between the delta O of Asn221 and the iron was 3.7 Å, which is too long to consider Asn221 a ligand. In the crystal structure of native BPDO, the corresponding position is occupied by glutamine226, located at 3.4 Å from the mononuclear iron, with the epsilon N pointing to the metal. This distance is decreased to 3.3 Å in the structure with biphenyl partially occupying the active site, and to 3.1 Å in the structure of the binary complex with the product, phenylcyclohexadienediol. Interestingly, this shortening of distance in the presence of the product is caused by a 1.4 Å movement of the mononuclear iron in the

active site. The distance between the epsilon N of Gln226 and the iron in the product complex is still too long to qualify Gln226 as a ligand, but the epsilon N provides a hydrogen bond to a hydroxyl group on the dihydroxycyclohexadiene ring of the product (Figure 4.1 A). To further investigate the role of Gln226, the variants Q226A, Q226N, and Q226E were produced by site-directed mutagenesis. If Gln226 were involved in coordination of the iron, the asparagine and alanine substitutions should abolish the iron coordination, whereas the glutamate substitution could fulfill a similar function.

According to the crystal structure of the binary product-BPDO complex, a methionine residue at position 231 lies directly opposite carbon 5 of the product (which corresponds to one of two equivalent carbons of the substrate). The distance between the sulfur gamma of Met231 and carbon 2 of biphenyl is 3.85 Å. According to previous steady-state kinetic studies, 2,2'-diClB induced uncoupling of the reaction with release of hydrogen peroxide (11). If uncoupling is related to improper orientation of the aromatic and molecular oxygen substrates at the active site, substitution of Met231 with alanine or threonine might result in an enzyme with a preference for 2,2'-diClB and/or stabilize the formation of the dichlorinated dihydrodiol product. (Figure 4.1 B).

Previous mutagenesis and crystallographic studies on naphthalene dioxygenase have suggested that an aspartate residue, located at the interface between adjacent alpha subunits, is involved in electron transfer between the Fe-S cluster and the mononuclear iron center (1:12). According to the crystal structure of BPDO, the corresponding aspartate at position 230 could hydrogen bond both the histidine 123 ligand of the Fe-S cluster and the histidine233 ligand of the mononuclear iron (Figure 4.2). A similar pattern was observed in cytochrome c peroxidase, where an Asp-His-Fe motif was shown

Figure 4.1 Crystal structure views of BPDO active site to depict the potential role of specific residues selected for site-directed mutagenesis studies. **A.** Gln226: **B.** Met231. Figures prepared with Swiss PDB Viewer v3.7b2 (13).

A.

B.

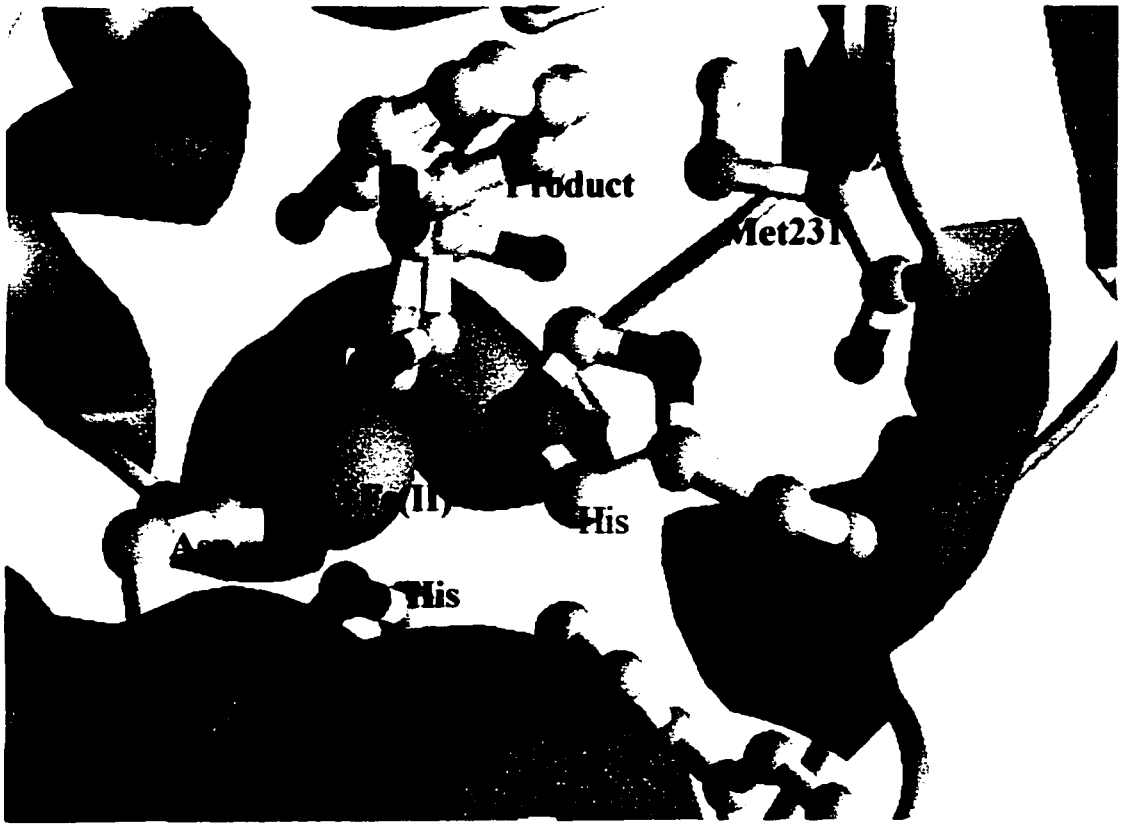

Figure 4.2 Diagram of the hypothetical internal electron transfer pathway in BPDO based on hydrogen bond network. The shades of green indicate adjacent α-subunits. His123 is hydrogen bonded (2.72 Å) to Asp230 in the adjacent subunit, which in turn hydrogen bonds to His233 (3.11 Å) (C. Colbert, Ph.D. Thesis, 2001).

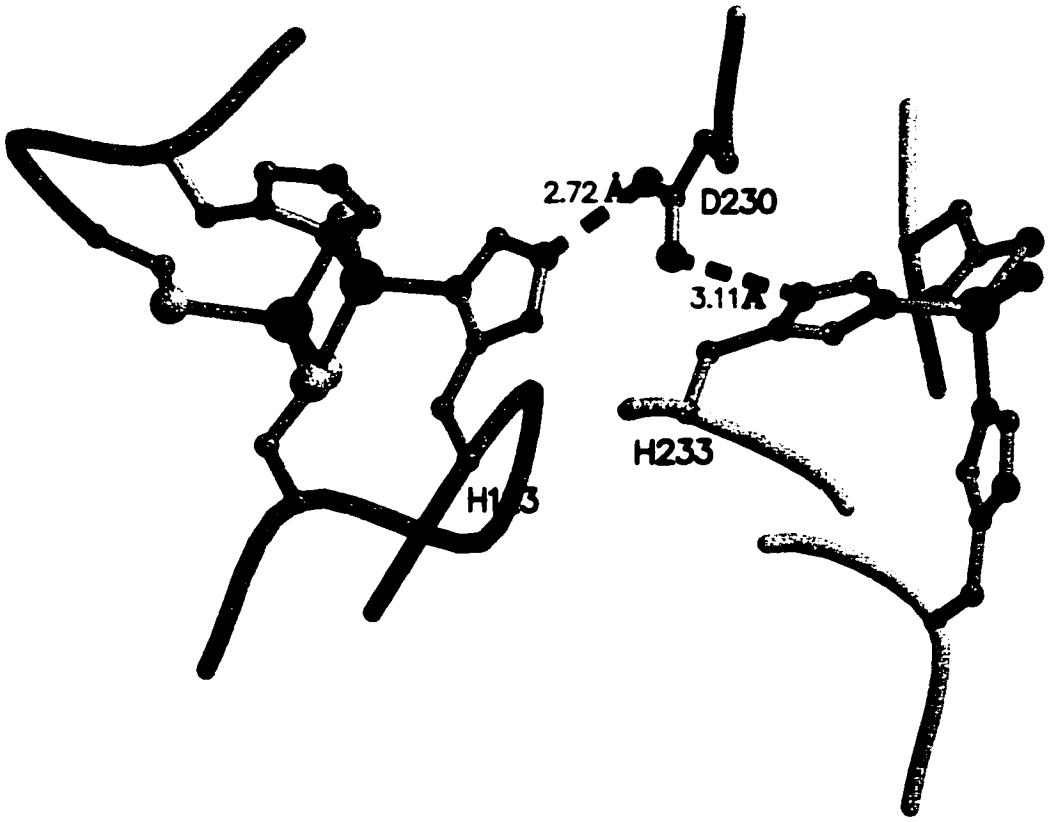
2.72 Å
D230
3.11 Å
H233

to regulate the oxidation-reduction potential of the heme-iron (14). If Asp230 were involved in electron transfer between the two metal centers, substitution by alanine would abolish electron transfer, whereas substitutions by glutamate or asparagine could modify electron transfer. If Asp230 were responsible for modulating the oxidation-reduction potentials of one or the two metal centers, the three substitutions would affect to various extents their mid-point potentials, and possibly the enzyme's ability to dihydroxylate biphenyl substrates.

In this study, the roles of three amino acid residues, Gln226, a potential mononuclear iron ligand, Met231, a potential substrate specificity determinant, and Asp230, a potential electron transfer mediator, were investigated by site-directed mutagenesis.

EXPERIMENTAL PROCEDURES

Materials- Synthetic oligonucleotide pairs described in Table 4.1 were purchased from BioCorp Inc. (Montreal, Canada). For DNA sequencing, the CEQ DTCS (dye terminator cycle sequencing) kit was from Beckman (Fullerton, CA, USA). Biphenyl was purchased from Aldrich (Mississauga, Ontario, Canada). Catechol and sodium dithionite were from Fisher (Fair Lawn, NJ, USA), while ferric ammonium citrate was obtained from ICN Biomedicals Inc. (Aurora, OH, USA). Restriction enzymes and *Pful* polymerase were purchased from Promega and Stratagene, respectively. All other chemicals were of analytical or HPLC grade.

Bacterial Strains and Plasmids- Strains used for protein expression or DNA propagation included *E. coli* DH5α (15), and *E. coli* C41[DE3] (16). *E. coli* strains were generally grown at 37 ^{0}C, and at 25 ^{0}C for after induction protein expression. Plasmids used were pT7-7AE for BPDO expression (N. Agar, Ph.D. thesis, Chapter 6), and pRKISC, which contains the *E. coli* genes required for iron-sulfur cluster assembly (17). For BPDO expression, cells were grown in Terrific Broth (18), supplemented with 0.1 mg/ml ferric ammonium citrate. For each purification, 2 liters of cell culture were grown. BPDO variants were overexpressed according to the protocol for wild type BPDO (N. Agar, Ph.D. thesis, Chapter 6).

DNA Manipulation and Amplification- DNA was purified using the Wizard *Plus* Minipreps kit (Promega), and DNA was extracted from agarose gels using the GFX Band

Table 4.1

Oligonucleotides for site directed mutagenesis of BPDO

Introduced mutation	Oligo name	Sequence (5'→ 3')
Q226A	Q226A-F	GGA AGT TCG CCG CCG AGG CGT TCT GCA GCG
	Q226A-R	CGC TGC AGA ACG CCT CGG CGG CGA ACT TCC
Q226E	Q226E-F	GGA AGT TCG CCG CCG AGG AGT TCT GCA GCG
	Q226E-R	CGC TGC AGA ACT CCT CGG CGG CGA ACT TCC
Q226N	Q226N-F	GGA AGT TCG CCG CCG AGA ACT TCT GCA GCG
	Q226N-R	CGC TGC AGA AGT TCT CGG CGG CGA ACT TCC
M231A	M231A-F	GCA GTT CTG CAG CGA CGC GTA CCA CGC CG
	M231A-R	CGG CGT GGT ACG CGT CGC TGC AGA ACT GC
M231T	M231T-F	GCA GTT CTG CAG CGA CAC GTA CCA CGC CG
	M231T-R	CGG CGT GGT ACG TGT CGC TGC AGA ACT GC
D230A	D230A-F	GCA GTT CTG CAG CGC CAT GTA CCA CGC C
	D230A-R	GGC GTG GTA CAT GGC GCT GCA GAA CTG C
D230E	D230E-F	GCA GTT CTG CAG CGA GAT GTA CCA CGC C
	D230E-R	GGC GTG GTA CAT CTC GCT GCA GAA CTG C
D230N	D230N-F	GCA GTT CTG CAG CAA CAT GTA CCA CGC C
	D230N-R	GGC GTG GTA CAT GTT GCT GCA GAA CTG C
Sequencing	Seq-Mlu	CGA CAA GGC CGA CTG GGG GCC GTT G
Sequencing	Seq-Sca	CCG AAC ATG TCC AGG ATC GGC AAC TGC

Prep kit (Pharmacia). DNA was digested, ligated, and transformed into *E. coli* using standard protocols (19). For DNA sequencing, DNA was amplified using polymerase chain reactions containing 165 ng of plasmid DNA, and 3.2 pmol of each oligonucleotide primer, Seq-Sca or Seq-Mlu (Table 4.1), in a final volume of 20 µl. The thermostable DNA polymerase, each dye-labeled terminator ddNTP, and each dNTP were used at concentrations of 25% of the recommended protocol (Beckman). Thirty temperature cycles were performed using a heated lid DNA thermal cycler (Perkin-Elmer), after a hot start of 1 min at 96 ^{0}C, as follows: 96 ^{0}C for 20 sec, 50 ^{0}C for 20 sec, and 60 ^{0}C for 4 min. After ethanol precipitation, the PCR products were analyzed using the Beckman CEQ DNA Analysis System at the Center for Structural and Functional Genomics (Concordia University, Montreal, Quebec, Canada).

Site-Directed Mutagenesis- Site-directed mutagenesis was done according to the Quickchange protocol (Stratagene), using the oligonucleotide primers described in Table 4.1. The mutations were introduced using polymerase chain reactions containing 200 ng of plasmid DNA, 2.5 units of *Pfu*I polymerase, 0.1 mM of each dNTP, and 27 pmol of each respective oligonucleotides primer (Table 4.1) in a final volume of 100 µl. Twenty temperature cycles were performed using a DNA thermal cycler (Perkin-Elmer) as follows: 96 ^{0}C for 30 sec, 52 ^{0}C for 45 sec, and 72 ^{0}C for 9 min.

Protein Purification- BPDO variants were purified and handled anaerobically using an FPLC system (Pharmacia) in a glove box (Vacuum Atmosphere) under an argon

atmosphere. Purification procedures were as described elsewhere (N. Agar, Ph.D. thesis, Chapter 6).

Analytical Methods- SDS-polyacrylamide gel electrophoresis with a 12% resolving gel was performed using a Bio-Rad MiniPROTEAN II apparatus, and gels were stained with Coomassie Blue according to established procedures (20). Protein quantitation was done using the bicinchoninic acid (BCA) protein assay reagent kit (Pierce) after removal of interfering substances (21), and using bovine serum albumin as a standard. Iron content was determined colorimetrically using Ferene S (Chapter 2).

Steady-state Kinetic and Coupling Measurements- Enzyme activity was estimated by following O_2 consumption using a computer-interfaced Clark-type polarographic O_2 electrode, as described previously (11). The degree of reaction coupling was estimated by adding catalase to the assay after 90 s to measure the amount of hydrogen peroxide released, as indicated by O_2 production.

UV-Visible Absorbance and Circular Dichroism Spectroscopies- Samples for UV-visible absorbance and circular dichroism spectroscopies were prepared in a Unilab glovebox (MBraun) under a nitrogen atmosphere (< 2 ppm O_2). The samples were reduced by adding 10 mM sodium dithionite, or oxidized with 10 mM potassium ferricyanide (approximately 20-fold excess), and desalted by passage through a 5 ml HiTrap (Pharmacia) desalting column. Absorbance spectra were monitored using a Cary 50 Bio spectrophotometer (Varian), and the visible circular dichroism spectra were obtained

using a Jasco J-710 CD spectrometer, in anaerobic quartz cuvettes of 1 cm pathlength with 3.4 μM BPDO. A 0.1 cm pathlength cell was used for the far-UV circular dichroism experiments. To remove the mononuclear iron from BPDO_wild-type and BPDO_Q226E, the proteins were incubated with a 10-fold excess of EDTA under aerobic conditions for 18 hours at 4 ^{0}C. The apo-protein preparations were desalted by passage through a 5 ml HiTrap desalting column (Pharmacia). Corresponding samples of holo-BPDO_wild-type and holo-BPDO_Q226E were similarly desalted to account for any effects of the desalting step, or of the extensive aerobic incubation. The enzyme activity of each sample was measured.

Mass Spectrometry Analysis - Mass spectra were obtained in the positive mode on a triple quadrupole spectrometer Model API-III (Sciex), calibrated with ammonium adduct ions of polypropylene glycol mixture supplied by the manufacturer. For accurate mass, a Pulsari QSTAR (Sciex) was calibrated in the two-point calibration mode, with an octapeptide ALILTLVS of exact mass 829.5398 amu, and cesium iodide of exact mass 132.9054 amu. The instrument was ready for sample injection when the drift from the theoretical readings was less than 4 ppm. Briefly, the samples and standards were dissolved in a solution (50% methanol, 45% water, 5% formic acid), and infused through a stainless steel capillary (100 μm ID) after removal of precipitated protein by centrifugation. A stream of air (pneumatic nebulization) was introduced to assist in the formation of submicron droplets. These droplets were evaporated at the interface by nitrogen gas producing highly charged ions, which were detected by the analyzer.

RESULTS

Site-directed Mutagenesis- Plasmids encoding eight site-directed variants of BPDO were generated as described in *Materials and Methods*: amino acid substitutions were Q226A, Q226E, Q226N, M231A, M231T, D230N, D230A, and D230E. DNA from two different clones of each mutagenesis experiment was isolated, and partially sequenced to confirm the mutations. The mutated pT7-7AE-based plasmids were subsequently transformed into *E. coli* C41[DE3]. Competent cells were prepared from one clone of each mutant, and were co-transformed with pRKISC, a plasmid encoding the *E. coli* iron-sulfur cluster assembly genes (17). The overexpression systems for Q226A, Q226E, Q226N, M231A, M231T, and D230N yielded high levels of soluble variant protein. In contrast, D230A was poorly expressed, and D230E was produced at high levels, but as an insoluble characteristically reddish fraction. Interestingly, the cell culture for the expression of D230N produced twice the amount of cell paste than the other cultures.

Purification of BPDO Variants- Yields, relative specific activities, and iron contents of anaerobically purified Q226A, Q226E, Q226N, M231A, M231T, and D230N are summarized in Table 4.2. All six variants were purified by the same method as for the wild-type, and according to SDS-PAGE appeared to be as pure or purer than wild-type (data not shown). Far-UV circular dichroism spectra were collected to assess the secondary structure of the proteins, and no significant changes were observed (data not shown). Electrospray mass spectrometry of the variants indicated masses of 21 556 ± 1 Da for unmutated β-subunits: unfortunately masses of the α-subunits could not be confirmed by this method due to the formation of multiple unidentifiable adducts.

Table 4.2

Yields and characteristics of purified BPDO variants

BPDO Variant	Yield (mg)	Fe : αβ dimer [a]	Specific Activity [b, c] (U/mg)
Q226A	69.0	3.02 (0.16)	1.4
Q226E	29.2	2.55 (0.16)	0.8
Q226N	32.5	3.27 (0.12)	2.5
M231A	106.0	2.80 (0.15)	3.1
M231T	66.0	3.06 (0.14)	2.8
D230N	122.0	2.15 (0.11)	0.3

[a] BPDO_wild-type has an Fe content of 2.8-4.0 Fe / αβ dimer; [b] BPDO_wild-type has a specific activity of 4.9 U/mg (11).
[c] Specific activities measured in the presence of 394 μM biphenyl.

Steady-State Kinetic Analysis- Under the standard assay conditions, in air-saturated buffer, Q226A, Q226N, M231A, M231T, and D230N showed Michaelis-Menten kinetics for the dependence of the initial rate of oxygen consumption on the concentration of biphenyl (Fig. 4.5, Appendix A). Estimates of the kinetic parameters for BPDO variants with biphenyl as substrate are presented in Table 4.3, and kinetic and coupling parameters for M231A and M231T with 2,2'-dichlorobiphenyl are presented in Table 4.4 (Appendix A). The dependence of initial velocity for Q226E on the biphenyl concentration did not conform to Michaelis-Menten kinetics, and data were consistent with substrate inhibition (Fig. 4.5, Appendix A).

To determine whether biphenyl utilization by Q226A, Q226E, and Q226N is uncoupled from oxygen consumption, the formation of hydrogen peroxide, a possible uncoupling product, was examined by adding catalase to the assay, as described previously (11). These experiments were done at biphenyl concentrations for which the variants exhibited maximum rates of oxygen uptake. Q226A and Q226N in the presence of 41.4 and 24.8 μM biphenyl, respectively, did not appear to produce any hydrogen peroxide. In contrast, Q226E in the presence of 1.7 μM biphenyl and 337 μM NADH produced at least 54.4 μM H_2O_2 after 90 sec of reaction.

Spectroscopic Characterization of BPDO Variants- The UV-visible absorption spectra of oxidized forms of M231A, M231T, and D230N were practically identical to the corresponding wild-type spectrum (22). Maxima observed at 323 and 455 nm, and a shoulder at ~ 575 nm, were indicative of the Rieske-type iron sulfur cluster integrity for these variants (data not shown). However, the absorbance spectra of oxidized and

Table 4.3

Steady-state kinetic parameters of BPDO variants for biphenyl

BPDO Variant	K_m (μM)	k_{cat} (s^{-1})	k_{cat} / K_m (x 10^6 $M^{-1}s^{-1}$)*
Q226A	9.7 (1.4)	0.8 (0.1)	0.08 (0.07)
Q226E	_	1.2 (0.2)	_
Q226N	3.4 (0.9)	0.8 (0.1)	0.2 (0.1)
M231A	9.4 (1.9)	2.1 (0.1)	0.2 (0.05)
M231T	11.1 (3.1)	2.9 (0.3)	0.3 (0.1)
D230N	0.3 (0.2)	0.3 (0.1)	1.0 (0.5)

*The corresponding value for BPDO_wild type is 1.2 (0.1) (11).
Standard deviation values are given in parentheses.

Figure 4.3 UV-Visible absorbance spectra of oxidized (A) and reduced (B) wild type and Q226 variants. Wild_type (____): Q226A (.....): Q226E (_ _ _): Q226N (_.._.._). Difference spectra of Q226E-wild_type are the lower solid lines traces on A and B. Samples were oxidized or reduced using a 20 fold excess concentration to the protein of respectively potassium ferricyanide or sodium dithionite. Samples were desalted into 25 mM HEPES pH 7.3 10% glycerol. and the spectra were normalized to their A_{280} (details in *Experimental Procedures*).

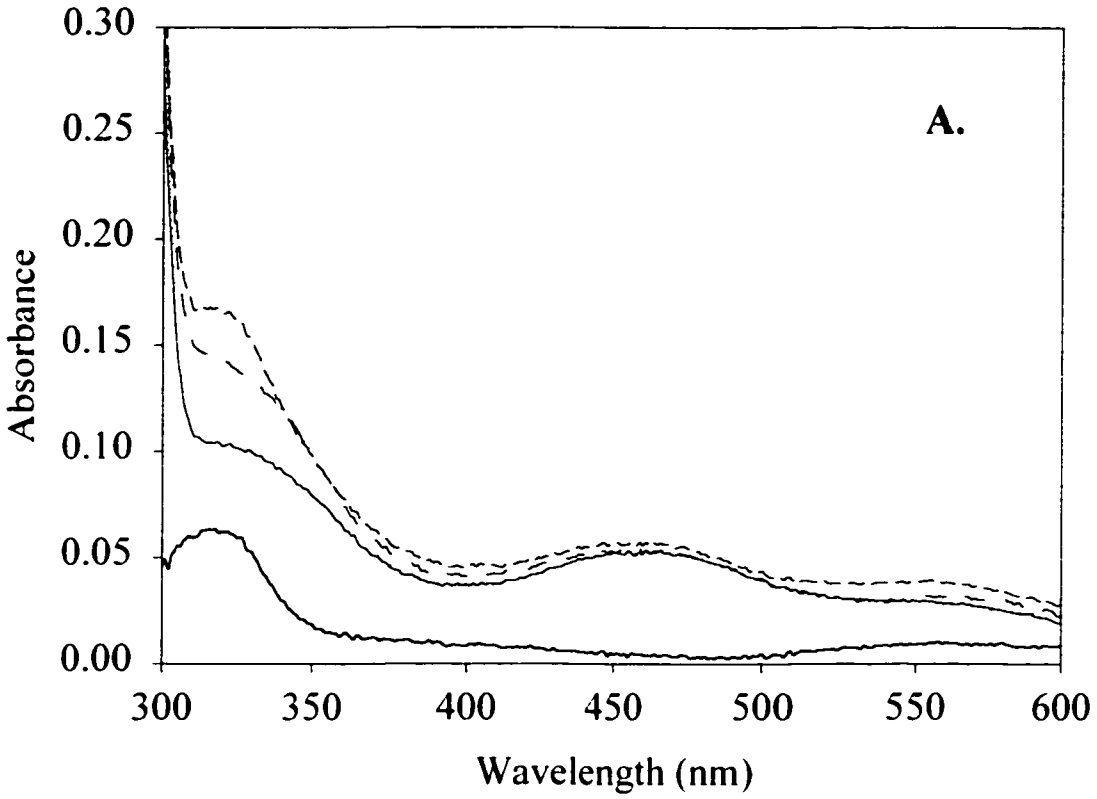
A.
Absorbance
0.30
0.25
0.20
0.15
0.10
0.05
0.00
300
350
400
450
500
550
600
Wavelength (nm)

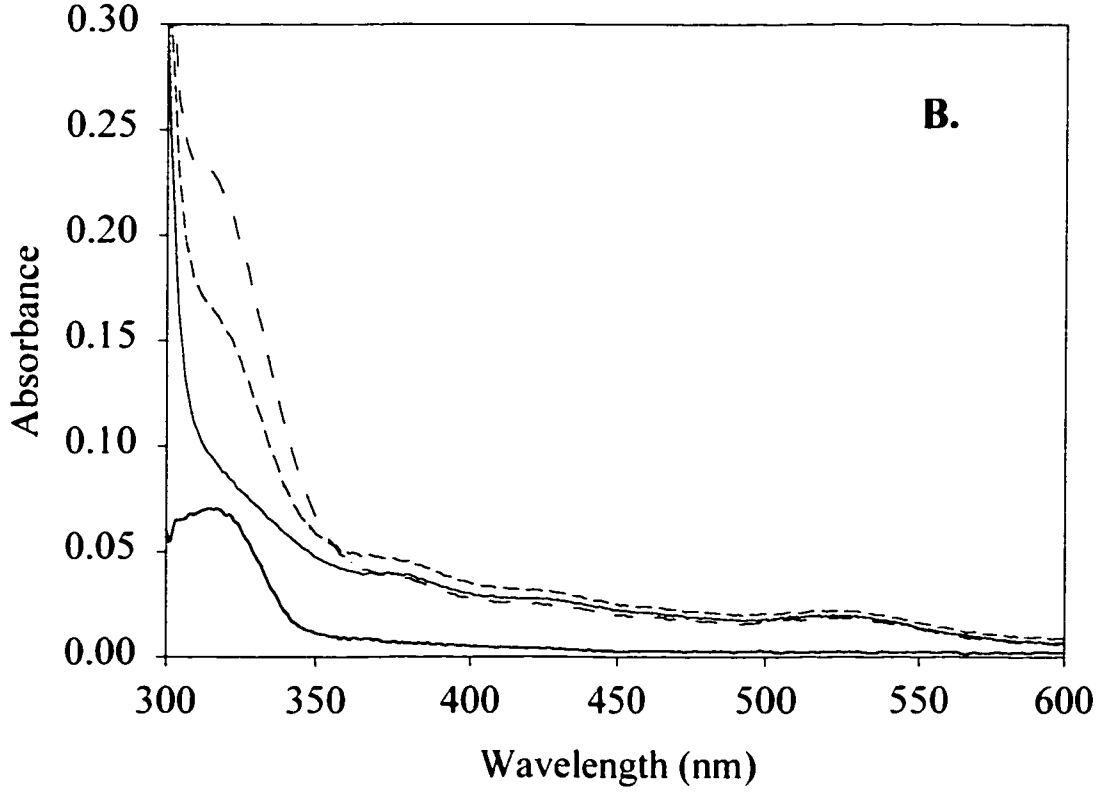
B.
Absorbance
0.30
0.25
0.20
0.15
0.10
0.05
0.00
300
350
400
450
500
550
600
Wavelength (nm)

reduced Q226E differed significantly from the corresponding wild-type spectra (Fig. 4.3). The main difference between Q226E and wild-type oxidized spectra is a peak centered at 318 nm (Fig. 4.3). The absorbance spectra of oxidized Q226N and Q226A showed intermediate degrees of this difference, with Q226A being the least affected (Fig. 4.3). To probe the possibility that this spectral change was related to a ligation rearrangement at the mononuclear iron, this iron was partially removed from wild-type and Q226E by aerobic incubation with EDTA (2). The enzymatic activity of the EDTA-desalted wild-type and Q226E samples were respectively 30 % and 52 % of their corresponding holo-forms, suggesting that these relative percentages of mononuclear iron remained bound at the active site. Despite the loss of activity upon incubation with EDTA, the absorbance spectra of wild-type and Q226E were unchanged. Therefore, it appears that the three different substitutions of Gln226 also affect the iron-sulfur cluster electronic environment.

The optical activities of the three Q226 variants were measured in the visible region, and compared to the wild type for both their oxidized and reduced forms (Fig. 4.4). Major differences were observed for the oxidized proteins between 300 and 330 nm, as the spectrum of Q226E undergoes a change in its ellipticity sign, and there are significant intensity differences between wild-type, Q226A, and Q226N. Intensity differences between the four BPDOs were also observed at 280 nm. For the reduced samples, the major differences are between 300 and 360 nm, and around 280 nm. Interestingly, the spectra of Q226A and Q226E overlay at 280 nm, while those for wild-type and Q226N were more intense and almost equivalent in that region.

Figure 4.4 Visible circular dichroism of wild type and Q226 variants oxidized (A) and reduced (B). Wild-type (___): Q226A (.....): Q226E (_ _ _): Q226N (_ .. _). Samples were oxidized or reduced using a 20 fold excess concentration to the protein of respectively potassium ferricyanide or sodium dithionite. Samples were desalted into 50 mM sodium phosphate buffer pH 7.3 10% glycerol. and the spectra were normalized to their A_{280} (details in *Experimental Procedures*).

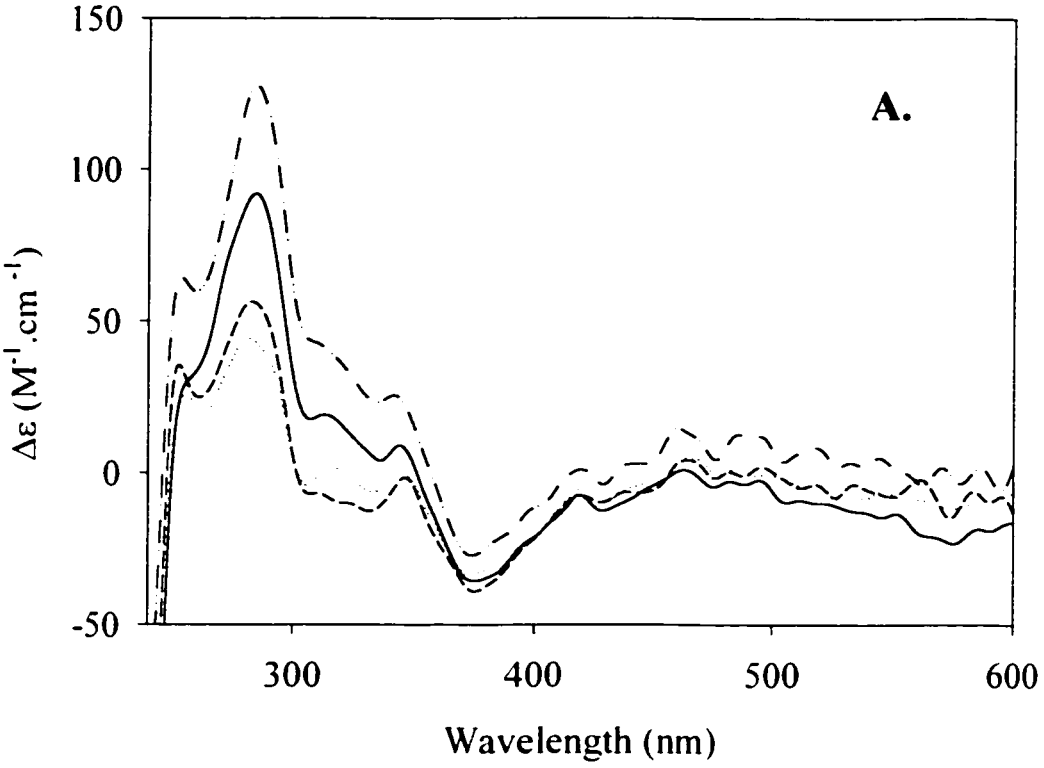
A.
150
100
50
0
-50
Δε (M-1.cm-1)
300
400
500
600
Wavelength (nm)

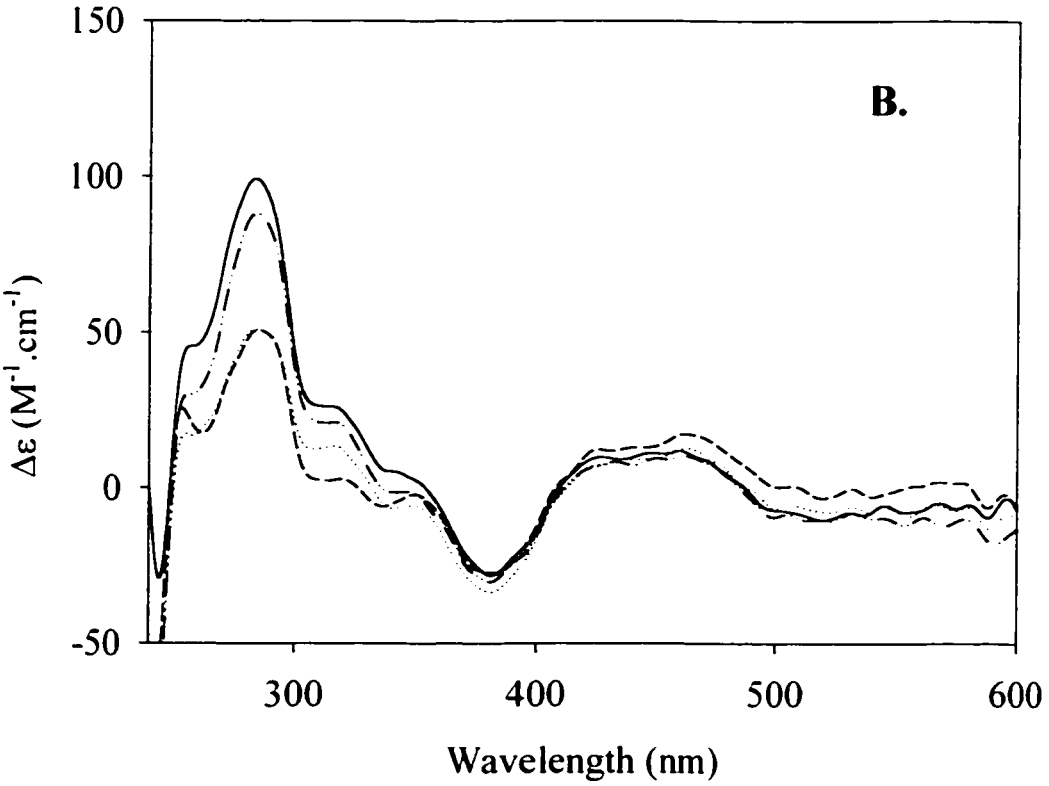
B.
150
100
50
0
-50
Δε (M-1.cm-1)
300
400
500
600
Wavelength (nm)

DISCUSSION

Site-directed mutagenesis of the three specific residues of BPDO reported here provides interesting insights into some determinants of enzyme activity. Q226A, Q226E, Q226N, M231A, M231T, and D230N were all highly expressed in soluble form, and successfully purified with high yields. According to SDS-PAGE results, each of the preparations was as pure or purer than wild-type preparations. Moreover, far-UV circular dichroism results indicated that the purified BPDO variants maintained secondary structure, therefore suggesting that characteristic differences from the wild-type protein arose from specific residue substitutions. In contrast, D230A was poorly expressed or degraded, while D230E was highly expressed in an insoluble characteristically reddish colored fraction. Since Asp230 is located at the interface of adjacent alpha subunits, it is possible that replacing this residue with alanine could prevent proper quaternary structure assembly. The fact that D230E is highly expressed and appears to contain its Fe-S cluster, but is compartmentalized into an insoluble fraction, suggests that this variant might be toxic to the cells.

Characterization of the Gln226 variants confirmed that Gln226 is not a ligand to the mononuclear iron, since all three variants were active with biphenyl, and appeared to have a full complement of Fe-S cluster and mononuclear iron. The preliminary steady-state kinetic parameters of Q226A and Q226N showed lower substrate specificity for biphenyl than the wild-type enzyme, but no hydrogen peroxide formation was detected. As for Q226E, the preliminary steady-state kinetic data for biphenyl could not be fit to the Michaelis-Menten equation, and suggested substrate inhibition. Moreover, in the presence of 1.9 μM biphenyl and excess NADH, the enzyme produced at least 54.4 μM

H_2O_2, indicating a high degree of uncoupling. According to the crystal structure of the binary product-bound complex, Gln226 forms hydrogen bonds with a hydroxyl group of the product and the aspartate ligand (Asp386) to the iron, suggesting a role for Gln226 in product formation and/or stabilization. Further investigation of biphenyl utilization, product formation, and detection of other possible reduced oxygen derivatives will be necessary to further delineate the role of Gln226. Interestingly, the substitution of Gln226 by a glutamate residue led to a change of the Fe-S cluster visible absorbance signal, and its optical activity. The possibility of the new feature at 318 nm of the oxidized protein arising from a rearrangement of ligation at the mononuclear iron site was ruled out by preparation of a partial apo-BPDO depleted of approximately 50% of activity. Further spectroscopic studies in conjunction with crystallography of the Gln226 variants will be necessary to assign the 318 nm-absorbing feature.

Inspection of the crystal structure suggested that substitution of Met231 with alanine or threonine might result in a preference for 2,2'-diClB. Steady-state kinetic characterization of M231A and M231T revealed that these variants indeed have higher k_{cat} and lower uncoupling for 2,2'-diClB.

The low activity of D230N with biphenyl, and its low iron occupancy at the mononuclear iron active site, clearly indicate the importance of this residue for biphenyl dioxygenase activity. To complete the investigation of the role of Asp230, more effort will have to be invested in the production of a soluble preparation of D230E. Due to the low activity of D230N on biphenyl, the steady-state kinetic characterization of this set of variants will be limited, but electron transfer and electrochemical investigations should be pursued.

REFERENCES

1. Kauppi, B., Lee, K., Carredano, E., Parales, R. E., Gibson, D. T., Eklund, H., and Ramaswamy, S. (1998) *Structure.* **6,** 571-586

2. Pavel, E. G., Martins, L. J., Ellis, W. R., Jr., and Solomon, E. I. (1994) *Chem.Biol.* **1,** 173-183

3. Gassner, G. T., Ballou, D. P., Landrum, G. A., and Whittaker, J. W. (1993) *Biochemistry* **32,** 4820-4825

4. Coulter, E. D., Moon, N., Batie, C. J., Dunham, W. R., and Ballou, D. P. (1999) *Biochemistry* **38,** 11062-11072

5. Tsang, H.T., Batie, C.J., Ballou, D.P., and Penner-Hahn, J.E. (1996) *Journal of Biological Inorganic Chemistry* **1,** 24-33

6. Bertini, I., Luchinat, C., Mincione, G., Parigi, G., Gassner, G.T., and Ballou, D.P. (1996) *Journal of Biological Inorganic Chemistry* **1,** 468-475

7. Carredano, E., Karlsson, A., Kauppi, B., Choudhury, D., Parales, R. E., Parales, J. V., Lee, K., Gibson, D. T., Eklund, H., and Ramaswamy, S. (2000) *J.Mol.Biol.* **296,** 701-712

8. Parales, R. E., Resnick, S. M., Yu, C. L., Boyd, D. R., Sharma, N. D., and Gibson, D. T. (2000) *J.Bacteriol.* **182,** 5495-5504

9. Parales, R. E., Lee, K., Resnick, S. M., Jiang, H., Lessner, D. J., and Gibson, D. T. (2000) *J.Bacteriol.* **182,** 1641-1649

10. Yu, C. L., Parales, R. E., and Gibson, D. T. (2001) *J.Ind.Microbiol.Biotechnol.* **27,** 94-103

11. Imbeault, N. Y., Powlowski, J. B., Colbert, C. L., Bolin, J. T., and Eltis, L. D. (2000) *J.Biol.Chem.* **275,** 12430-12437

12. Parales, R. E., Parales, J. V., and Gibson, D. T. (1999) *J.Bacteriol.* **181,** 1831-1837

13. Schwede, T., Diemand, A., Guex, N., and Peitsch, M. C. (2000) *Res.Microbiol.* **151,** 107-112

14. Goodin, D. B. and McRee, D. E. (1993) *Biochemistry* **32,** 3313-3324

15. Hanahan, D. (1983) *J.Mol.Biol.* **166,** 557-580

16. Miroux, B. and Walker, J. E. (1996) *J.Mol.Biol.* **260,** 289-298

17. Nakamura, M., Saeki, K., and Takahashi, Y. (1999) *J.Biochem.(Tokyo)* **126,** 10-18

18. Ausubel, F. M. and et al. (1997) *Current Protocols in Molecular Biology*, John Wiley & Sons Inc., New York

19. Sambrook, J., Fritsch, E. F., and Maniatis, T. (1989) *Molecular Cloning: A Laboratory Manual*, Cold Spring Harbour, New York

20. Laemmli. U. K. (1970) *Nature* **227,** 680-685

21. Brown. R. E.. Jarvis. K. L.. and Hyland. K. J. (1989) *Anal.Biochem.* **180,** 136-139

22. Hurtubise. Y.. Barriault. D.. Powlowski. J.. and Sylvestre. M. (1995) *J.Bacteriol.* **177,** 6610-6618

Chapter 5

A Comparison of the Specificities of BPDO from Psychrotolerant and Mesophilic PCB-Degrading Bacteria

ABSTRACT

Biphenyl dioxygenases from the psychrotolerant bacterium *Pseudomonas* sp. strain Cam-1 ($BPDO_{Cam1}$) and the mesophile *Burkholderia* sp. strain LB400 ($BPDO_{LB400}$) were purified and their activities and thermostability were compared. $BPDO_{Cam1}$ transformed biphenyl and dichlorobiphenyls (diClBs) in the following order of apparent maximal rates at 25°C: biphenyl > 3,3'-diClB > 4,4'-diClB > 2,2'-diClB. This is probably representative of KF707-type dioxygenases as the sequence of the $BPDO_{Cam1}$ α-subunit, which harbors the major determinants of specificity, shares 99.8% sequence identity with that of BPDO from *P. pseudoalcaligenes* KF707. In contrast, $BPDO_{LB400}$ transformed the diClBs in the following order of apparent maximal rates: biphenyl > 2,2'-diClB > 3,3'-diClB > 4,4'-diClB. However, the apparent specificity of $BPDO_{LB400}$ for 2,2'-diClB was approximately twice that for biphenyl. In both enzymes, O_2 utilization was well coupled to biphenyl transformation. In contrast, diClB transformation was uncoupled from O_2-utilization to varying extents. Indeed, the data suggest that the positioning of the congener in the active site of the dioxygenase is an important determinant of the BPDO's reactivity. At 4°C, $BPDO_{Cam1}$ had a k_{cat}^{app} for biphenyl of 1.1 ± 0.1 s^{-1} (50 mM MES, pH 6.0). In contrast, $BPDO_{LB400}$ did not detectably transform biphenyl under these conditions. At 10 and 25°C, the respective specificity constants ($k_{cat}^{app} / K_m^{app}$) of $BPDO_{Cam1}$ and $BPDO_{LB400}$ for biphenyl were very similar. However, the k_{cat}^{app} of $BPDO_{Cam1}$ was approximately 10 times higher than that of $BPDO_{LB400}$ under these conditions. This is consistent with the observation that strain Cam-1 removes some congeners up to 10 times faster than strain LB400 at 7°C. The thermostability of $BPDO_{Cam1}$ was significantly lower than that of $BPDO_{LB400}$ (half-lives at 57°C of 16 ± 2 and 38 ± 8 min, respectively).

INTRODUCTION

A wide variety of microorganisms have evolved to use naturally occurring aromatic compounds as growth substrates. It has become clear that aromatic biotransformations can be applied for the production of enantiomerically pure compounds as well as the degradation of harmful contaminants (24). An example of the latter is the microbial degradation of biphenyl, which has been extensively studied as a possible means of removing polychlorinated biphenyls (PCBs) from the environment (1). In the US, PCBs were commercially produced for over 50 years, until this production was banned in 1977. However, they continue to cause a variety of environmental and health problems due to their persistence and pervasiveness (1).

PCBs are aerobically transformed by the biphenyl catabolic pathway (21, 29). The initial transformation is catalyzed by biphenyl dioxygenase (BPDOS), a multicomponent enzyme consisting of an FAD-containing reductase (BphG), a Rieske-type ferredoxin (BphF) and a two-subunit oxygenase (BPDO) with $\alpha_3\beta_3$ constitution (Fig.5.1). BphG and BphF transfer electrons from NADH to the terminal oxygenase, which transforms biphenyl to *cis*-(2*R*,3S)-dihydroxy-1-phenylcyclohexa-4,6-diene. The α-subunit of the terminal oxygenase, encoded by *bphA*, contains a Rieske-type [2Fe-2S] cluster and a mononuclear Fe^{2+} center (25), which are essential for catalysis. The successive activities of the subsequent enzymes in the biphenyl pathway convert the phenylcyclohexadiene to TCA cycle intermediates.

Bacterial strains possessing different PCB-degrading capabilities have been characterized. For example, *Burkholderia* sp. strain LB400 (46) (originally identified as a member of the genus *Pseudomonas* [7]) oxidizes an exceptionally broad spectrum of PCBs (1, 5), including congeners with up to six chloro substituents, and preferentially transforms *ortho*-substituted biphenyls (23). In contrast, PCB-degrading bacteria such as *Pseudomonas pseudoalcaligenes* KF707 and *Comamonas testosteroni* B-356

Figure 5.1 The reaction catalyzed by biphenyl dioxygenase (BPDOS). The enzyme comprises an FAD-containing reductase (BphG), a Rieske-type ferredoxin (BphF), and an oxygenase (BphAE or BPDO) that contains a Rieske-type [2Fe-2S] cluster and a catalytic mononuclear Fe^{2+} center. Biphenyl is stereospecifically hydroxylated at adjacent positions yielding *cis*-(2*R*,3*S*)-dihydroxy-2,3-dihydrobiphenyl. ox. oxidized; red. reduced.

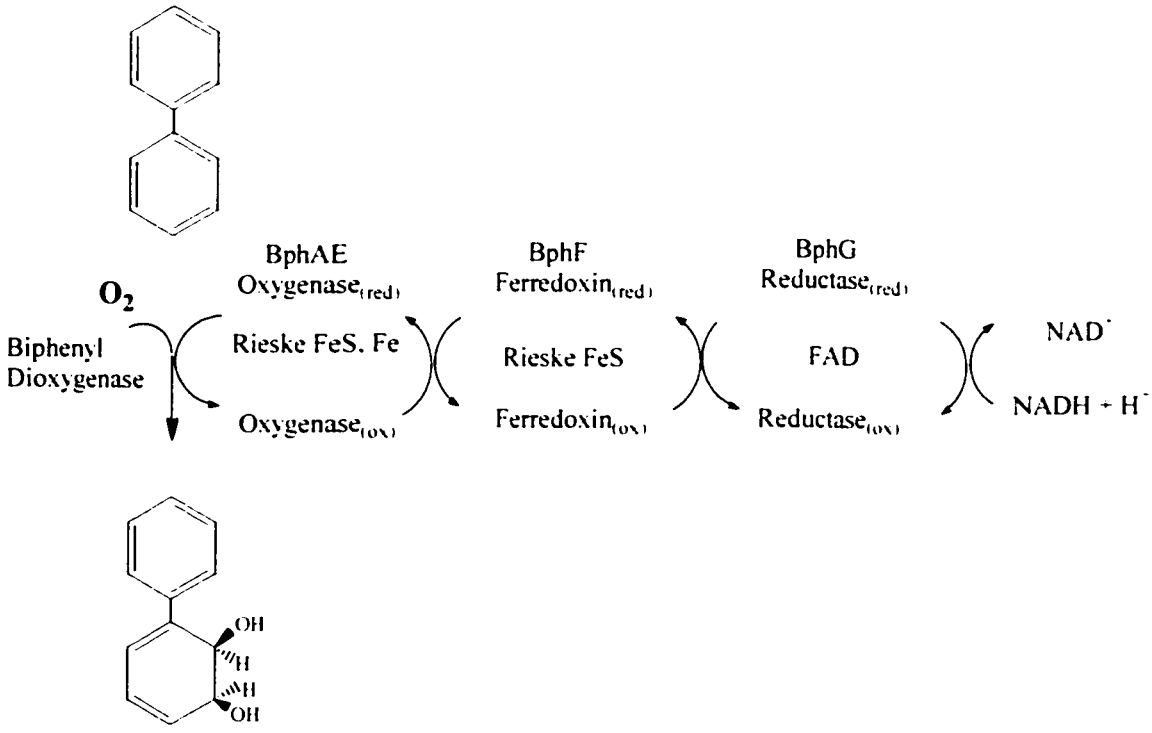
BphAE
Oxygenase(red)
BphF
Ferredoxin(red)
BphG
Reductase(red)
O2
Biphenyl
Dioxygenase
Rieske FeS, Fe
Rieske FeS
FAD
NAD+
NADH + H+
Oxygenase(ox)
Ferredoxin(ox)
Reductase(ox)
OH
H
H
OH

preferentially transform *para*-substituted biphenyls or *meta*-substituted biphenyls, respectively, and do not oxidize PCBs with more than four chloro substituents (4, 23). As the initial enzyme in the pathway, BPDO is a major determinant of PCB transformation. For instance, the ability of LB400 to transform a comparatively wide range of PCB congeners results from 2,3- and 3,4-dihydroxylation activities of BPDO from LB400 ($BPDO_{LB400}$) and the ability of $BPDO_{LB400}$ to dechlorinate certain *ortho*-substituted PCBs (14, 26). Despite their markedly different reactivities, $BPDO_{LB400}$ and $BPDO_{KF707}$ share approximately 95% sequence identity.

Due to its key role in PCB transformation, BPDO has been engineered to develop more efficient PCB-degrading bacteria (20). Site-directed mutagenesis of $BPDO_{LB400}$ and $BPDO_{KF707}$ (14) and exchanging domains of the genes that encode BPDOs (4b, 34, 41, 44), indicate that the major determinants of congener preference are located in the carboxyl-terminal region of the α-subunit. Moreover, shuffling the *bphA* genes of different BPDOs generated enzymes with different substrate preferences than the parent enzymes (9, 20, 36). Interestingly, exchanging the *bphE*-encoded β-subunits of different BPDOs also affected substrate preference (10, 32), indicating that the β-subunit may also play a role in determining the substrate specificity of BPDO. Despite many studies of BPDO, many aspects of the reactivity of this enzyme remain unknown. Fortunately, recent improvements in purifying BPDO, and an oxygraph assay to continuously monitor dioxygenase activity, facilitate studies to provide needed insight (33). Thus, it has been demonstrated that the transformation of certain PCB congeners by $BPDO_{B356}$ is poorly coupled to O_2 consumption (33). Such uncoupling depletes reducing equivalents from the cell, with concomitant production of reactive oxygen species. Clearly, additional insights into BPDO function will facilitate the effective design of recombinant BPDOs.

Pseudomonas sp. strain Cam-1, a psychrotolerant bacterium previously isolated from PCB-contaminated Arctic soil, is of interest due to its ability to transform PCBs at

low temperatures (38). Cam-1 transforms a narrower range of PCBs than LB4000, and preferentially degrades *para*-substituted biphenyls over *ortho*-substituted biphenyls (38). Indeed the congener preference of Cam-1 is similar to that of KF707, consistent with the high sequence identity of $BPDO_{KF707}$ and BPDO from Cam-1 ($BPDO_{Cam1}$) (39). However, PCB congeners that are transformed by both Cam-1 and LB400 at 7°C are removed up to 10 times faster by Cam-1 (38). Moreover, the rates of PCB removal by LB400 are higher at 50°C than at 37°C, whereas the rates of PCB removal by Cam-1 are significantly decreased at 50°C (38). Higher rates of PCB transformation at 7°C by Cam-1 than LB400, and decreased PCB transformation at high temperatures by Cam-1 suggest that Cam-1 may express a cold-adapted BPDO (15, 16).

In the current study, we purified the BPDO components of biphenyl dioxygenase from LB400 ($BPDO_{LB400}$) and Cam-1 ($BPDO_{Cam1}$) and used an oxygraph assay to compare the respective BPDO activities *in vitro*. The apparent specificities of $BPDO_{LB400}$ and $BPDO_{Cam1}$ were determined using biphenyl and each of three dichlorobiphenyls (diClBs): 2,2'-diClB, 3,3'-diClB and 4,4'-diClB. The efficiencies of PCB transformation at 25°C by $BPDO_{LB400}$ and $BPDO_{Cam1}$ were further compared by determining the ratio biphenyl/O_2 consumed by each enzyme in the presence of each biphenyl. Furthermore, the activities and stability of these enzymes were determined at various temperatures. The results are discussed in light of previous reports of cold-adapted enzymes and the high sequence identity of $BPDO_{Cam1}$ and $BPDO_{LB400}$.

MATERIALS AND METHODS

Chemicals. Biphenyl (99%) and catalase were purchased from Sigma-Aldrich (Oakville, Ontario). 2,2'-diClB (99%) was purchased from Accu Standard (New Haven, CT, USA). Ferene S was purchased from ICN Biomedicals Inc. 3,3'-diClB, 4,4-diClB and 2,3-dihydroxybiphenyl were gifts from Prof. Victor Snieckus. All other chemicals were of analytical or HPLC grade.

Bacterial strains, plasmids and culture conditions. $BPDO_{LB400}$ was overexpressed in *E. coli* strain C41(DE3) (40) from pT7-6a, which contains *bphAEFG* genes from LB400 (29, 43). $BPDO_{Cam1}$ was overexpressed in *E. coli* strain C41(DE3) from pT7-7a, which contains *bphAEFG* genes from Cam-1 (39). The nucleotide sequence of all expression constructs was verified (39). The expression of the *isc* genes from *E. coli* enhances the expression of iron-sulfur proteins (42). Consequently, the *isc* genes from *Pseudomonas putida* KT2442 were cloned and coexpressed in *E. coli* strain C41(DE3) with the *bph* genes (Agar *et al.*, in prep). For expression of $BPDO_{LB400}$ and $BPDO_{Cam1}$, recombinant *E. coli* strains were grown at 37°C on Terrific broth containing 100 μg/ml ampicillin, 10 μg/ml tetracycline, an HCl-solubilized solution of minerals (10 ml/L) (45), and ferric ammonium citrate (0.1 mg/ml). When the OD_{610} of the culture reached approximately 0.7, the culture was cooled to 22°C. Isopropyl-1-thio-β-D-galactopyranoside (IPTG) was added to a final concentration of 1 mM and cultures were incubated for an additional 18 h at 22°C before harvesting by centrifugation. The harvested cell pellet was washed with PAS buffer (7) and stored at –70 °C until use.

Purification and handling of proteins. Proteins were purified and handled anaerobically in a glovebox maintained at less than 2 ppm O_2 unless otherwise specified. High resolution chromatographic procedures were performed using an ÄKTA Explorer (Amersham Pharmacia Biotech, Baie d'Urfé, Québec, Canada) interfaced to a glovebox

as described previously (45). Buffers were prepared using water purified on a Barnstead NANOpure UV apparatus to a resistivity of greater than 17 MΩcm. Buffers for anaerobic procedures were filtered (Ahlstrom Filtration), bubbled with argon for 20 min, and equilibrated in the glovebox for 24 h prior to addition of dithiothreitol and iron. Buffer A contained 25 mM HEPES (pH 7.3), 10 % glycerol, 2 mM dithiothreitol and 0.5 mM ferrous ammonium sulfate; buffer B was buffer A with 1 M NaCl; and buffer PS was buffer A containing 0.205 M ammonium sulfate (~5% saturation). Protein-containing fractions were concentrated by ultrafiltration using an Amicon stirred cell equipped with a YM30 membrane.

For purification of BPDOs, frozen cell pellets were thawed and suspended in 80 ml 25 mM HEPES (pH 7.3) and 10% glycerol containing 2 mM dithiothreitol and 0.1 mg/ml DNase I. Cell suspensions were divided into two batches and sonicated using an ultrasonic liquid processor (Misonix Incorporated, Farmingdale, NY) with 10 X 12 s pulses adjusted to 30% of maximum output. The cell debris was removed by ultracentrifugation at 4°C for 70 min at 300 000 g. Centrifuge tubes were transferred to the glove box and the clear supernatant was carefully decanted, passed through a 0.45 μm filter, then diluted with 40 ml buffer A. Samples of 20 ml crude extract were loaded onto a Mono Q HR 10/10 anion-exchange column (Pharmacia Biotech) equilibrated with buffer A and operated at a flow rate of 3 ml/min. Bound proteins were eluted using a linear gradient of 0 to 20% buffer B over 80 mL. Brown-colored BPDO-containing fractions (*i.e.*, absorbing at 323 nm and 455 nm, characteristic of the [2Fe-2S] Rieske-type center, and containing subunits of the expected size as seen by denaturing gel electrophoresis), were pooled and concentrated to less than 50 ml by ultrafiltration. The samples were brought to 0.205 M with ammonium sulfate, filtered, then loaded onto a phenyl-Sepharose column (1 X 9 cm; Amersham Pharmacia Biotech) equilibrated with buffer PS. The column was operated at a flow rate of 5 ml/min. Bound proteins were

eluted using a linear gradient of 0.205 to 0 M ammonium sulfate over 5 column volumes. $BPDO_{Cam1}$ eluted at 0% ammonium sulfate. $BPDO_{LB400}$ eluted as a comparatively broad peak centered at 40 mM ammonium sulfate. BPDO-containing fractions were concentrated to between 20 and 30 mg/ml and flash-frozen as beads in liquid nitrogen.

His-tagged ferredoxin from *Burkholderia* sp. LB400 (ht-$BphF_{LB400}$) and his-tagged reductase from *Comamonas testosteroni* B-356 (ht-$BphG_{B356}$) were prepared using immobilized metal affinity chromatography as described previously (13, 31).

Steady-state Kinetic Measurements. Enzymatic activity was measured by following the consumption of O_2 as described previously using a Clark-type polarographic O_2 electrode (Yellow Springs Instruments Model 5301, Yellow Springs, OH; 44). The activity assay was performed in a thermojacketted Cameron Instrument Co. model RCI respiration chamber (Port Arkansas, TX) connected to a Lauda Model RM6 circulating bath. For assays performed at temperatures other than 25°C, the reaction buffer was pre-equilibrated at the desired temperature using ice or a hot plate, as appropriate. Initial velocities were determined from progress curves by analyzing the data using Microsoft Excel.

The standard activity assay was performed in a total volume of 1.4 ml of air-saturated 50 mM MES, pH 6.0 (25°C) containing 160 μM biphenyl, 320 μM NADH, 1.8 μM ht-$BphG_{B356}$, 3.6 μM ht-$BphF_{LB400}$, and 0.6 μM of BPDO. The assay was initiated by adding the oxygenase after equilibrating the assay with all other components for 30 s. The reaction buffer and stock solutions used in the assay were prepared fresh daily. Stock solutions and protein samples were prepared anaerobically, stored under argon on ice, and withdrawn using a gas-tight syringe. The O_2 electrode was zeroed and calibrated on the day of use, as described previously (45). One unit of enzyme activity was defined as the quantity of enzyme required to consume 1 μmol of O_2/min.

Apparent steady-state kinetic parameters were determined as described previously (33). Biphenyl concentrations were varied from 0.5 μM to 160 μM. The solubility of biphenyl in 50 mM MES buffer (pH 6.0, 25°C), 44 μM, is similar to that in water (19, 33). Initial velocities determined at different substrate concentrations were fitted to the Michaelis-Menton equation using the least-squares fitting and dynamic weighting options of LEONORA (12).

Coupling Measurements. Coupling experiments were carried out using 50 mM MES (pH 6.0) at 25°C and either 160 μM biphenyl, 68 μM 2,2'-diClB, 80 μM 3,3'-diClB or 40 μM 4,4'-diClB. The same concentrations of BPDO components were used as in the standard assay, and reactions were initiated by adding the BPDO. Reactions were analyzed for the production of hydrogen peroxide and the depletion of biphenyl. Hydrogen peroxide production was determined by adding 650 U of catalase to the reaction mixture 3 min after initiation of the reaction. The amount of O_2 that was detected upon the addition of catalase was taken to represent 50% of the hydrogen peroxide produced during biphenyl transformation. Biphenyl depletion was determined by stopping the reaction after 1.5, 3, or 10 min by extracting the reaction mixtures using 1.5 volumes of hexane. The hexane extractions were analyzed for congener content by gas chromatography. Standard curves were prepared by using known amounts of each biphenyl; standards were treated identically to the test treatments.

Half-life Measurements. The respective half-lives of $BPDO_{Cam}$ and $BPDO_{LB400}$ at 57°C were determined spectrophotometrically. A sample of each BPDO was diluted 2.2 μM in MES buffer (pH 6.0) pre-equilibrated to 57°C. The sample was incubated at 57°C and its absorbance was continuously monitored at 323 nm.

Analytical Methods. SDS-PAGE analyses were performed using 12% resolving gels and Coomassie Blue staining according to standard protocols (3). Protein

concentration was determined using a bicinchoninic acid protein assay (Pierce) after removing interfering substances (8). Iron assays were performed using Ferene S and $FeCl_3$ as a standard (27). The content of acid-labile sulfur in the BPDO preparations was determined using *N,N*-dimethyl-*p*-phenylenediamine and Na_2S as a standard (11).

Spectrophotometric measurements were performed using a Varian, Cary 1E UV-Vis spectrophotometer equipped with a thermostatted cuvette holder and a circulating water bath. Concentrations of ht-$BphF_{LB400}$, ht-$BphG_{B356}$, and BPDO were determined spectrophotometrically using $\varepsilon_{326} = 9\ mM^{-1}cm^{-1}$ (13), $\varepsilon_{450} = 11.8\ mM^{-1}cm^{-1}$ (31), and $\varepsilon_{450} = 10.1\ mM^{-1}cm^{-1}$ (25), respectively. Gas chromatography was performed using a model 5890 gas chromatograph flame ionization detector, an HP 7673 autoinjector (Hewlett-Packard) and a DB-5 column. Nucleotide sequences were determined by the Nucleic Acid and Protein Services unit at the University of British Columbia using AmpliTaq FS DyeDeoxy terminator cycle sequencing chemistry (Applied Biosystems) and Centri-Sep columns (Princeton Separation, Adelphia, N.J.) to purify the extension products.

RESULTS

Purification of BPDO components. The respective yields of anaerobically purified $BPDO_{LB400}$ and $BPDO_{Cam1}$ were approximately 15 and 23 mg/L cell culture. Oxidized preparations of $BPDO_{LB400}$ and $BPDO_{Cam1}$ had R-values (A_{280}/A_{323}) of 10.8 and 8.6, respectively. Purified $BPDO_{LB400}$ contained 3.4 ± 0.5 mol of iron and 2.1 ± 0.7 mol of sulfur per mol of αβ-heterodimer. Purified $BPDO_{Cam1}$ contained 2.5 ± 0.4 mol of iron and 1.8 ± 0.3 mol of sulfur per mol of αβ-heterodimer. The R-values and Fe- and S-content of these preparations are similar to those reported for anaerobically purified preparations of $BPDO_{B356}$ (33), and indicate that the BPDOs essentially contain their full complements of Rieske-type [2Fe-2S] clusters and mononuclear Fe^{2+} centers.

Reconstitution of BPDO activity. The activity of BPDO was reconstituted under steady-state conditions using ht-$BphG_{B356}$ and ht-$BphF_{LB400}$ and monitored using an oxygen electrode. The sequences of $BphF_{LB400}$ and $BphF_{Cam1}$ are identical (39). Moreover, steady-state experiments performed using recombinant BphF in which the his-tag was removed established that the tag did not detectably affect O_2 utilization by BPDO. Finally, a previous study indicated the use of ht-$BphG_{B356}$ and the exchange of electron transfer components between closely related BPDOs does not significantly affect enzyme activity (32). It was thus concluded that differences in steady-state parameters of $BPDO_{LB400}$ and $BPDO_{Cam1}$, as determined using the conditions described in "Materials and Methods", reflect differences in the respective BPDOs of these systems. As observed for $BPDO_{B356}$, the steady-state parameters of $BPDO_{LB400}$ and $BPDO_{Cam1}$ depended on the concentrations of BphG and BphF. The determined kinetic parameters are thus referred to as apparent parameters as they were determined at fixed concentrations of O_2, ht-$BphG_{B356}$ and ht-$BphF_{LB400}$. The specific activities of $BPDO_{LB400}$ and $BPDO_{Cam1}$ were 0.27 ± 0.01 U/mg and 3.1 ± 0.4 U/mg, respectively. The R-value and specific activity of two different preparations of $BPDO_{LB400}$ were not significantly different.

Apparent specificities of BPDOs. Under all conditions studied, the steady-state consumption of O_2 by BPDO as a function of biphenyl concentration obeyed classical Michaelis-Menten kinetics (*i.e.*, random trends in the residuals were observed). At 25°C, the respective apparent specificities of $BPDO_{Cam1}$ and $BPDO_{LB400}$ for biphenyl were very similar (Table 5.1). However, their respective k_{cat}^{app} and K_m^{app} were very different: both parameters of $BPDO_{Cam1}$ were approximately an order of magnitude higher than those of $BPDO_{LB400}$. The apparent kinetic parameters of $BPDO_{LB400}$ were confirmed using two independent enzyme preparations.

The Michealis-Menten equation could also be fit to the initial rates of O_2 consumption by $BPDO_{Cam1}$ and $BPDO_{LB400}$ observed in the presence of 2,2'- and 3,3'-diClB. As observed for biphenyl, the K_m^{app}s of $BPDO_{LB400}$ for these two diClBs were significantly lower than those for $BPDO_{Cam1}$ (Table 5.1). Indeed, the K_m^{app}s of $BPDO_{Cam1}$ for 2,2'- and 3,3'-diClBs were so high, that the maximum rates occurred at concentrations of these compounds that apparently exceeded their respective solubility limits. A similar phenomenon was reported for $BPDO_{B356}$, and was suggested to arise from the partitioning of the diClB to the active site of the enzyme from the solid phase (33). Interestingly, the apparent specificity of $BPDO_{LB400}$ for 2,2'-diClB was approximately 2 times that for biphenyl (Table 5.1). The steady-state parameters of $BPDO_{Cam1}$ and $BPDO_{LB400}$ for 4,4'-diClB could not be estimated due to the low solubility of this compound (~0.27 μM in aqueous buffer) and the low initial rates of O_2 consumption. Thus, for 4,4'-diClB, only the maximum initial rates of O_2 consumption by $BPDO_{Cam1}$ and $BPDO_{LB400}$ are reported (Table 5.1).

Coupling of biphenyl transformation to O_2 utilization. In the presence of 160 μM biphenyl, the amount of O_2 consumed by each BPDO corresponded to the amount of biphenyl utilized (Table 5.1). Furthermore, no hydrogen peroxide, a possible uncoupling product, was detected upon the addition of catalase to these reaction mixtures. In

Table 5.1

Apparent steady state kinetic and coupling parameters of different BPDOs for selected biphenyl substrates

Congener	BPDO	k_{cat}^{app}	K_m^{app}	$k_{cat}^{app} / K_m^{app}$	H_2O_2[a]/O_2	rate of congener removal
		s^{-1}	μM	$\mu M^{-1} s^{-1}$		nmol· min^{-1}
biphenyl	Cam1	4.6 (0.2)	28.8 (2.6)	0.17 (0.05)	ND[b]	95[c]
	LB400	0.51 (0.03)	3.5 (1.4)	0.13 (0.07)	ND	41[c]
	B-356	7.3 (0.2)[d]	6.2 (0.5)	1.2 (0.1)	ND	89[c]
2,2'	Cam1	0.30 (0.02)	2.6 (0.7)	0.12 (0.03)	0.36 (0.007)	3.2 (0.3)[f]
	LB400	0.25 (0.004)	0.97 (0.1)	0.26 (0.02)	0.11 (0.005)	21 (4)[f]
	B-356	1.2 (0.1)[d]	2.6 (0.9)	0.5 (0.4)	0.56	4.5[f]
3,3'	Cam1	1.2 (0.08)	6.2 (0.8)	0.19 (0.02)	0.4 (0.05)	7.8 (2)[f]
	LB400	0.25 (0.01)	0.58 (0.09)	0.44 (0.06)	0.26 (0.06)	1.3[g]
	B-356	4.2 (0.1)[d]	3.3 (0.5)	1.3 (0.2)	0.16	17.3[f]
4,4'	Cam1	0.26 (0.08)[c]			0.26 (0.05)	2.6 (0.07)[f]
	LB400	0.13 (0.03)[c]			0.33 (0.06)	0.25 (0.2)[f]
	B-356	2.0 (0.1)[d]			0.33	4.3[f]

Experiments were performed using air-saturated 50 mM MES, pH 6.0 at 25°C. Numbers in parenthesis indicate standard deviation. [a]Includes the assumption that the amount of O_2 detected accounts for 50% of H_2O_2 produced; [b]ND, not detectable; [c]calculated from specific activity using 40 μM 4,4'-diClB; [d]data taken from Imbeault *et al.* (32); rates of congener removal and H_2O_2/O_2 ratios are based on data obtained after 1.5 min[c], 3 min[f] or 10 min[g].

contrast, the utilization of O_2 by each BPDO in the presence of each of the diClBs was uncoupled (Table 5.1). Consideration of the amount of congener removed clearly indicates that not all uncoupling resulted in H_2O_2 production. This is particularly striking in the case of 3,3'-diClB utilization by $BPDO_{LB400}$: surprising little congener was removed at saturating concentrations although the k_{cat}^{app} was comparable to that for 2,2'-diClB and the H_2O_2/O_2 ratio was not that much higher. This suggests that a significant amount of uncoupling resulted in H_2O production.

The extent of uncoupling between O_2- and diClB-utilization was dependent on both the isozyme and the diClB. For example, $BPDO_{Cam}$ was significantly more uncoupled in the presence of 2,2'-diClB than $BPDO_{LB400}$, although their k_{cat}^{app} with this substrate were similar. Moreover, there was no discernable trend between the degree of uncoupling and the steady-state kinetic parameters. Thus, uncoupling was not necessarily lowest for diClBs that were better substrates (higher $k_{cat}^{app} / K_m^{app}$) or that were turned over at higher maximal rates (higher k_{cat}^{app}). In $BPDO_{LB400}$ for example, the transformation of both 2,2'-diClB and 3,3'-diClB were uncoupled from O_2-utilization, although the dioxygenase had a higher apparent specificities for both of these congeners than for biphenyl.

Taking into account the k_{cat}^{app} and the degree of uncoupling (biphenyl/O_2), $BPDO_{Cam}$ transformed biphenyl and diClBs in the following order of apparent maximal rates at 25°C: biphenyl > 3,3'-diClB > 4,4'-diClB > 2,2'-diClB. In contrast, $BPDO_{LB400}$ transformed these compounds in the following order of apparent maximal rates: biphenyl > 2,2'-diClB > 3,3'-diClB > 4,4'-diClB. These results are consistent with the % congener removal as determined by GC analyses. More particularly, congener removal studies were performed with saturating quantities of congeners (*i.e.*, concentration >> K_m^{app}) and should thus reflect k_{cat}^{app}.

Temperature dependence of BPDO activity. The dependence of BPDO activity on temperature was investigated by performing the standard activity assay at temperatures from 4°C to 60°C. Under these conditions, BPDO is saturated with biphenyl, thus at temperatures below 45°C, the measured initial velocities reflect k_{cat}^{app}, which is consistent with what is generally observed in enzymatic reactions (12). Moreover, at any given temperature in this range, the activity of $BPDO_{Cam1}$ was higher than that of $BPDO_{LB400}$ (Fig. 5.2). Indeed, at 4°C, $BPDO_{LB400}$ had no detectable activity whereas $BPDO_{Cam1}$ still transformed biphenyl at a significant rate. However, the highest observed activity of $BPDO_{Cam1}$ occurred at a lower temperature than that of $BPDO_{LB400}$ (47°C vs. 55°C). As the drop in activity of the two isozymes probably reflects thermal denaturation of the respective BPDOs during the assay, the observed rates are referred to as k_{rel}. Thermodynamic parameters (Table 5.3) were derived from Arrhenius plots (30, 37) using the data up to 42.5°C and 35°C for $BPDO_{Cam1}$ and $BPDO_{LB400}$, respectively. The lower free energy of activation ($\Delta G^{\ddagger}$) of $BPDO_{Cam1}$ as compared to $BPDO_{LB400}$ is consistent with the former's higher k_{cat}^{app}. Finally, determination of the apparent steady-state parameters of the two BPDOs at 10°C revealed that their respective $k_{cat}^{app} / K_m^{app}$ were not significantly different, as observed at 25°C (Table 5.2).

Thermostability of BPDO. To better characterize the relative thermal stabilities of $BPDO_{Cam1}$ and $BPDO_{LB400}$, the respective half-lives of these proteins were determined spectrophotometrically at 57°C by continuously monitoring the decrease in absorbance due to loss of the Rieske-type [2Fe-2S] cluster. Accordingly, the half-lives of $BPDO_{Cam1}$ and $BPDO_{LB400}$ were 16 ± 2 min and 38 ± 8 min, respectively. The longer half-life of $BPDO_{LB400}$ at 57°C is consistent with the higher k_{rel} of $BPDO_{LB400}$ observed at temperatures above 50°C.

Figure 5.2 The effect of increasing temperature on the activities of $BPDO_{Cam1}$ (◆) and $BPDO_{LB400}$ (■) (n=3, error indicates standard deviation).

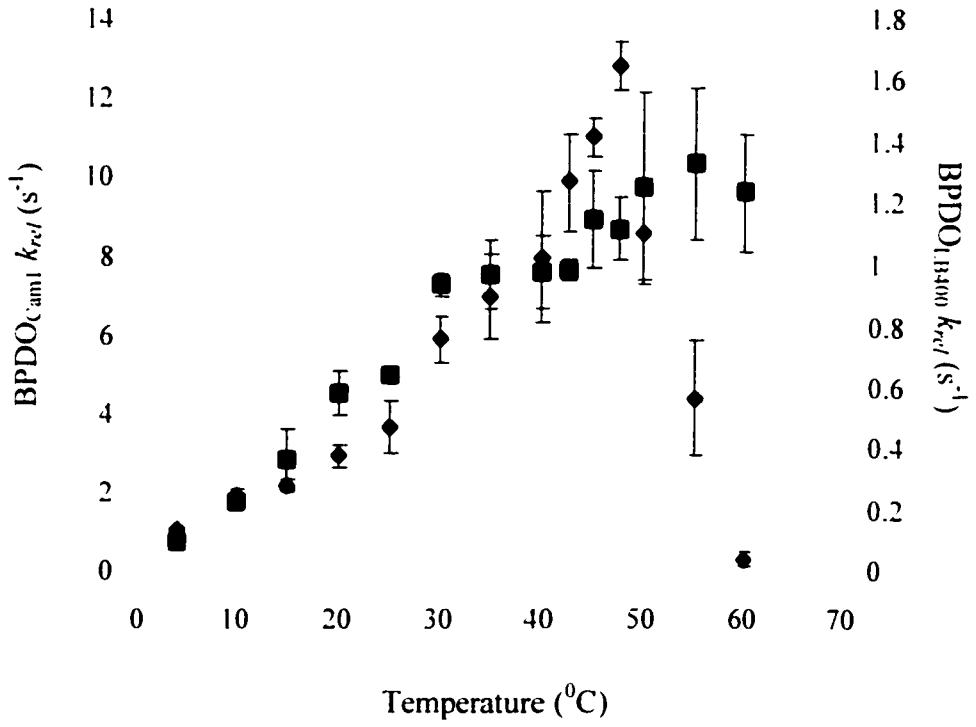
14
12
10
8
6
4
2
0
1.8
1.6
1.4
1.2
1
0.8
0.6
0.4
0.2
0
0
10
20
30
40
50
60
70
BPDO$_{Cam1}$ k_{rel} (s^{-1})
BPDO$_{H400}$ k_{rel} (s^{-1})
Temperature (^{0}C)

Table 5.2

Apparent steady-state kinetic parameters of BPDOs for biphenyl at two temperatures.

Temperature (°C)	BPDO	k_{cat}^{app}	K_m^{app}	$k_{cat}^{app} / K_m^{app}$
		s^{-1}	μM	X 10^6 $M^{-1}s^{-1}$
4	Cam-1	1.1 (0.1)	18.1(2.9)	0.06 (0.001)
	LB400	-[a]	-	-
10	Cam-1	2.2 (0.06)	10.8 (1.1)	0.20 (0.02)
	LB400	0.26 (0.01)	1.6 (0.3)	0.16 (0.03)

Experiments were performed using air-saturated 50 mM MES, pH 6.0. Values in parentheses represent standard errors. (n=3 or 4) . [a]No detectable O_2 utilization.

Table 5.3

Thermodynamic parameters of $BPDO_{Cam1}$ and $BPDO_{LB400}$ at 25 °C with biphenyl.

BPDO	$\Delta G^{\ddagger}$ (kJ mol^{-1})	$\Delta H^{\ddagger}$ (kJ mol^{-1})	$T\Delta S^{\ddagger}$ (kJ mol^{-1} K^{-1})
Cam1	69.9 ± 0.05	37.7 ± 2	-32.1 ± 2
LB400	74.2 ± 0.07	48.4 ± 5	-25.7 ± 5

DISCUSSION

The co-expression of either BPDO with the Fe-S-cluster-inserting machinery in *E. coli* yielded larger amounts of BPDOs from less starting culture and/or in fewer purification steps, than previously reported procedures for purification of BPDO oxygenases from either *E. coli* (2, 25, 32) or *Pseudomonas* (33). The specific activity of $BPDO_{LB400}$ was greater than that reported for aerobically purified preparations of the enzyme (2, 25), and the purities of $BPDO_{Cam1}$ and $BPDO_{LB400}$ were similar to that reported for anaerobically purified preparations of $BPDO_{B356}$ (33). In addition, preparations of $BPDO_{Cam1}$ and $BPDO_{LB400}$ contained a full complement of Rieske-type [2Fe-2S] cluster and mononuclear Fe^{2+} centers.

The kinetic parameters of $BPDO_{Cam1}$ and $BPDO_{LB400}$ for biphenyl and the diClBs are consistent with previous *in vivo* and *in vitro* studies. Thus, whole cells of Cam-1 removed a higher percentage of 4,4'-diClB than 2,2'-diClB in a PCB mixture (38). Similarly, both strain LB400 (23, 38) and an aerobic preparation of $BPDO_{LB400}$ (32) removed diClBs in the same order of preference as the order of maximal rates reported here (2,2'-diClB > 3,3'-diClB > 4,4'-diClB). Interestingly, the removal of 2,2'-diClBs by $BPDO_{Cam1}$ was detected although whole cells of Cam-1 did not transform pure 2,2'-diClB (data not shown). It is possible that other factors, such as PCB transport across the cell membranes, might determine PCB transformation by whole cells. Nevertheless, the reactivities of $BPDO_{LB400}$ and $BPDO_{B356}$ (33) for diClBs reflect the congener preferences of their respective parent strains. It is more likely that differences between the *in vitro* and whole cell assays reflect the greater sensitivity of the former. Finally, it is noted that previous experiments failed to detect the significant differences in the reactivities of $BPDO_{B356}$ and $BPDO_{LB400}$ (32). However, those studies were performed using aerobic preparations of the oxygenases, a discontinuous enzyme assay, and different reaction

conditions. Moreover, they reported a lower k_{cat}^{app} s for biphenyl, and higher K_m^{app} s by 3 to 10 fold lower (32).

The preference of $BPDO_{Cam1}$ for 3,3'-diClB is particularly interesting in light of the sequence similarity of this enzyme with that of $BPDO_{KF707}$. The α-subunits of these enzymes, which harbor the principal specificity determinants, differ by a single residue (Ala178 in $BPDO_{Cam1}$ is Val in $BPDO_{KF707}$: Fig. 5.3) whereas their β-subunits differ by five residues. Although KF707-type BPDOs have been noted for their strong preference for 4,4'-diClB over 2,2'-diClB (41), the reactivity of these enzymes for 3,3'-diClB has not been reported. The specificity of $BPDO_{Cam1}$ is very similar to that of $BPDO_{B356}$ (33). Although the latter enzyme is less related to $BPDO_{Cam1}$, $BPDO_{KF707}$, and $BPDO_{LB400}$ (the respective BPDOs share approximately 75% sequence identity), regions III and IV of the $BPDO_{B356}$ α-subunit, identified by Mondello as key specificity determinants (41), are very similar to those of $BPDO_{KF707}$ (Figure 5.3). These considerations suggest that the substrate specificity of $BPDO_{Cam1}$ represents that of KF707-type BPDOs.

The kinetic data clearly indicate that 2,2'-diClB is a better substrate for $BPDO_{LB400}$ than biphenyl. Previous *in vitro* studies had indicated that the specific activity of $BPDO_{LB400}$ for 3-chlorobiphenyl (3-ClB) and 2,5-diClB is higher than for biphenyl (2). The latter data probably reflect maximal turnover rates and not specificity constants. Nevertheless, these data present the interesting possibility that $BPDO_{LB400}$ may have adapted to PCB degradation.

The uncoupling data point to an important factor in the reactivities of BPDOs: how the PCB congeners fit into the active site. Thus, uncoupling is thought to occur in oxygenases when the substrate is not optimally positioned in the active site with respect to the activated oxygen intermediate that is generated during the catalytic cyclic (*e.g.*, 42c). Suboptimal positioning can reflect the occurrence of more than one binding

configuration or substrate mobility in the active site. Under such conditions, H_2O_2 or water can be produced, presumably due to reaction of the activated oxygen intermediate with solvent species. The observation of multiple transformation products from particular congeners (2, 42d) suggests that those congeners are bound by BPDO in more than one orientation or are mobile in the active site. The existence of multiple binding modes is distinct from binding affinity. For example, $BPDO_{LB400}$ does not transform 4,4'-diClB efficiently, but the enzyme clearly binds 4,4'-diClB fairly well as O_2 is consumed at a considerable rate in the presence of this congener. Thus, it is possible that $BPDO_{LB400}$ binds 4,4'-diClB with the same affinity as KF707-type BPDOs, including $BPDO_{Cam1}$, but that this congener is bound in an unproductive orientation in LB400-type enzymes.

The principal distinguishing characteristic of cold-adapted enzymes is a significant decrease of $\Delta H^{\ddagger}$ with respect to their mesophilic homologs, which leads to a higher k_{cat}, especially at lower temperatures (37). Cold-adapted enzymes also tend to be less thermostable than their mesophilic homologs. This is thought to be a consequence of the increased flexibility of the structure required to improve catalysis at low temperatures (37). The comparative study of $BPDO_{Cam1}$ and $BPDO_{LB400}$ could be interpreted to indicate that $BPDO_{Cam1}$ is cold-adapted. The apparent optimal k_{rel} of $BPDO_{Cam1}$ is reached at lower temperature than $BPDO_{LB400}$, and the half-life of $BPDO_{Cam1}$ at 57°C is approximately half that of $BPDO_{LB400}$. These two observations indicate that the T_m of $BPDO_{Cam1}$ is much lower than that of $BPDO_{LB400}$. While T_m is not a thermodynamic parameter of protein stability, lower T_m's appear to be always associated with decreased stability (4c, 42b). However, two considerations indicate that $BPDO_{Cam1}$ is not cold-adapted. First, the steady-state kinetic parameters of $BPDO_{Cam1}$ for biphenyl at 25°C are similar to those reported for a mesophilic enzyme, $BPDO_{B356}$, determined under similar conditions (33). Second, as noted above, the α-subunit of $BPDO_{Cam1}$ is so similar to that

of another mesophilic enzyme, $BPDO_{KF707}$, that it is highly likely that these enzymes have identical catalytic properties.

It is nonetheless possible that $BPDO_{Cam1}$ is less stable than $BPDO_{KF707}$. Consideration of the five amino acid differences between β-subunits of $BPDO_{Cam1}$ and $BPDO_{LB400}$ (Figure 5.3b) in the context of the three dimensional structure of $BPDO_{B356}$ reveals that Arg41Ser occurs at the interface of two β-subunits, and corresponds to an increase in the polarity of this residue in $BphE_{Cam1}$. Hydrophobic interactions are stabilized by heat; thus, decreasing the hydrophobicity of interactions between β_{Cam1} subunits might reduce the thermostability of $BPDO_{Cam1}$ (22). Residues 58 and 59 of β_{356} are located at an interface of the α- and β-subunits, whereas residues 65 and 104 of β_{356} are located at a possible interface of two β-subunits.

Although the current data suggest that $BPDO_{Cam1}$ is not cold-adapted, the differences between $BPDO_{Cam1}$ and $BPDO_{LB400}$ nevertheless are consistent with the differences between their respective parental strains, Cam-1 and LB400 (38). Thus, whole cells of Cam-1 remove certain PCB congeners more efficiently than LB400 at 7°C. Furthermore, PCB removal by LB400 increased at high temperature; in contrast, high temperature inhibited PCB removal by Cam-1. Both observations are consistent with the higher k_{cat}^{app} of $BPDO_{Cam1}$ for biphenyl at low temperature and its low thermal stability compared to $BPDO_{LB400}$.

Thus, it will be interesting to compare the activity of $BPDO_{KF707}$ with $BPDO_{Cam1}$ and $BPDO_{LB400}$. If $BPDO_{KF707}$ has similar activities and thermostability as $BPDO_{Cam1}$, then determining the kinetic parameters of recombinant BPDOs previously generated by shuffling *bphA* genes from LB400 and KF707 may reveal if broad substrate range and low specific activity are necessarily linked. Otherwise, if $BPDO_{KF707}$ has similar

activities and thermostability as $BPDO_{LB400}$, then the relation between subunit interaction and BPDO activity should be further investigated.

Thus, this analysis can be applied to generate recombinant enzymes, which could reveal if broad substrate specificity and low catalytic activity are necessarily linked. Furthermore, applications of the current analysis could determine the effectiveness of rationally designing BPDOs that have improved characteristics.

Figure 5.3 Alignment of amino acid sequences of terminal oxygenase subunits BphA (A) and BphE (B) from $BPDO_{Cam1}$ and $BPDO_{LB400}$. Differences in amino acid sequences are highlighted. Arrows indicate residues that coordinate the mononuclear Fe^{2+} center: (*) indicate residues that coordinate the Rieske-type [Fe2-S2] cluster.

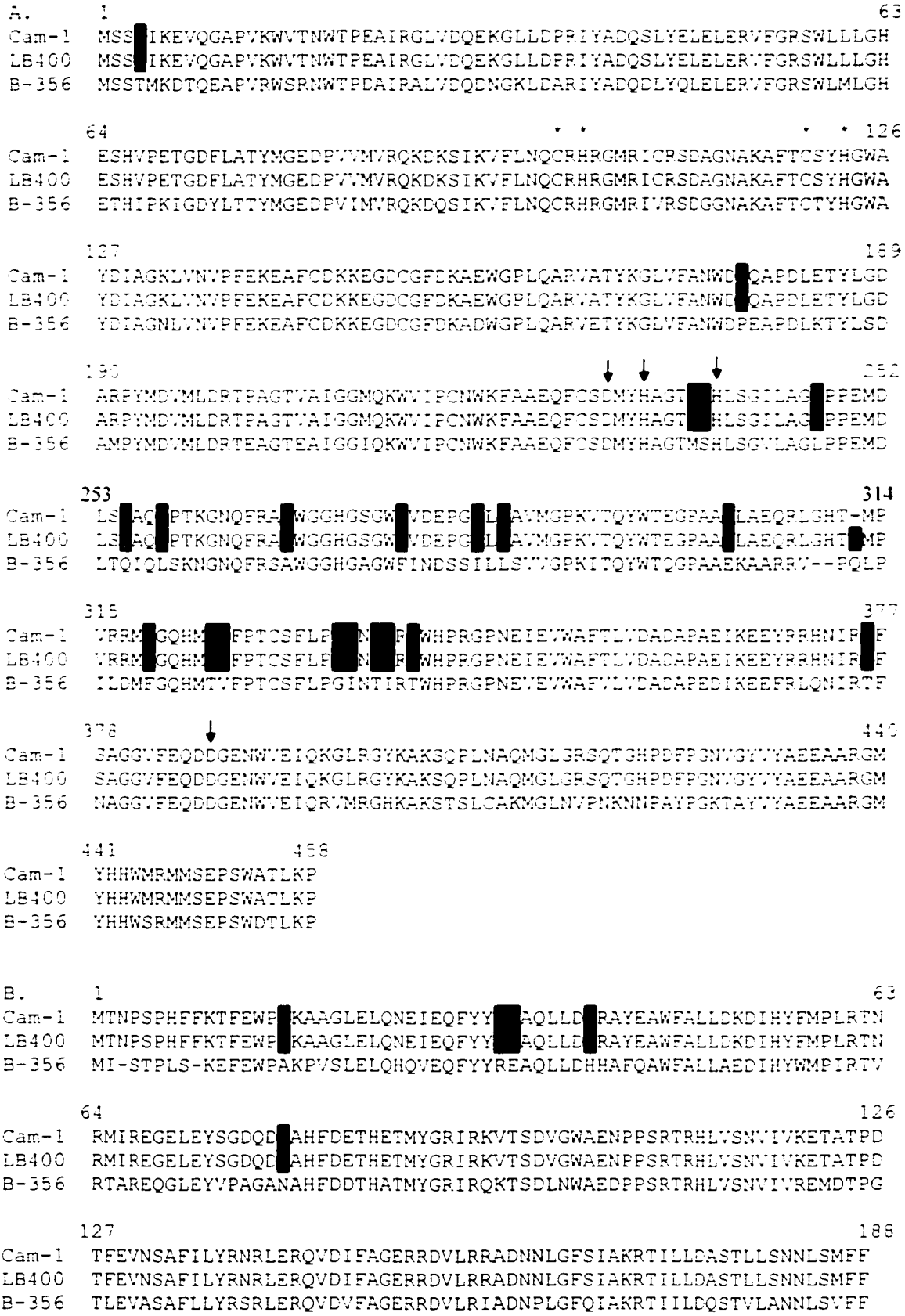
A.
Cam-1
LB400
B-356
B.
Cam-1
LB400
B-356

ACKNOWLEDGEMENTS

This work was supported by Natural Sciences and Engineering Research Council of Canada Strategic Grants 224153-99 (to L.D.E. and J.B.P.) and to W.W.M. E.R.M. and N.Y.R.A. are recipients of Natural Sciences and Engineering Research Council of Canada postgraduate scholarships.

We thank Professor Michel Sylvestre (Institut National de la Recherche Scientifique-Santé, Université du Québec) for providing the expression system for ht-$BphG_{B356}$; Manon M.J. Couture for providing the expression system for ht-$BphF_{LB400}$, and Pascal D. Fortin and Yong Ge (Department of Microbiology and Immunology, University of British Columbia) for constructing pPAISC. Frederic H. Vaillancourt (Department of Microbiology and Immunology, University of British Columbia) generously provided DHBD.

REFERENCES

1. Abramowicz, D. A. (1990) *Critical Reviews in Biotechnology*. **10**:241-251

2. Arnett, C. M., Parales, J. V., and Haddock, J.D. (2000) *Applied and Environmental Microbiology*. **66**:2928-2933

3. Ausubel, F. M., Brent, R., Kingston, R.E., Moore, D.D., Seidman, J.G., and J. A. S., and Struhl, K. (1992) *Short Protocols in Molecular Biology*, 2 ed. Greene Publishing Associates and John Wiley & Sons, New York.

4. Barriault, D., Pelletier, C., Hurtubise, Y., and Sylvestre, M. (1997) *Int. Biodeterior. Biodegrad.* **39**:311-316

4b. Barriault, D., Simard, C., Chatel, H., and Sylvestre, M. (2001) *Can. J. Microbiol.* **47**:1025-32

4c. Becktel W.J., and Schellman, J.A. (1987) *Biopolymers*. **26**:1859-1877

5. Bedard, D. L., Unterman, R., Bopp, L.H., Brennan, M.J., Haberl, M.L., and Johnson, C. (1986) *Applied and Environmental Microbiology*. **51**:761-768

6. Bedard, D. L., and Haberl, M. L. (1990) *Microbial Ecology*. **20**:87-102

7. Bopp,L. H. 1986. *Journal of Industrial Microbiology*. **1**:23-29

8. Brown, R. E., Jarvis, K. L., and Hyland, K. J. (1989) *Analytical Biochemistry*. **180**:136-139

9. Bruhlmann F., and Wilfred, C. (1999) *Biotechnology and Bioengineering*. **63**: 544-551

10. Chebrou, H., Hurtubise, Y., Barriault, D., and Sylvestre, M. (1999) *Journal of*

Bacteriology. **181**:4805-4811

11. Chen, J.-S., and Mortenson, L. (1977) *Analytical Biochemistry*. **79**:157-165

12. Cornish-Bowden, A. (1995) *Fundamentals of enzyme kinetics*. Portland Press, London

13. Couture, M. M.-J., Colbert, C. L., Babini, E., Rosell, F.I., Mauk, G., Bolin, J.T., and Eltis, L.D. (2001) *Biochemistry*. **40**:84-92

14. Erickson B. D., and Mondello, F.J. (1993) *Applied and Environmental Microbiology*. **59**:3858-3862

15. Feller, G., Arpigny, J. L., Narinx, E., and Gerday, C. (1997) *Comp. Biochem. Physiol*. **3**:495-499

16. Feller, G., and Gerday, C. (1997) *Cellular and Molecular Life Sciences*. **53**:830-841

17. Feller, G., Narinx, E., Arpigny, J.L., Aittaleb, M., Baise, E., Genicot, S., and Gerday, C. (1996) *FEMS Microbiology Reviews*. **18**: 189-202

18. Feller, G., Sonnet, P., and Gerday, C. (1995) *Applied and Environmental Microbiology*. **61**: 4474-4476

19. Foreman, W. T., and Bidleman, T. F. (1985) *Journal of Chromatography*. **330**:203-216

20. Furukawa, K. (2000) *Current Opinion in Biotechnology*. **11**:244-249

21. Furukawa, K., and Miyazaki, T. (1986) *Journal of Bacteriology*. **166**:392-398

22. Gerday, C., Aittaleb, M., Arpigny, J.L., Baise, E., Chessa, J.-P., Garsoux, G., Petrescu, I., and Feller, G. (1997) *Biochimica et Biophysica Acta*. **1342**: 119-131

23. Gibson, D. T., Cruden, D. L., Haddock, J. D., Zylstra, G. J., and Brand, J. M. (1993) *Journal of Bacteriology*. **175**:4561-4564

24. Gibson, D.T., and Parales, R.E. (2000) *Current Opinion in Biotechnology*. **11**:236-243

25. Haddock, J. D., and Gibson, D.T. (1995) *Journal of Bacteriology*. **177**:5834-5839

26. Haddock, J. D., Horton, J. R., and Gibson, D.T. (1995) *Journal of Bacteriology*. **177**:20-26

27. Haigler, B. E., and Gibson, D.T. (1990) *Journal of Bacteriology*. **172**:457-464

28. Hall, J.G. (1985) *Molecular Biol. Evol.* **2**:251-269

29. Hofer, B., Eltis, L. D., Dowling, D. N., and Timmis, K. N. (1993) *Gene*. **130**:47-55

30. Hoyoux, A., Jennes, I., Dubois, P., Genicot, S., Dubail, F., Francois, J.M., Baise, E., Feller, G., and Gerday, C. (2001) *Applied and Environmental Microbiology*. **67**:1529-1535

31. Hurtubise, Y., Barriault, D., Powlowski, J., and Sylvestre, M. (1995) *Journal of Bacteriology*. **177**:6610-6618

32. Hurtubise, Y., Barriault, D., and Sylvestre, M. (1998) *Journal of Bacteriology*. **180**:5828-5835

33. Imbeault, N. Y. R., Powlowski, J. B., Colbert, C. L., Bolin, J. T., and Eltis, L. D. (2000) *Journal of Biological Chemistry*. **275**: 12430-12437

34. Kimura, N., Nishi, A., Goto, M., and Furukawa, K. (1997) *Journal of Bacteriology*. **179**:3936-3943

35. Kulakova, L., Galkin, A., Kurihara, T., Yoshimura, T., and Esaki, N. (1999) *Applied and Environmental Microbiology*. **65**:611-617

36. Kumamaru, T., Suenaga, H., Mitsuoka, M., Watanabe, T., and Furukawa, K. (1998) *Nature Biotechnology*. **16**:663-666

37. Lonhienne, T., Gerday, C., and Feller, G. (2000) *Biochimica et Biophysica Acta*. **1543**:1-10

38. Master, E. R., and Mohn, W. W. (1998) *Applied and Environmental Microbiology*. **64**: 4823-4829

39. Master, E. R., and Mohn, W.W. (2001) *Applied and Environmental Microbiology*. **67**: 2669-2676

40. Miroux, B., and Walker, J. E. (1996) *Journal of Molecular Biology*. **260**: 289-298

41. Mondello, F. J., Turcich, M. P., Lobos, J. H., and Erickson, B. D. (1997) *Applied and Environmental Microbiology*. **63**:3096-3103

42. Nakamura, M., Saeki, K., and Takahashi, Y. (1999) *J. Biochem*. **126**:10-18

42b. Privalov P.L., and Potekhin, S.A. (1986) *Methods Enzymol*. **131**:4-51

42c. Raag, R., and Poulos, T.L. (1991) *Biochemistry* **30**:2674-2684

42d. Seeger, M., Zielinski, M., Timmis, K.N., Hofer, B. (1999) *Appl. Environ. Microbiol*. **65**:3614-3621

43. Studier, F. W., Rosenberg, A. H., Dunn, J. J., and Dubendorff, J. W. (1990) *Methods in Enzymology*. **185**:60-89

44. Suenaga, H., Nishi, A., Watanabe, T., Sakai, M., and Furukawa, K. (1999) *Journal*

of Bioscience and Bioengineering. **87**:430-435

45. Vaillancourt, F. H., Han, S., Fortin, P. D., Bolin, J. T., and Eltis, L. D. (1998) *Journal of Biological Chemistry*. **273**: 34887-34895

46. Viallard, V., Poirier, I., Cournoyer, B., Haurat, J., Wiebkin, S., Ophel-Keller, K., and Balandreau, J. (1998) *International Journal of Systematic Bacteriology*. **48**:549-563

Chapter 6

Rieske-Type Iron-Sulfur Cluster Assembly and Reassembly in Biphenyl Dioxygenase Mediated by the Iron-Sulfur Cluster Assembly Gene Products from *Pseudomonas aeruginosa* PA01

ABSTRACT

In the aerobic microbial degradation of a variety of aromatic hydrocarbons including biphenyl, naphthalene, benzene, and toluene, the initial reaction is generally catalyzed by a multicomponent oxygenase system including one or more Fe-S clusters. One such enzyme is biphenyl dioxygenase (BPDO), an NADH-dependent aromatic ring-hydroxylating dioxygenase that transforms biphenyl and various polychlorinated biphenyls (PCBs) to their dihydrodihydroxy-derivatives. The iron-sulfur cluster (*isc*) assembly genes, *iscRSUAhscBAfdxorf3*, were cloned from *Pseudomonas aeruginosa* PA01, and shown to bolster the production of Rieske-type iron-sulfur containing oxygenase components of biphenyl dioxygenases in an *E. coli* coexpression system. Two methods of generating apo-BPDO were developed, and these preparations were used to test *in vitro* reconstitution of the Fe-S clusters by crude extracts containing overexpressed *isc* gene products. On the basis of visible CD spectroscopy and enzymatic activity measurements, it appeared that the iron-sulfur cluster was reassembled in oxidatively-damaged BPDO. These results suggest that co-expression of the *isc* gene cluster may allow engineering of bioremediation systems that not only allow more efficient expression of key degradative oxygenases, but that also maintain the levels of active proteins during time of localized oxidative stress.

INTRODUCTION

The initial reaction in aerobic microbial degradation of aromatic hydrocarbons is generally catalyzed by a multicomponent oxygenase system requiring one or more Fe-S cluster prosthetic groups. Biphenyl dioxygenase is a typical aromatic ring-hydroxylating dioxygenase, utilizing O_2 and NADH to transform biphenyl and polychlorinated biphenyls (PCBs) to the corresponding dihydrodihydroxy derivatives (Fig. 6.1). Dihydroxylation destabilizes the ring and prepares it for subsequent enzymatic cleavage. The biphenyl dioxygenase system comprises an FAD-containing reductase, a Rieske-type [2Fe-2S] ferredoxin, and a two-subunit oxygenase component (BPDO) of $\alpha_3\beta_3$ constitution that contains a Rieske-type [2Fe-2S] cluster and a mononuclear iron center (1-6). The iron atoms of Rieske-type [2Fe-2S] clusters are ligated by two histidine and two cysteine residues, differing from the four-cysteine ligation pattern found in plant-type ferredoxins (7). Structural and spectroscopic studies of related dioxygenases indicate that catalysis occurs at the mononuclear iron center, while the reductase component, the [2Fe-2S] cluster ferredoxin, and the oxygenase [2Fe-2S] cluster transfer electrons from NADH to the active site iron (8-10).

Although it is possible for the Fe-S clusters of proteins to be assembled *in vitro* using free iron and sulfide, iron-sulfur cluster assembly in living organisms is coordinated by a set of highly conserved gene products encoded by *iscSUAhscBAfdx* (11). A wealth of genetic and biochemical data has implicated these gene products at various steps in the iron-sulfur cluster assembly process. The first step in Fe-S cluster biosynthesis appears to involve sulfur transfer from IscS to IscU (12;13). IscS is an L-cysteine desulfurase that converts cysteine to alanine and elemental sulfur (14;15). The sulfur is transferred to the scaffold protein, IscU, where a transient cluster is assembled for donation to a target apoprotein (16;17): IscA is proposed to be an alternate scaffold protein (18;19). The *isc* cluster-encoded adrenodoxin-type ferredoxin (20), Fdx, may be

involved in the reduction of S^0 and/or Fe^{3+} (21), or it might provide the reducing equivalents necessary for Fe-S cluster transfer into an apoprotein. The molecular chaperone homologues, HscA and HscB, have been shown to form a complex with IscU *in vitro*, but the physiological relevance of this complex still remains to be elucidated (22-24). Finally, it has been suggested that IscR senses the Fe-S cluster assembly status in the cell, autoregulates its own expression, and consequently represses the expression of the Fe-S cluster assembly proteins (25).

Isc gene products have been implicated in both *de novo* iron-sulfur cluster assembly and iron-sulfur cluster repair. Thus, Takahashi and coworkers have shown that the overexpression of a variety of Fe-S cluster-containing ferredoxins is significantly improved when co-expressed with the *isc* gene cluster from *E. coli* (26). They have also shown that the process of Fe-S cluster assembly relies on the sequential association and dissociation of IscS, IscU, IscA, HscB, HscA, Fdx, and Orf3 (24). A repair function has recently been attributed to IscS, which was shown to convert a dinitrosyl iron complex, formed by exposure of a ferredoxin to nitric oxide, to the [2Fe-2S] cluster form in the presence of L-cysteine *in vitro* (27).

In our studies of biphenyl dioxygenases, we encountered some enzymes whose Fe-S cluster containing α-subunit, specifically, was very difficult to express in soluble form. Furthermore, it has recently been shown that in the presence of certain dichlorinated biphenyls, O_2 utilisation is significantly uncoupled from aromatic substrate hydroxylation, releasing O_2 derivatives such as H_2O_2 (28). Such reactive oxygen species are capable of destroying iron-sulfur clusters, a situation that could easily arise in the case of BPDO, where the catalytic site and the Fe-S cluster are separated by 12 Å (8, Colbert *et al.*, in preparation). Limitations in the assembly and repair of the Fe-S cluster of BPDO represent potential impediments to the application of this enzyme for bioremediation. Such limitations might be overcome by co-expression with the *isc* cluster proteins.

In this study, we report the cloning and sequencing of the *isc* gene cluster from *Pseudomonas aeruginosa* PA01, comprising *iscRSUAhscBAfdxorf3*, and demonstrate its ability to bolster the expression levels of various BPDOs. We also examine the capacity of the *isc*-encoded proteins to repair oxidatively-damaged BPDO Fe-S cluster. Taken together, these findings may eventually lead to the engineering of chlorinated biphenyl-degrading strains that not only make more BPDO, but also maintain the levels of competent enzymes during times of localized oxidative stress.

Figure 6.1 BPDO of *Comamonas testosteroni* B-356. The enzyme comprises an FAD-containing reductase (BphG), a Rieske-type ferredoxin (BphF), and an oxygenase, which contains a Rieske-type [2Fe-2S] cluster and a catalytic mononuclear iron center. Biphenyl is stereospecifically hydroxylated at positions 2 and 3, yielding *cis*-(2*R*,3*S*)-dihydroxy-2,3-dihydrobiphenyl.

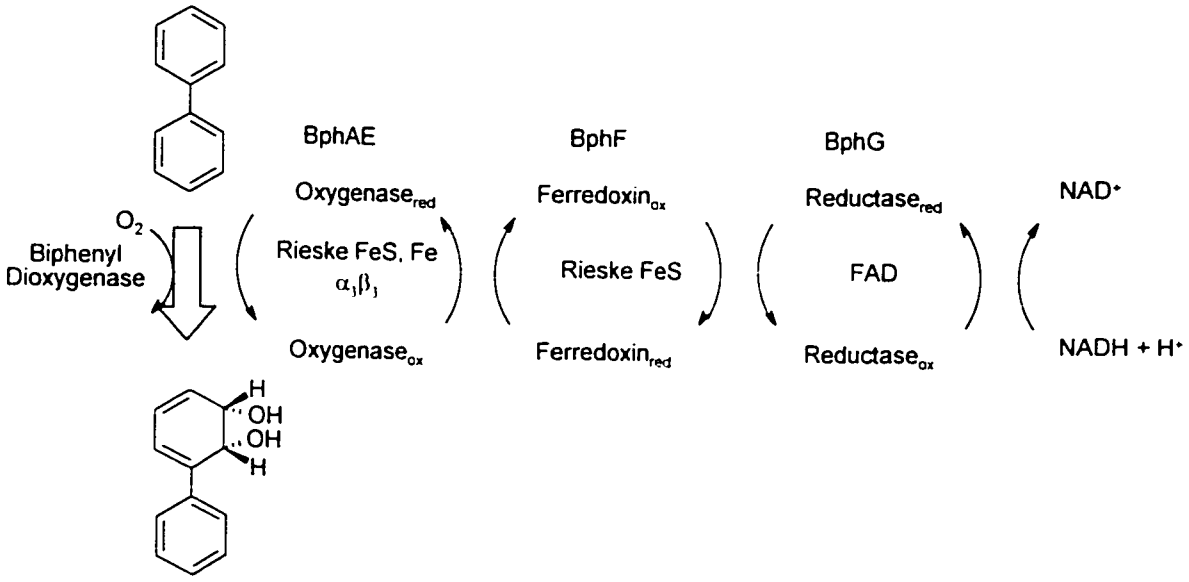
BphAE
BphF
BphG
Oxygenase$_{red}$
Ferredoxin$_{ox}$
Reductase$_{red}$
NAD$^+$
O_2
Biphenyl
Dioxygenase
Rieske FeS, Fe
$\alpha_3\beta_3$
Rieske FeS
FAD
Oxygenase$_{ox}$
Ferredoxin$_{red}$
Reductase$_{ox}$
NADH + H$^+$
H
OH
OH
H

EXPERIMENTAL PROCEDURES

Materials- Biphenyl was purchased from Anachemia (Quebec, Canada), and L-cysteine (minimum 98% (TLC)) from Sigma Chemical Co. (MO, USA). Restriction enzymes and *Pfu*I polymerase were purchased from Promega (WI, USA) and Stratagene (CA, USA), respectively. The thermostable polymerase, *Taq* Hifi, purchased from Invitrogen (ON, Canada), was used for the cloning of the *isc* genes from *Pseudomonas*. Synthetic oligonucleotides for the construction of pT7-7AE-3_{B356}, and for cloning of the *isc* genes from *Pseudomonas aeruginosa* PA01, are described in Table 6.1, and were obtained either from the Sheldon Biotechnology Center (McGill University, Montreal, Canada), or the Nucleic Acid and Protein Services unit (NAPS), Biotechnology Laboratory, University of British Columbia (Vancouver, Canada). Oligonucleotides for *isc* gene sequencing were purchased from BioCorp Inc. (Montreal, Canada) (sequences not shown), and were used in conjunction with the CEQ DTCS (dye terminator cycle sequencing) kit (Beckman, USA). All other chemicals were of analytical or HPLC grade.

Bacterial Strains and Plasmids- Strains used for DNA propagation or protein expression, and plasmids, are described in Table 6.1. The plasmid, pQE31AE (2), for cloning of *bphAE* from *Comamonas testosteroni* B-356 was generously provided by Dr. Michel Sylvestre (INRS-IAF, Montreal, Canada). Strains harboring pT7-7, or its derivatives, pT7-7AE-3, pT7-7a, and pT7-6a, were grown in the presence of ampicillin (100 μg/ml) or carbenicillin (100 μg/ml). Strains harboring pRKNMC, pRKISC, pPAISC-1, or pPAISC-2 were grown in the presence of tetracycline (20μg/ml). For BPDO expression, strains were grown in Terrific Broth (29)

Table 6.1 Plasmids, strains and oligonucleotides used in this study

Strain, plasmid, or oligonucleotide	Relevant genotype/properties	Reference
Pseudomonas aeruginosa PA01	Chromosomal DNA encoding *iscRSUAhscBAfdxorf3* between 4267115 and 4274299 bp	(30)
E.coli C41[DE3]	Mutant *E.coli* BL21[DE3]	(31)
Plasmids		
pT7-7 and pT7-6	T7 promoter, ColE1 origin, Ap^r	(32)
pT7-7AE-3_{B356}	pT7-7 carrying $bphAE_{B356}$, Ap^r	This study
pT7-7a	pT7-7 carrying $bphAE_{Cam1}$, Ap^r	(Chapter 5)
pT7-6a	pT7-6 carrying $bphAE_{LB400}$, Ap^r	(33)
pUC18Not	Ap^r, polylinker in the *lacZ* gene	(34)
pRKNMC	IncP1 replicon, *lac* promoter, Tc^r	(26;35)
pRKISC	pRKNMC carrying *iscRSUAhscBAfdxorf3* from *Escherichia coli*, Tc^r	(26;35)
pPAISC-1 and pPAISC-2	pRKNMC carrying *iscRSUAhscBAfdxorf3* cluster from *Pseudomonas aeruginosa* PA01, Tc^r	This study
Oligonucleotides		
AE-NdeI (*NdeI* restriction site underlined)	5'-CAGTGGATCCCCATATGAGTTC GACTATGAAAGA-3'	This study
AE-BglII (*BglII* restriction site underlined)	5'-GCGTTGGTAAAGATCTTGGTCC GCGT-3'	This study
ISC9 (*XbaI* restriction site underlined)	5'-GC T CTA GAT GGC TAG TCC CGT TCC TC-3'	This study
ISC8 (*XbaI* restriction site underlined)	5'-CAC TCT AGA CCT AAT TAC TCG GAT AAG AGC-3'	This study

Ap^r, ampicillin resistance; Tc^r, tetracycline resistance

supplemented with 0.1 mg/ml ferric ammonium citrate. Culture media were inoculated with 1% (v/v) of an overnight culture and grown at 37^0C until the A_{600} of the culture reached 0.9-1.0. Expression was then induced by addition of isopropyl-1-thio-β-D-galactopyranoside to a final concentration of 1 mM, and the culture was transferred to 20^0C (Cam-1 and LB400) or 25^0C (B-356), and incubated for an additional 18 hours before harvesting by centrifugation.

DNA Manipulations and Amplification- Plasmid DNA was purified using the Wizard Plus Minipreps kit (Promega, WI, USA). Purified chromosomal DNA from *Pseudomonas aeruginosa* PA01 was kindly provided by Professor Robert E.W. Hancock from The University of British Columbia (BC, Canada). DNA was digested, ligated, and transformed into *E. coli* using standard protocols (36).

For the construction of pT7-7AE-3, DNA corresponding to the initial fragment of *bphA* from *Comamonas testosteroni* B-356 was amplified by polymerase chain reactions containing: 265 ng of template DNA (pQE31AE), 2.5 units of *Pfu* polymerase, 10 nmol of each dNTP, and 30 pmol of each oligonucleotide primer, AE-NdeI and AE-BglII (Table 6.1), in a final volume of 25 µl. Twenty temperature cycles were performed using a DNA thermal cycler (Perkin-Elmer) as follows: 94^0C for 1 min, 55^0C for 2 min, and 72^0C for 45 s.

For cloning of the *isc* genes from *Pseudomonas aeruginosa*, DNA was amplified by polymerase chain reactions containing 100 ng of chromosomal DNA, 8 units of *Taq* HiFi polymerase, 80 nmol of each dNTP, and 120 pmol of each oligonucleotide primer, ISC8 and ISC9 (Table 6.1), in a final volume of 50 µl. A total of twenty-two temperature cycles were performed using a DNA thermal cycler as follows: one cycle 94^0C for 5 min, 52^0C for 2 min, and 70^0C for 5 min; four cycles 94^0C for 1 min, 52^0C for 1 min, and 70^0C for 5 min; seventeen

cycles 94^{0}C for 1 min, 63^{0}C for 1 min, and 70^{0}C for 5 min; an additional 7 min at 70^{0}C. The resulting DNA fragment was cloned as an *XbaI* fragment into pUC18Not.

For DNA sequencing, DNA was amplified using polymerase chain reactions containing 165 ng of plasmid DNA, and 3.2 pmol of each oligonucleotide primer (sequences not shown), in a final volume of 20 µl. Primers were designed based on the reported genomic sequence of the *isc* gene cluster (30). The thermostable DNA polymerase, each dye-labeled terminator ddNTP, and each dNTP were used at concentrations of 25% that of the recommended protocol (Beckman). Thirty temperature cycles were performed using a heated lid DNA thermal cycler (Perkin-Elmer), after a hot start of 1 min at 96 ^{0}C, as follows: 96 ^{0}C for 20 sec, 50 ^{0}C for 20 sec, and 60 ^{0}C for 4 min. After ethanol precipitation, the PCR products were analyzed using the Beckman CEQ DNA Analysis System at the Center for Structural and Functional Genomics (Concordia University, Montreal, Quebec, Canada). The *isc* genes were also sequenced at BioS&T Inc. (Montreal, Canada).

Anaerobic Manipulations- All anaerobic manipulations were performed in a Vacuum Atmospheres glove box under an argon atmosphere (< 2 ppm O_2) (University of Georgia), or in a nitrogen atmosphere (< 2 ppm O_2) MBraun UniLab Workstation.

Crude Extract Preparation- For expression tests, a culture sample was centrifuged, resuspended in 1 ml of 25 mM HEPES, pH 7.3, containing 10% glycerol, to an A_{600} corresponding to 15, and sonicated. Insoluble material was removed by centrifugation at 15,000 x g for 20 min at 4 ^{0}C. Samples of 15 µl of whole cells, supernatant, or

resuspended pellet were prepared and loaded on SDS-PAGE gels. For reconstitution experiments, frozen cell pellets were resuspended in a ratio of 0.5 g of cells in 1 ml of resuspension buffer (25 mM HEPES pH 7.3, containing 10% glycerol and 2 mM DTT). Crude extracts were prepared fresh for every reconstitution experiment. The cells were lysed by sonication, and the extract was clarified by ultracentrifugation for 1 hour at 64 330 x *g* at 4^0C, and filtered anaerobically through a 0.45 μm pore diameter filter.

Activity Measurements- Enzymatic activity in crude extracts and with purified preparations was measured by following O_2 consumption using a computer-interfaced Hansatech DW1 O_2 electrode. The assay, data collection, and analysis were performed as described previously (28). The standard activity assay contained 440 μM biphenyl, 377 μM NADH, 1.2 μM $BphG_{B\text{-}356}$, 2.8 μM $BphF_{LB400}$, and aliquots of 10 uL of oxygenase crude extracts prepared as described above.

Protein Purification- Chromatography was performed using a Pharmacia FPLC system installed inside a Vacuum Atmospheres glove box under an argon atmosphere (< 2 ppm O_2) for rigourous anaerobic conditions (28). The cell pellets from 2 L of cell culture were resuspended in 50 ml of 25 mM HEPES, pH 7.3, containing 10% glycerol, 0.01 mg/ml Dnase I, and 2 mM DTT. Cell suspensions were sonicated using a Branson Sonifier 250 apparatus with 10 X 12 sec pulses. The extract was clarified by ultracentrifugation for 90 min at 166 580 x *g*. The supernatant was passed through a 0.45- μm filter and loaded onto a 17 ml Source 15Q anion-exchange column (Amersham Pharmacia Biotech), eluted, and concentrated as previously described. The resulting

preparation was brought to 5% saturation with ammonium sulfate, filtered and loaded onto a 14 ml phenyl-Sepharose column (Amersham Pharmacia Biotech), eluted, and concentrated as previously described (28).

Analytical Methods- SDS-polyacrylamide gel electrophoresis with a 12% resolving gel was performed using a Bio-Rad MiniPROTEAN II apparatus, and gels were stained with Coomassie Blue according to established procedures (37). Protein concentrations were estimated using the bicinchoninic acid protein assay reagent kit (Pierce) after removal of interfering substances by TCA precipitation (38). Bovine serum albumin was used as a standard.

Preparation of Apo-Oxygenase - The Fe-S cluster of BPDO was removed by precipitation with ammonium sulfate at pH 2.0. The enzyme was diluted 10 fold into a solution of 50 mM sodium phosphate, pH 2.0, that was saturated with $(NH_4)_2SO_4$, and incubated at room temperature under aerobic conditions for 5 min. Precipitated protein was pelleted by centrifugation in a microcentrifuge at 15 000 x g for 15 min, and redissolved under anoxygenic conditions in HEPES buffer pH 7.5, I = 0.032 M, containing 10 % glycerol and 0.35 % SDS.

In vitro Oxidative Stress on the Oxygenase- $BPDO_{B356}$ was incubated at room temperature under aerobic conditions in 50 mM sodium phosphate buffer, pH 7.8, in the presence of 22 mU xanthine oxidase, and 0.2 mM xanthine. Controls were prepared with either only BPDO and xanthine oxidase, or BPDO and xanthine, under the same

conditions. The reaction catalyzed by xanthine oxidase with xanthine and oxygen releases superoxide, which further dismutates to hydrogen peroxide. The effects of superoxide and hydrogen peroxide on the [2Fe-2S] cluster of the oxygenase were monitored by UV-Vis absorbance of the characteristic Fe-S cluster signal. The reaction and the control mixtures were monitored for 20-hour periods. In order to observe the effects of hydrogen peroxide only, a control mixture containing 0.173 mM H_2O_2 and 4.2 uM $BPDO_{B356}$ in 50 mM sodium phosphate, pH 7.3, containing 10% glycerol, was monitored by UV-Vis absorbance as described above.

Apo-BPDO was also prepared by incubation at 37^{0}C of 11.6 μM BPDO in 25 mM HEPES, pH 7.8, containing 10% glycerol, 0.2 mM xanthine, and a total of 12 mU xanthine oxidase and 1.9 mM GSH (which were added in two equal aliquots, at 0 and 1 hour) for 5 hours.

Analytical-Ultracentrifugation- The holooxygenase and its acid-resolved apo-form were subjected to sedimentation velocity runs using a Beckman Optima XL1 analytical ultracentrifuge. The holooxygenase was dialysed against 25 mM HEPES, pH 7.3, containing 10% glycerol, and the apo-form was dialysed against HEPES buffer pH 7.5, I = 0.032 M, containing10 % glycerol and 0.35 % SDS. Both oxygenase forms (volumes of 17 μl holo, and 150 μl apo) were dialysed for one hour under aerobic conditions, and the respective dialysis buffers were used as blanks in the analytical ultracentrifugation cells. Samples (420 μl) of 0.5 mg/ml protein were loaded into an An 60 Ti rotor at 20 ^{0}C. The oxygenase and its apo-form were respectively sedimented at 57 996 x *g*, and 161 101 x *g*. Data were analyzed using both the DCDT$^+$ (39) and the Svedberg (40) software

packages for comparison. The buffer density and the protein partial specific volume were estimated using the Sednterp software (www.jphilo.mailway.com).

Oxygenase Fe-S Cluster In vitro Reassembly- Bacterial crude extracts and apooxygenase were prepared as described above. The reassembly of the Fe-S cluster into the acid-resolved apooxygenase was monitored by using visible absorbance spectroscopy over a period of 17 hours to detect the appearance of the Rieske [2Fe-2S] cluster signal. The anaerobic reconstitution assay was composed of 6.6 μM apooxygenase, and a crude extract equivalent to 0.1 g of *E.coli* C41[DE3] pRKISC. The assay was supplemented with 156 μM each of $Fe(SO_4)_2(NH_4)_2$, L-cysteine, and NADH. The assay blank contained the same components, but omitting the apooxygenase. A control assay was prepared using a corresponding amount of crude extract from *E.coli* C41[DE3] pRKNMC, an extract lacking the *Pseudomonas* iron-sulfur cluster assembly proteins. The control blank was the equivalent, without the apooxygenase.

Apo-BPDO generated by incubation with xanthine and xanthine oxidase was also used for reconstitution experiments monitored by visible circular dichroism (CD) spectroscopy, and enzymatic activity assays. In these cases, the anaerobic reconstitution assays were composed of 3.2 μM BPDO (with approximately 40 % remaining cluster), and a crude extract equivalent to 0.1 g of *E.coli* C41[DE3] pPAISC-2. The assay was supplemented with 310 μM each of $Fe(SO_4)_2(NH_4)_2$, L-cysteine, NADH, and ATP. The controls and blanks were similar to the ones described above. An additional control involved incubating the apo-oxygenase produced by oxidative stress with $Fe(SO_4)_2(NH_4)_2$, L-cysteine, NADH, and ATP, but omitting crude extract.

Spectroscopic Characterization- The absorbance spectroscopy experiments were done using a Cary 50 Bio spectrophotometer from Varian, with 1 cm pathlength quartz anaerobic cuvettes. The experiments monitored by CD spectroscopy were conducted using a JASCO 710 spectropolarimeter. In the far-UV CD region, a 0.1 cm pathlength quartz cell was used with solutions containing 0.93 mg/ml BPDO. For the reconstitution experiments monitored in the visible CD region, an anaerobic quartz cuvette with both 1 cm and 0.3 cm pathlengths was used.

RESULTS

Cloning and sequencing of the isc genes from Pseudomonas aeruginosa PA01 - The region encoding the *isc* gene cluster in *Pseudomona aeruginosa PA01* was defined by the *Pseudomonas* genome sequencing effort (30). Two primers, ISC8 and ISC9, were designed to hybridize to sequences flanking the cluster, at positions 4 267 108 and 4 272 648 (Fig. 6.2). Polymerase chain reaction using chromosomal DNA from *Pseudomonas aeruginosa* PA01 with oligonucleotides ISC8 and ISC9 rendered a 5591 bp fragment that was cloned into pUC18Not as an *XbaI* fragment. Two different clones were selected for further characterization. For coexpression of the *isc* genes, the *XbaI* fragment of each clone was first transferred into the *XbaI* site pRKNMC, producing pPAISC-1 and pPAISC-2, respectively. Sequencing of the *isc* gene clusters of these plasmids revealed some point mutations introduced by the cloning PCR. Although most of the mutations were silent, some generated amino acid substitutions: in HscA (E62G; S69G), IscU (M77T), and IscS (V148A) for clone 1; and in HscA (T81A; P104L) and HscB (K124R) for clone 2. Each point mutation was sequenced twice to confirm differences with the published sequence.

Construction of the $BPDO_{B356}$ expression plasmid - To clone *bphAE* from *Comamonas testosteroni* B-356 into the pT7-7 vector, an *NdeI* restriction site was introduced at the ATG start codon of *bphA* by PCR, using pQE31AE (2) as the template, and the primers AE-NdeI and AE-BglII (Table 6.1). The 3' primer overlapped the *BglII* restriction site in the *bphA* gene. The amplified 128 bp fragment was purified from an agarose gel, and then cut with *NdeI* and *BglII* restriction enzymes. A second fragment, corresponding to

Figure 6.2 *Isc* gene cluster map from *Pseudomonas aeruginosa* PA01 (30) (GenBank AE004091).

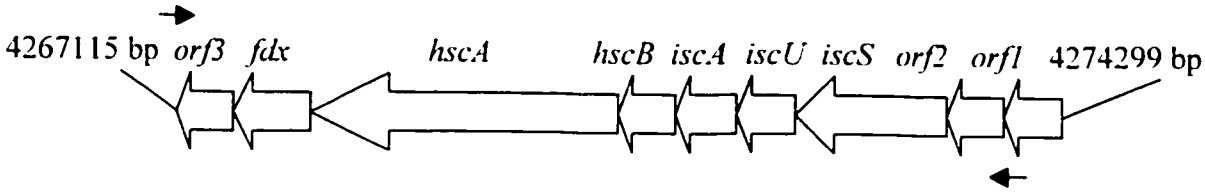
4267115 bp
orf3
fdx
hscA
hscB
iscA
iscU
iscS
orf2
orf1
4274299 bp

the rest of the coding region for *bphA*, as well as *bphE*, was prepared by cleaving pQE31AE with *BglII* and *HindIII*. The purified *BglII-HindIII* fragment was 1870 bp. The two fragments were directly ligated into pT7-7 opened with *NdeI* and *HindIII*, rendering pT7-7AE-3. The new construct was checked by cleaving with *XbaI* and *HindIII*, which gave the expected 2038 bp fragment of full-length *bphAE* (data not shown).

The pT7-7a (Chapter 5), and pT7-6a plasmids (33) for the expression of BPDO from *Pseudomonas* sp. Cam-1, and *Burkholderia* sp. LB400, respectively, were generously provided by Emma Master and Lindsay D.Eltis from The University of British Columbia, Canada.

Expression of BPDOs in the presence and absence of the Pseudomonas isc genes- Co-expression of the *isc* gene cluster together with Rieske-type iron-sulfur cluster containing proteins has not been previously reported. The effects of coexpression of the *Pseudomonas* gene cluster, comprising *iscR-iscS-iscU-iscA-hscB-hscA-fdx-ORF3*, on the expression levels of three different BPDOs were therefore investigated. Control strains harboring only the vector, pRKNMC, were used to account for potential stabilizing effects of the coexpression plasmid (26).

Crude extracts from strains expressing $BPDO_{B356}$, $BPDO_{LB400}$, or $BPDO_{Cam1}$ together with the *isc* genes were noticeably darker than crude extract from cells harbouring the vector only: the Rieske cluster is brown-colored, and the *isc* gene products do not appear to contribute significantly to the color (26). In the absence of coexpression with the *isc* genes, only a trace of α-subunit expression from $BPDO_{Cam1}$ was observed by

SDS-PAGE, while the cofactorless β-subunit was highly expressed in a soluble form (Fig. 6.3). However, in the presence of the *isc* genes expressed from either pPAISC-1 or pPAISC-2, high levels of expression were observed for both oxygenase subunits (Fig. 6.3). Similar results were observed for coexpression of $BPDO_{Cam1}$ with the *isc* genes from *E. coli*, confirming the functionality of the *isc* genes cloned from *Pseudomonas*. Coexpression of the *isc* genes with either $BPDO_{B356}$ or $BPDO_{LB400}$, monitored by SDS-PAGE, indicated an apparent increase in the portion of soluble oxygenase, rather than the expression level of the α-subunits (data not shown).

Activity measurements in crude extracts- To confirm that the expression levels of $BPDO_{B356}$ and $BPDO_{LB400}$ actually increased, enzyme activities were estimated by measuring biphenyl-dependent oxygen consumption by crude extracts supplemented with reductase, ferredoxin, and NADH under standard conditions, as described previously (28). The crude extracts containing $BPDO_{B356}$ or $BPDO_{LB400}$ and the coexpressed *isc* gene products showed about 1.4 times more total activity than the corresponding crude extracts from cells lacking co-expressed *isc* genes.

Purification of $BPDO_{B356}$ from an E. coli strain coexpressing the isc gene products- Additional evidence of enhanced $BPDO_{B356}$ formation by coexpression of the *isc* gene cluster was obtained by comparing purification yields from strains either harboring or lacking the *isc* gene cluster expression plasmid. $BPDO_{B356}$ was purified anaerobically from both *E. coli* C41[DE3] pT7-7AE pRKNMC and *E. coli* C41[DE3] pT7-7AE pRKISC, under identical conditions. In agreement with the crude extract enzymatic

Figure 6.3 SDS-PAGE of $BPDO_{Cam1}$ expression from pT7-7a in the presence or absence of co-expression with *isc* genes from pPAISC-1 or pPAISC-2. Lane 1- LMW marker; lanes 2, 3, 4-pRKNMC (vector control); lanes 5,6,7- pPAISC-1; and lanes 8,9,10-pPAISC-2. The three lanes contain samples of whole cells, supernatant, and pellet from left to right. Culture conditions were as described in *Materials and Methods*.

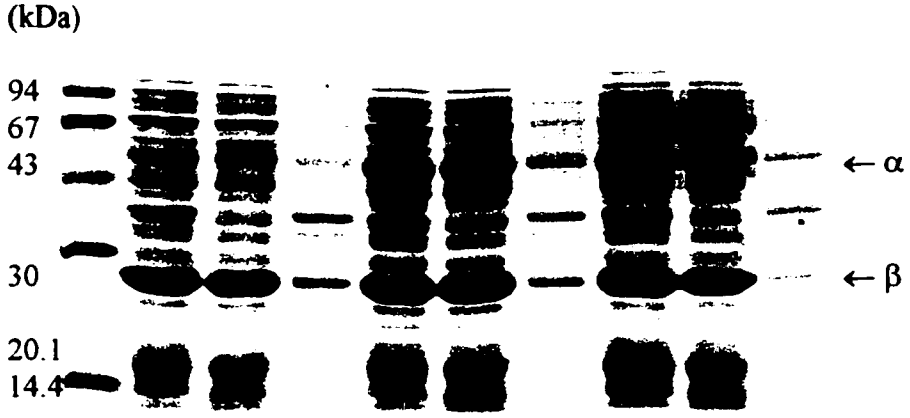
(kDa)
94
67
43
30
20.1
14.4
← α
← β

activity measurements, the yield of holooxygenase isolated from the strain coexpressing the *isc* genes was 1.4 times that isolated from the vector control strain. The spectral properties, specific activities, and purities of the two preparations were not significantly different (data not shown). The absorbance and circular dichroism spectra of the oxidized and reduced forms of $BPDO_{B356}$ isolated from *E. coli* C41[DE3] pRKISC pT7-7AE-3 are presented in figure 6.4.

Apo-oxygenase preparation and characterization – In order to examine Fe-S cluster assembly *in vitro*, apooxygenase free of the Fe-S cluster is required. However, $BPDO_{B356}$ was remarkably resistant to Fe-S cluster removal under both oxidizing and reducing conditions using several published protocols. The oxidative procedure developed for aconitase (41), even with an extended incubation period at room temperature, did not disrupt the Fe-S cluster significantly, nor did a reductive procedure involving incubation with excess β-mercaptoethanol and EDTA under anaerobic conditions (data not shown). Conditions used for disruption of the Fe-S cluster of SoxR in the presence of reduced glutathione (GSH) with either H_2O_2 or L-cysteine (42;43) also failed to efficiently produce preparations of apo-BPDO (data not shown). The two latter methods disrupted less than 7% of the Fe-S cluster over 5 hours.

An apooxygenase preparation was successfully obtained by quantitatively precipitating the oxygenase with 90%-saturated ammonium sulfate in 50 mM sodium phosphate buffer at pH 2.0. The white protein precipitate was redissolved in 25 mM HEPES pH 7.5, containing 10% glycerol and 0.35% SDS. Omission of SDS prevented

Figure 6.4 UV-vis (**A**) and visible CD (**B**) spectra of $BPDO_{B356}$. Solid lines represent oxidized-BPDO, and dotted lines reduced-BPDO. BPDO was oxidized with a 20-fold excess of potassium ferricyanide, desalted in 50 mM sodium phosphate 10% glycerol pH 7.3, and diluted to 1.7 μM. BPDO was reduced with a 20 fold excess sodium dithionite, desalted anaerobically, and diluted to 3.3 μM. The spectra were normalized to A_{280} for comparison.

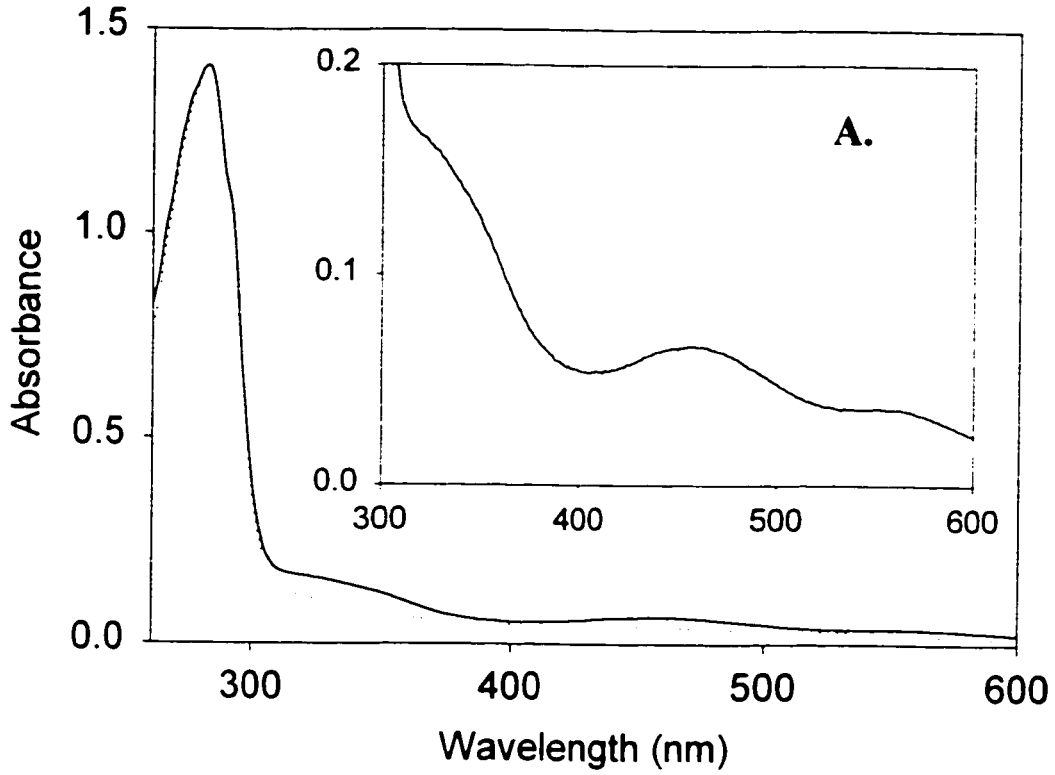
A.
Absorbance
Wavelength (nm)
1.5
1.0
0.5
0.0
0.2
0.1
0.0
300
400
500
600

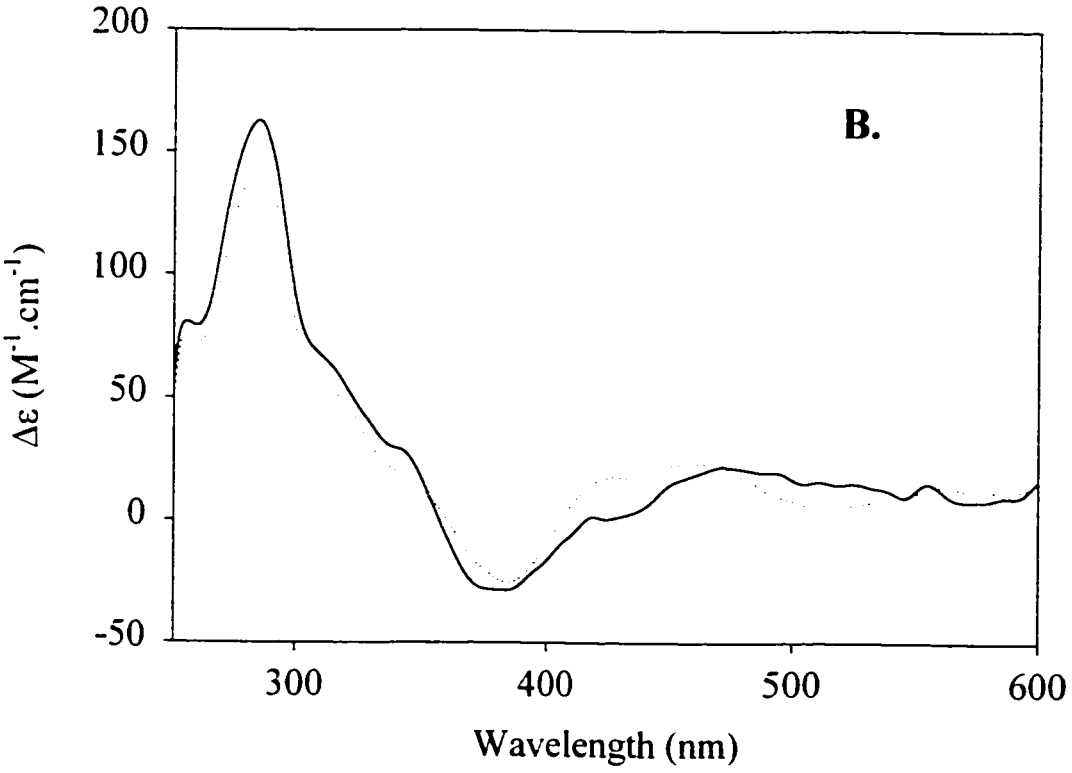
B.
Δε (M-1.cm-1)
Wavelength (nm)
200
150
100
50
0
-50
300
400
500
600

redissolution of the precipitate. Low yields of soluble apo-BPDO were obtained when SDS was replaced by 0.5-2 M urea, 10% trifluoroethanol, or 12 mM CHAPS.

Cluster removal was confirmed by the bleached UV-Vis absorption and visible CD spectra of the redissolved preparation (data not shown). Comparison of far-UV CD spectra indicates that the apooxygenase retained most of the secondary structure features found in the holoenzyme either in the presence or absence of SDS (Fig. 6.5). However, analytical ultracentrifugation experiments showed that the quaternary structure of the apoprotein was disrupted. Sedimentation velocity data for holo-BPDO were fit to a single-species model using DCDT$^+$, with a molecular weight of 209.8 ± 13.6 kDa corresponding to the hexamer ($\alpha_3\beta_3$) form of the oxygenase (219 kDa). The acid-resolved apo-BPDO behaved as a single species with molecular weight of 50.9 ± 5.0 kDa, indicating loss of the $\alpha_3\beta_3$ quaternary structure.

Oxidative stress effect on the Rieske [2Fe-2S] cluster of $BPDO_{B356}$ - Reactive oxygen species released from BPDO during turnover of certain dichlorinated biphenyls (28) have the potential to disrupt the [2Fe-2S] cluster. In order to test this, the oxygenase was submitted to oxidative stress *in vitro* by incubating it with xanthine oxidase and xanthine, which generates both superoxide and hydrogen peroxide (44). In the presence of xanthine oxidase or xanthine alone, no significant loss of the iron-sulfur cluster absorbance signal was observed under aerobic conditions over a 20-hour period at room temperature. Incubation in the presence of both xanthine oxidase and xanthine under the same conditions resulted in loss of 60% of the iron-sulfur, as indicated by the change in visible absorbance. To distinguish the effect of superoxide from hydrogen peroxide, the

Figure 6. 5 Far UV CD spectra to compare secondary structure of holo- and apo-oxygenase. Dotted line is for holo-BPDO, dashed line holo-BPDO with SDS, and solid line apo-BPDO with SDS. Samples were 0.93 mg/ml in 0.1 cm pathlength cell.

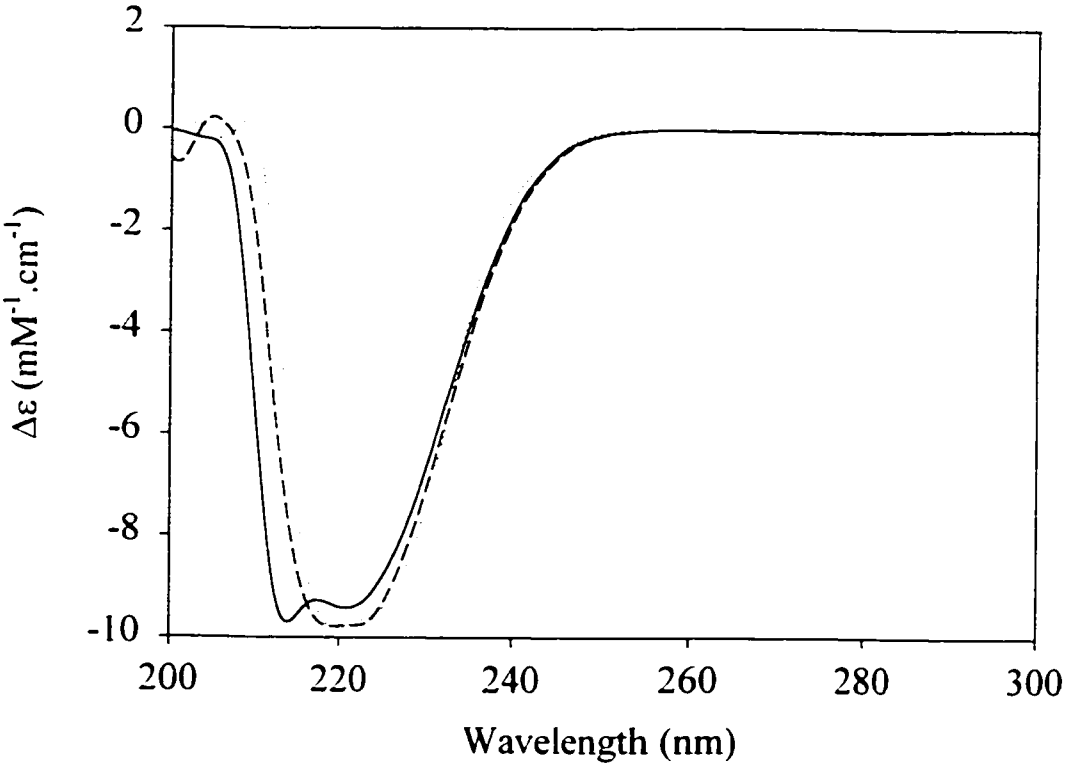
2
0
-2
-4
-6
-8
-10
Δε (mM-1.cm-1)
200
220
240
260
280
300
Wavelength (nm)

oxygenase was incubated aerobically in the presence of hydrogen peroxide at a concentration equivalent to the xanthine concentration in the previous experiment. Since the UV-visible absorbance signal of the Fe-S cluster only decreased by 14%, it appears that superoxide is a more effective disruptor of the Fe-S cluster than is peroxide. These results suggested that incubation with xanthine/xanthine oxidase might be an appropriate way to prepare SDS-free apoenzyme for reconstitution. Accordingly, incubation of holo-$BPDO_{B356}$ with xanthine, xanthine oxidase, and GSH at 37^0C resulted in disassembly of 57% of the cluster after 6 hours, as indicated by bleaching of the spectrum (Fig. 6.6). Such preparations were used for in vitro reassembly experiments.

In vitro reassembly of the Rieske-type [2Fe-2S] cluster in $BPDO_{B356}$ using crude extracts containing the isc gene products- Apo-oxygenase preparations produced by the acidic ammonium sulfate and oxidative stress methods were used to examine the capacity of the *isc* gene products to reassemble the Rieske-type [2Fe-2S] cluster of BPDO *in vitro*. Anaerobic reconstitution of the iron-sulfur cluster, together with measurements of enzymatic activity using crude extracts containing the overexpressed *isc* proteins, was compared to corresponding controls using extracts from cells lacking overexpressed *isc* protein.

UV-vis spectroscopy of acid-resolved apo-BPDO incubated with crude extracts from *E.coli* C41[DE3] harboring the *isc* expression plasmid was consistent with reassembly of a [2Fe-2S] cluster over a 21 hour period at room temperature (Fig. 6.7). The development of a peak at 323 nm is consistent with formation of Fe-S bonds (7), and an increase in absorbance around 425-455 nm is characteristic of a Rieske-type Fe-S

Figure 6.6 Oxidative stress on the oxygenase [2Fe-2S] cluster using the xanthine / xanthine oxidase system in presence of GSH at 37^0C. Details in *Experimental Procedures*.

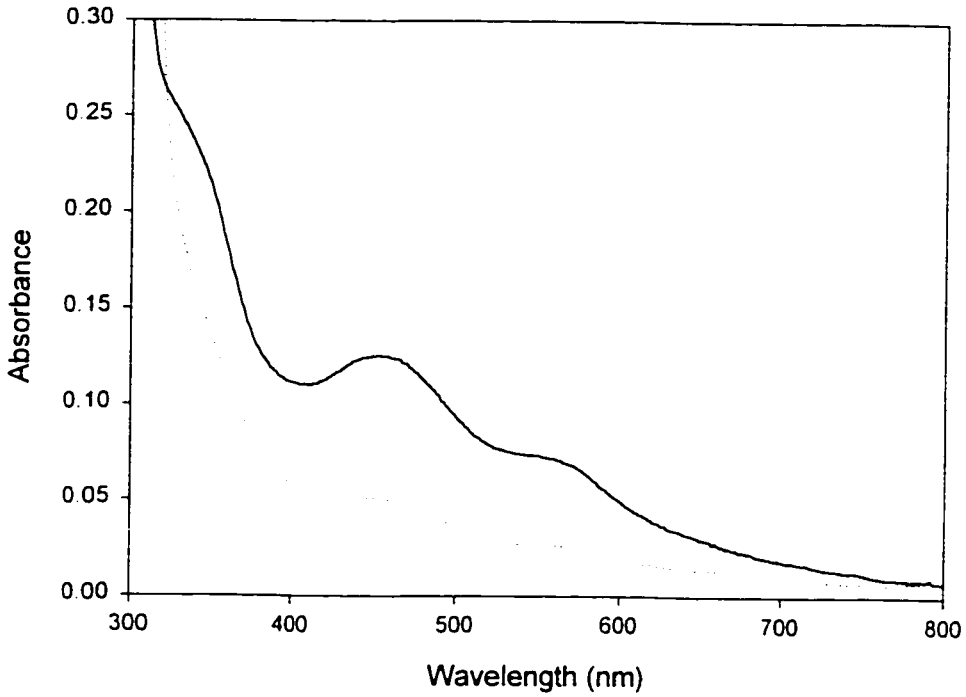
0.30
0.25
0.20
0.15
0.10
0.05
0.00
Absorbance
300
400
500
600
700
800
Wavelength (nm)

Figure 6.7 *In vitro* reconstitution of iron-sulfur cluster in acid-resolved apo-BPDO using crude extracts of *E. coli* C41[DE3] pRKNMC and pRKISC, monitored by visible absorbance spectroscopy of anaerobic samples. A. Reconstitution using crude extract with overexpressed *isc* genes; initial time (___); 5 hours (....); 21 hours (_ _). B. Reconstitution using crude extract lacking the overexpressed *isc* genes; initial time (___); 21 hours (....). Conditions are detailed in *Experimental Procedures*. The reference cell cuvette contained an identical mixture, but lacking apo-BPDO.

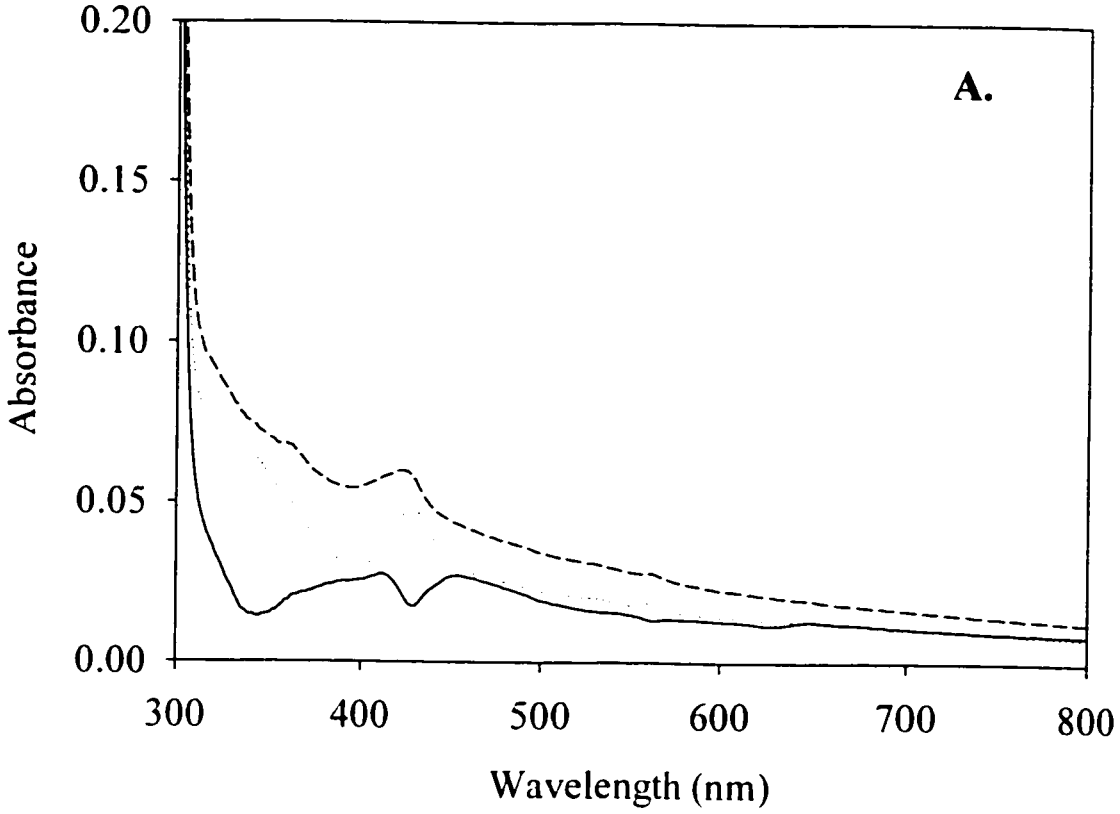
A.
0.20
0.15
0.10
0.05
0.00
Absorbance
300
400
500
600
700
800
Wavelength (nm)

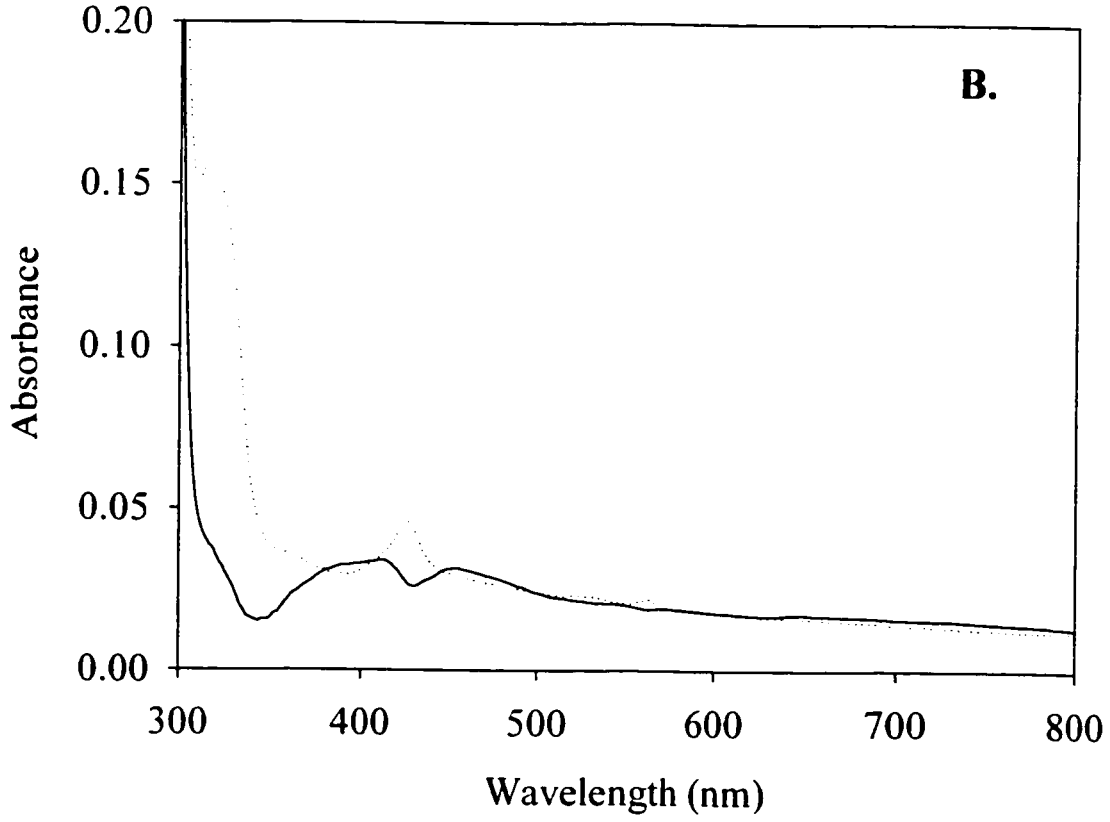
B.
0.20
0.15
0.10
0.05
0.00
Absorbance
300
400
500
600
700
800
Wavelength (nm)

cluster (Fig. 6.7A). The appearance of peaks centered at 425 and 560 nm could be due to heme assembly: if so there is relatively little contibution by heme to the absorbance at 323 nm. Under these conditions, the apparent maximal absorbance at 323 nm was approximately 0.1, corresponding to approximately 30% cluster reassembly according to the absorbance of the original oxidized holo-BPDO sample. In a control experiment, where crude extract was from *E.coli* C41[DE3] lacking the overexpressed *isc* gene products, these spectral changes were not observed (Fig. 6.7B). Interestingly, when the reconstitution assays were supplemented with $Fe(SO_4)_2(NH_4)_2$, L-cysteine, and NADH the maximal absorbance at 323 nm reached during the reaction was 0.4, suggesting over 90% reassembly of the cluster. However, after reaching this maximum, the absorbance began to decrease, suggesting some instability in the cluster under the experimental conditions. The control reconstitution assay did not show similar increases in absorbance (data not shown). Despite apparent cluster reassembly, none of these reconstitution experiments yielded reactivated enzyme, possibly due to the denaturing effects of the SDS that was unavoidably present in the acid-resolved apo-BPDO preparation.

Similar experiments were performed with apo-BPDO prepared by incubation with superoxide, since these samples did not contain SDS. Reconstitution reactions were monitored by CD spectroscopy, which is spectroscopically selective for the Rieske [2Fe-2S] cluster signal (7). Quantitation of the 340-377 nm peak to trough ratio (Table 6.2) indicates that the apo-BPDO sample had approximately 4% of the cluster present relative to starting holo-BPDO (Fig. 6.8). Heme does not interefere in this region of the CD spectrum (ref). Incubation of apo-BPDO in the presence of crude extract containing the overexpressed *isc* gene products yielded approximately 49% cluster, while incubation

with extracts lacking overexpressed *isc* genes only yielded approximately 32 % cluster (Table 6.2).

The superoxide-treated apo-BPDO used in these experiments had a residual enzymatic activity with biphenyl of 1.84 ± 0.06 U/ml: the activity of holo-BPDO used to prepare the apo-form was 7.31 ± 0.4 U/ml. Reconstitution of apo-BPDO with extract lacking overexpressed *isc* gene products yielded an activity of 1.6 ± 0.02 U/ml, compared to 2.00 ± 0.02 U/ml in reconstitution reactions done with crude extract from cells overexpressing the *isc* gene products. A control reaction where apo-BPDO was incubated under the same conditions but without *E. coli* extract showed a decrease in activity to 1.39 ± 0.05 U/ml.

Figure 6.8 *In vitro* reconstitution of iron-sulfur cluster using crude extracts of *E.coli* C41[DE3] pRKNMC and pPAISC-2 monitored by visible circular dichroism spectroscopy of oxidized samples. Holo-BPDO (_ _); apo-BPDO (_.._); reconstitution using crude extract lacking the overexpressed *isc* genes (___); reconstitution using crude extract with overexpressed *isc* genes (....). Each spectrum represents accumulation of 20 scans. Conditions are detailed in *Experimental Procedures*.

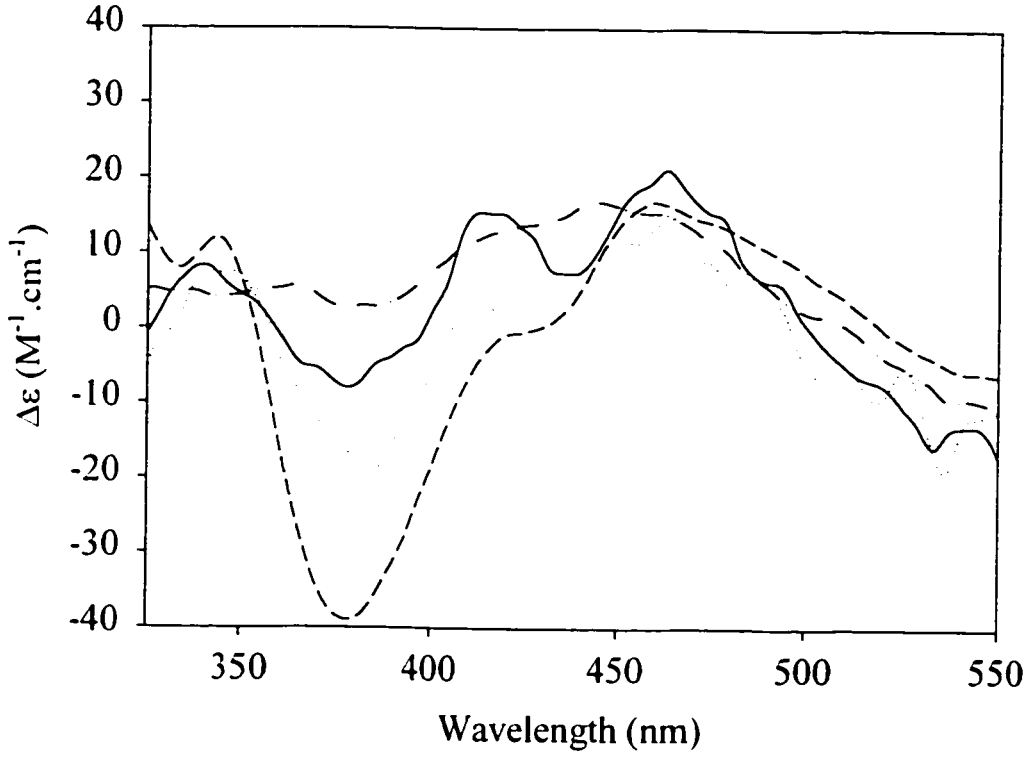
40
30
20
10
0
-10
-20
-30
-40
Δε (M-1.cm-1)
350
400
450
500
550
Wavelength (nm)

Table 6.2 Molar CD absorptivities of BPDO and BPDO Fe-S cluster reassembly assays

Sample	λ (nm)	CD $\Delta\varepsilon$ ($M^{-1}.cm^{-1}$)	$\Delta CD_{340-377}$ $\Delta\varepsilon$ ($M^{-1}.cm^{-1}$)
BPDO	340	10.7	49.7
	377	-39.0	
Apo-BPDO	340	4.5	1.9
	377	2.6	
Nmc reassembly	340	7.8	15.8
	377	-8.0	
Isc reassembly	340	7.8	24.2
	377	-16.4	

DISCUSSION

Our experience with overexpression of bacterial biphenyl dioxygenases suggested that the Fe-S cluster-containing alpha subunit was often limiting in the production of high levels of soluble oxygenase. In most cases, the cofactorless beta subunit was expressed to higher levels than the alpha subunit, and excess beta subunit was found in the insoluble fraction of the cell extract. Different approaches to improving yield have included optimizing the ribosome binding site of the alpha subunit, using different vectors and expression strains, supplementing growth media with metals, and using slower rates of expression (Agar *et al.*, unpublished). However, the ratio of alpha:beta subunit was consistently less than one using all of these approaches. Our best previous results for $BPDO_{B356}$ were obtained using *Pseudomonas putida* KT2442 as the overexpression host, together with a pVLT31-based plasmid construct, where 5.6 mg of soluble oxygenase per liter of culture were obtained (28).

This method failed for $BPDO_{Cam1}$, where the beta subunit was highly expressed in most of the tested expression systems, but soluble alpha Fe-S cluster-containing subunit was barely observable on SDS-PAGE (Fig. 6.3). Following the findings of Takahashi *et al.*, that expression of ferredoxins containing Fe-S clusters could be significantly improved by coexpression with the *isc* gene cluster from *E. coli* (26), improved expression of BPDO in the presence of the *Pseudomonas aeruginosa* PA01 *isc* gene cluster was tested. The results summarized in Fig. 6.3 are striking: both $BPDO_{Cam1}$ subunits are highly expressed only when co-expressed with the *isc* gene cluster. These results indicate a requirement for increased levels of the iron-sulfur cluster assembly

proteins for the efficient production of high levels of $BPDO_{Cam1}$. To our knowledge, this is also the first evidence of the ability of the *isc* proteins to assemble a Rieske-type Fe-S cluster.

Although the effect was the most striking for $BPDO_{Cam1}$, improved yields of other BPDOs were also obtained when co-expressed with the *isc* gene cluster. For $BPDO_{B356}$, comparative measurements of enzyme activity in crude extracts, and yields of purified protein, indicated a 1.4-fold higher level of expression of active enzyme in the *isc*-expressing strain than in the control strain. Furthermore, this expression system allowed the purification of 50 mg of pure BPDO per liter of culture (Agar *et al.*, unpublished results), compared to 5.6 mg/liter using expression in *Pseudomonas* (28). Similar results were observed for the coexpression of $BPDO_{LB400}$ with the *isc* gene cluster (data not shown).

Comparison of the *isc* cluster sequences in two independent clones, pPAISC-1 and pPAISC-2, to the published genome sequence revealed point mutations introduced by the cloning PCR. Each point mutation responsible for an amino acid substitution was sequenced two times to eliminate the possibility of sequencing artifacts, and was unique to one or the other clone. Despite these substitutions, similar functionality was observed for each clone, and both clones yielded results comparable to experiments done using the plasmids expressing the *E. coli isc* cluster (26;35). Therefore, the mutations do not appear to affect functionality.

The ability of the *isc* assembly proteins to provide apo-BPDO with a Rieske-type Fe-S cluster was examined *in vitro*. It proved to be very difficult to remove the cluster, which is perhaps not surprising considering the large size of the protein and the buried

position of the cluster within the structure (8), Colbert *et al.*, in preparation). Soluble apo-oxygenase was finally obtained by precipitation with ammonium sulfate under acidic conditions, followed by dissolution in buffer supplemented with 0.35% SDS. Although the far-UV circular dichroism spectrum of the apo-oxygenase indicated intact secondary structure, analytical ultracentrifugation results revealed loss of the $\alpha_3\beta_3$ quaternary structure in these preparations.

In vitro reassembly of the cluster in the absence of oxygen was attempted using crude extracts containing the complete *isc* assembly protein ensemble, together with acid-resolved apo-BPDO. Without supplementing the assay with iron and cysteine, an absorption signal around 323 nm, consistent with formation of approximately 30% of a fully reconstituted oxygenase, was observed in the presence of *isc*-containing crude extract, but not control extracts. When the assay was supplemented with iron, L-cysteine, and NADH, the signal increased to a level suggesting more than 90% reconstitution of Fe-S cluster, but appeared to be unstable. Even though visible absorbance changes were consistent with reassembly of a reduced [2Fe-2S] cluster, a signal that appears to correspond to simultaneous heme synthesis interfered. Unfortunately, the reconstitution assay could not be brought to high enough concentration for EPR measurements of cluster reassembly without formation of significant amounts of precipitate. In any event, no enzymatic activity was observed after completion of these reconstitution reactions. This may be due to failure of the subunits to reassemble, either because of the presence of SDS or because they do not reassemble spontaneously *in vitro* (2;45).

Additional studies were done with partially-resolved apoprotein preparations that were generated by exposure to superoxide. The fact that the cluster was relatively easily

destroyed by superoxide, compared to other methods of generating apoprotein, indicates that the Fe-S center may be sensitive to the reactive oxygen species generated under some turnover conditions (28). Using preparations of superoxide-resolved apo-BPDO, and a reconstitution assay supplemented with iron, L-cysteine, NADH, and ATP, an increase in the signal of the Rieske Fe-S cluster was observed between 350-400 nm by circular dichroism spectroscopy, together with a partial recovery of enzymatic activity on biphenyl. According to the CD spectra, it appears that the reconstitution of Fe-S cluster is more extensive than the recovery of enzymatic activity. However, that could be related to other modifications of the enzyme by reactive oxygen species, or the lack of active site mononuclear iron, that prevent the enzyme from being fully active.

The initial evidence of a repair function for an *isc* gene product was the catalytic formation of a nitrogenase iron-sulfur cluster by NifS (46). Subsequently, identification of the housekeeping *isc* gene cluster from *Azotobacter vinelandii* led Dean and coworkers to propose a repair function for the *isc* gene products (11). In addition to these studies, other evidence of Fe-S cluster repair that was independent of new protein synthesis was observed in *E. coli* systems (47-49), and the existence of active mechanisms to actively dispose of altered clusters was postulated (48). Moreover, the ability of IscS to convert a dinitrosyl iron complex formed upon nitric oxide exposure of an Fe-S cluster to the original [2Fe-2S] cluster was recently shown *in vitro* (27).

The present studies clearly illustrate the advantages of coexpressing the *isc* assembly proteins to produce high yields of active Fe-S cluster containing oxygenases, and suggest the possibility of repairing damaged clusters in these enzymes. Since reactive oxygen species are released during turnover of dichlorinated biphenyls (28), the

presence of the *isc* assembly proteins might improve the ability of strains to degrade these and more highly chlorinated congeners. We are in the process of using these strains to investigate their usefulness in improved degradation of PCB mixtures.

ACKNOWLEDGMENTS

We thank Professor J.E. Walker from the Medical Research Council Laboratory of Molecular Biology, Cambridge, UK for providing the *E.coli* C41[DE3] strain. Professor Yasuhiro Takahashi from Osaka University generously provided us with the pRKNMC, and pRKISC plasmids. Dr. Emma R. Master and Professor William W. Mohn from University of British Columbia provided the pT7-7a plasmid. We thank Professor Michael K. Johnson for anaerobic purification facilities, and Dr. Jeffrey N. Agar for EPR analysis. Work supported by NSERC to J.B.P, and to L.D.E. N.Y.R.A. was the recipient of an NSERC fellowship.

REFERENCES

1. Hurtubise, Y., Barriault, D., Powlowski, J., and Sylvestre, M. (1995) *J.Bacteriol.* **177,** 6610-6618

2. Hurtubise, Y., Barriault, D., and Sylvestre, M. (1996) *J.Biol.Chem.* **271,** 8152-8156

3. Haddock, J. D. and Gibson, D. T. (1995) *J.Bacteriol.* **177,** 5834-5839

4. Ensley, B. D. and Gibson, D. T. (1983) *J.Bacteriol.* **155,** 505-511

5. Haigler, B. E. and Gibson, D. T. (1990) *J.Bacteriol.* **172,** 465-468

6. Haigler, B. E. and Gibson, D. T. (1990) *J.Bacteriol.* **172,** 457-464

7. Fee, J. A., Findling, K. L., Yoshida, T., Hille, R., Tarr, G. E., Hearshen, D. O., Dunham, W. R., Day, E. P., Kent, T. A., and Munck, E. (1984) *J.Biol.Chem.* **259,** 124-133

8. Kauppi, B., Lee, K., Carredano, E., Parales, R. E., Gibson, D. T., Eklund, H., and Ramaswamy, S. (1998) *Structure.* **6,** 571-586

9. Carredano, E., Karlsson, A., Kauppi, B., Choudhury, D., Parales, R. E., Parales, J. V., Lee, K., Gibson, D. T., Eklund, H., and Ramaswamy, S. (2000) *J.Mol.Biol.* **296,** 701-712

10. Carredano, E., Kauppi, B., Choudhury, D., and Ramaswamy, S. (2000) *Acta Crystallogr.D.Biol.Crystallogr.* **56,** 313-321

11. Zheng, L., Cash, V. L., Flint, D. H., and Dean, D. R. (1998) *J.Biol.Chem.* **273,** 13264-13272

12. Smith, A. D., Agar, J. N., Johnson, K. A., Frazzon, J., Amster, I. J., Dean, D. R., and Johnson, M. K. (2001) *J.Am.Chem.Soc.* **123,** 11103-11104

13. Urbina, H. D., Silberg, J. J., Hoff, K. G., and Vickery, L. E. (2001) *J.Biol.Chem.* **276,** 44521-44526

14. Zheng, L., White, R. H., Cash, V. L., Jack, R. F., and Dean, D. R. (1993) *Proc.Natl.Acad.Sci.U.S.A* **90,** 2754-2758

15. Zheng, L., White, R. H., Cash, V. L., and Dean, D. R. (1994) *Biochemistry* **33,** 4714-4720

16. Agar, J. N., Zheng, L. M., Cash, V. L., Dean, D. R., and Johnson, M. K. (2000) *Journal of the American Chemical Society* **122,** 2136-2137

17. Agar, J. N., Krebs, C., Frazzon, J., Huynh, B. H., Dean, D. R., and Johnson, M. K. (2000) *Biochemistry* **39,** 7856-7862

18. Krebs, C., Agar, J. N., Smith, A. D., Frazzon, J., Dean, D. R., Huynh, B. H., and Johnson, M. K. (2001) *Biochemistry* **40,** 14069-14080

19. Ollagnier-de-Choudens, S., Mattioli, T., Takahashi, Y., and Fontecave, M. (2001) *J.Biol.Chem.* **276,** 22604-22607

20. Jung, Y. S., Gao-Sheridan, H. S., Christiansen, J., Dean, D. R., and Burgess, B. K. (1999) *J.Biol.Chem.* **274,** 32402-32410

21. Kakuta, Y., Horio, T., Takahashi, Y., and Fukuyama, K. (2001) *Biochemistry* **40,** 11007-11012

22. Hoff, K. G., Silberg, J. J., and Vickery, L. E. (2000) *Proc.Natl.Acad.Sci.U.S.A* **97,** 7790-7795

23. Hoff, K. G., Ta, D. T., Tapley, T. L., Silberg, J. J., and Vickery, L. E. (2002) *J.Biol.Chem., ahead of print*

24. Tokumoto, U., Nomura, S., Minami, Y., Mihara, H., Kato, S., Kurihara, T., Esaki, N., Kanazawa, H., Matsubara, H., and Takahashi, Y. (2002) *J.Biochem.(Tokyo)* **131,** 713-719

25. Schwartz, C. J., Giel, J. L., Patschkowski, T., Luther, C., Ruzicka, F. J., Beinert, H., and Kiley, P. J. (2001) *Proc.Natl.Acad.Sci.U.S.A* **98,** 14895-14900

26. Nakamura, M., Saeki, K., and Takahashi, Y. (1999) *J.Biochem.(Tokyo)* **126,** 10-18

27. Yang, W., Rogers, P. A., and Ding, H. (2002) *J.Biol.Chem.* **277,** 12868-12873

28. Imbeault, N. Y., Powlowski, J. B., Colbert, C. L., Bolin, J. T., and Eltis, L. D. (2000) *J.Biol.Chem.* **275,** 12430-12437

29. Ausubel, F. M. and et al. (1997) *Current Protocols in Molecular Biology*, John Wiley & Sons Inc., New York

30. Stover, C. K., Pham, X. Q., Erwin, A. L., Mizoguchi, S. D., Warrener, P., Hickey, M. J., Brinkman, F. S., Hufnagle, W. O., Kowalik, D. J., Lagrou, M., Garber, R.

L., Goltry, L., Tolentino, E., Westbrock-Wadman, S., Yuan, Y., Brody, L. L., Coulter, S. N., Folger, K. R., Kas, A., Larbig, K., Lim, R., Smith, K., Spencer, D., Wong, G. K., Wu, Z., Paulsen, I. T., Reizer, J., Saier, M. H., Hancock, R. E., Lory, S., and Olson, M. V. (2000) *Nature* **406,** 959-964

31. Miroux, B. and Walker, J. E. (1996) *J.Mol.Biol.* **260,** 289-298

32. Studier, F. W., Rosenberg, A. H., Dunn, J. J., and Dubendorff, J. W. (1990) *Methods Enzymol.* **185,** 60-89

33. Hofer, B., Eltis, L. D., Dowling, D. N., and Timmis, K. N. (1993) *Gene* **130,** 47-55

34. Herrero, M., de, L., V, and Timmis, K. N. (1990) *J.Bacteriol.* **172,** 6557-6567

35. Takahashi, Y. and Nakamura, M. (1999) *J.Biochem.(Tokyo)* **126,** 917-926

36. Sambrook, J., Fritsch, E. F., and Maniatis, T. (1989) *Molecular Cloning: A Laboratory Manual*, Cold Spring Harbour, New York

37. Laemmli, U. K. (1970) *Nature* **227,** 680-685

38. Brown, R. E., Jarvis, K. L., and Hyland, K. J. (1989) *Anal.Biochem.* **180,** 136-139

39. Philo, J. S. (2000) *Anal.Biochem.* **279,** 151-163

40. Philo, J. S. (1997) *Biophys.J.* **72,** 435-444

41. Kennedy, M. C. and Beinert, H. (1988) *J.Biol.Chem.* **263,** 8194-8198

42. Ding, H. and Demple, B. (1996) *Proc.Natl.Acad.Sci.U.S.A* **93,** 9449-9453

43. Ding, H. and Demple, B. (1998) *Biochemistry* **37,** 17280-17286

44. Porras, A. G., Olson, J. S., and Palmer, G. (1981) *J.Biol.Chem.* **256,** 9006-9103

45. Maeda, T., Takahashi, Y., Suenaga, H., Suyama, A., Goto, M., and Furukawa, K. (2001) *J.Biol.Chem.* **276,** 29833-29838

46. Zheng, L. and Dean, D. R. (1994) *J.Biol.Chem.* **269,** 18723-18726

47. Flint, D. H., Smyk-Randall, E., Tuminello, J. F., Draczynska-Lusiak, B., and Brown, O. R. (1993) *J.Biol.Chem.* **268,** 25547-25552

48. Ding, H. and Demple, B. (2000) *Proc.Natl.Acad.Sci.U.S.A* **97,** 5146-5150

49. Rogers, P. A. and Ding, H. (2001) *J.Biol.Chem.* **276,** 30980-30986

Chapter 7

Summary

The achievements presented in this thesis required the production of substantial quantities of high-quality BPDO, and the development of a reliable enzymatic activity assay. Overexpression of BPDO in a pseudomonad followed by purification under strictly anoxygenic conditions accomplished the first goal. Purified BPDO appeared to contain a full complement of [2Fe-2S] center and catalytic iron, and had a specific activity of 4.9 Units/mg under defined conditions. Highly homogeneous samples prepared using this method reproducibly rendered crystals under anaerobic conditions that diffracted to 1.6 Å resolution. Biphenyl dioxygenase activity was quantitated by monitoring O_2 consumption in the presence of biphenyl or selected dichlorinated biphenyl substrates (1). Steady-state kinetic assays for biphenyl and 2,2'-, 3,3'-, and 4,4'-diClB revealed a different order of substrate preference than observed in whole cells (2). The dependence of steady-state kinetic parameters on the concentration of oxygen in the presence of the dichlorinated biphenyls revealed that the ability of BPDO to utilize oxygen efficiently depended strongly on the substitution pattern of the dichlorobiphenyl substrate. Moreover, the dihydroxylation reaction was uncoupled from O_2 consumption in the presence of the dichlorinated biphenyls, producing hydrogen peroxide.

The first crystal structures of BPDO and its binary complexes with substrate and product were solved, and contributed to the study of structure-function relationships in BPDO. The crystal structure revealed an $\alpha_3\beta_3$ quaternary arrangement, with the [2Fe-2S] Rieske-type cluster and the catalytic mononuclear iron residing on the α-subunit. The two metal centers within one subunit were 43 Å apart, which is too distant for electron transfer. The distance between the two metal centers in adjacent subunits was 12 Å, which would allow inter-subunit electron transfer in BPDO. Pentacoordinate ligation

geometry of the mononuclear iron was observed in resting and substrate-bound BPDO and involved two histidine residues, one aspartate side-chain in a bidentate manner, and one water molecule. In the presence of product at the active site, the coordination geometry of the iron increased to hexacoordinate with the addition of a second water molecule. Many of these structural features were first observed in naphthalene dioxygenase (4.5).

The high-resolution crystal structure information was used to address the roles of specific residues in BPDO activity. Glutamine 226, located 3.1 Å away from the catalytic iron, forms a hydrogen bond with the product: the equivalent asparagine residue in naphthalene dioxygenase has been suggested to be a ligand to the iron (3.4). Site-directed mutagenesis was used to substitute glutamine 226 by alanine, asparagine, or glutamate. The Q226A and Q226N variants showed apparent steady-state kinetic parameters with biphenyl similar to those of wild-type BPDO, while Q226E kinetics were consistent with substrate inhibition. Moreover, in the presence of limiting biphenyl, Q226E consumed an excessive quantity of oxygen, which was mostly accounted for as hydrogen peroxide. Interestingly, a new feature around 318 nm appeared in the absorbance spectra of reduced and oxidized Q226E, suggesting a modified electronic environment around the [2Fe-2S] cluster, or perhaps the mononuclear iron. Future crystallographic studies of these variants will provide more information on the nature of the changes imposed by the substitutions of glutamine 226.

Another residue selected for investigation by site-directed mutagenesis was methionine 231. The crystal structure of BPDO indicates that this residue is in close contact with a modeled chlorine substituent on the distal ring of the biphenyl product in a

way suggesting that substitution by alanine or threonine would favor dihydroxylation of 2,2'-diClB. Steady-state kinetic characterization of M231A and M231T with biphenyl as substrate showed that these variants had decreased substrate specificity, but increased rate of 2,2'-diClB dihydroxylation with lower uncoupling. Kinetic characterization of these variants suggests that Met231 is involved in substrate specificity.

Aspartate 230 was also targeted for site-directed mutagenesis to assess its role in internal electron transfer, and in regulation of the enzyme's redox properties. This residue is located between the [2Fe-2S] center and the catalytic iron, and can form hydrogen bonds with histidine ligands from both metal centers. Problems were encountered with two of the constructed variants: D230A was poorly expressed, while D230E was highly expressed but was insoluble. However, D230N was successfully purified under anaerobic conditions and found to have low activity on biphenyl, and a low iron occupancy at the mononuclear iron active site. The role of Asp230 in internal electron transfer and in redox regulation remains to be investigated.

Part of the approach undertaken to identify some molecular determinants of BPDO enzymatic activity consisted of a comparison of related biphenyl dioxygenases sharing from 70-95 % sequence identity (5). BPDOs from *Comamonas testosteroni* B-356, *Burkholderia cepacia* LB400, and an Arctic soil isolate, *Pseudomonas sp.* strain Cam-1, were overexpressed and purified to homogeneity. The steady-state kinetics properties of these isozymes for biphenyl, and 2,2'-, 3,3'-, and 4,4'-diClB were investigated. $BPDO_{B356}$ and $BPDO_{Cam1}$ transformed biphenyl and diClBs in the following order of apparent maximal rates at 25°C: biphenyl > 3,3'-diClB > 4,4'-diClB > 2,2'-diClB. In contrast, $BPDO_{LB400}$ followed the order of apparent maximal rates:

biphenyl > 2,2'-diClB > 3,3'-diClB > 4,4'-diClB. In the three enzymes, O_2 utilization was well-coupled to biphenyl transformation, but the transformations of diClBs were uncoupled from oxygen consumption to varying extents, ranging from 0.11 ± 0.005 H_2O_2 : O_2 for $BPDO_{LB400}$ to 0.56 ± 0.05 H_2O_2 : O_2 for $BPDO_{B-356}$ in presence of 2,2'-diClB. These results suggest that the positioning of the congener in the active site of the dioxygenase is an important determinant of the BPDO's reactivity.

Limitations in production of high levels of $BPDO_{Cam1}$ led to the development of an improved overexpression system for BPDOs. The iron-sulfur cluster (*isc*) assembly gene cluster was cloned from *Pseudomonas aeruginosa* PA01, and coexpressed in *E. coli* together with *bphAE* genes encoding BPDOs B-356, LB400, or Cam1 (6). The availability of larger quantities of the *isc* gene products during overexpression of the [2Fe-2S] Rieske-type containing BPDOs enabled the production of larger amounts of highly active, soluble, holo-BPDOs than previous methods. Oxidative stress studies on $BPDO_{B356}$ demonstrated the lability of the [2Fe-2S] cluster in the presence of an enzymatic superoxide-producing system: by contrast, the cluster was relatively stable in the presence of oxygen or hydrogen peroxide. Evidence for reconstitution of the oxidatively damaged cluster by an *E. coli* crude extract with overexpressed *isc* gene products was obtained by absorbance and circular dichroism spectroscopic studies, and supported by a regain of enzymatic activity. These results suggest that the *isc* genes are not only involved in *de novo* iron sulfur cluster biosynthesis, but could also have the ability to repair damaged Fe-S clusters in BPDO.

REFERENCES

1. Imbeault, N. Y. R., Powlowski, J. B., Colbert, C. L., Bolin, J. T., and Eltis, L. D. (2000) *J. Biol. Chem.* **275**, 12430-12437
2. Barriault, D., Pelletier, C., Hurtubise, Y., and Sylvestre, M. (1997) *Int. Bioterior. Biodegrad.* **39**, 311-316
3. Kauppi, B., Lee, K., Carredano, E., Parales, R. E., Gibson, D. T., Eklund, H., and Ramaswamy, S. (1998) *Structure*, **6**, 571-586
4. Carredano, E., Karlsson, A., Kauppi, B., Choudhury, D., Parales, R. E., Parales, J. V., Lee, K., Gibson, D. T., Eklund, H., and Ramaswamy, S. (2000) *J. Mol. Biol.* **296**, 701-712
5. Master, E.R., Agar, N.Y.R., Powlowski, J.B., Mohn, W.W., and Eltis, L.D. (2002) *Submitted.*
6. Agar, N.Y.R., Fortin, P. D., Ge, Y., Eltis, L.D., and Powlowski, J.B. (2002) *In preparation.*

APPENDIX A

Figure 4.5 The steady-state dihydroxylation of biphenyl by BPDO variants: dependence of the initial velocity of O_2-uptake on biphenyl concentration in air-saturated buffer. **A.** BPDO_Q226A: **B.** BPDO_Q226E: **C.** BPDO_Q226N: **D.** BPDO_D230N: **E.** BPDO_M231A: **F.** BPDO_M231T. Results and experimental conditions as in Chapter 4. The fitted parameters are shown in Table 4.3.

A.

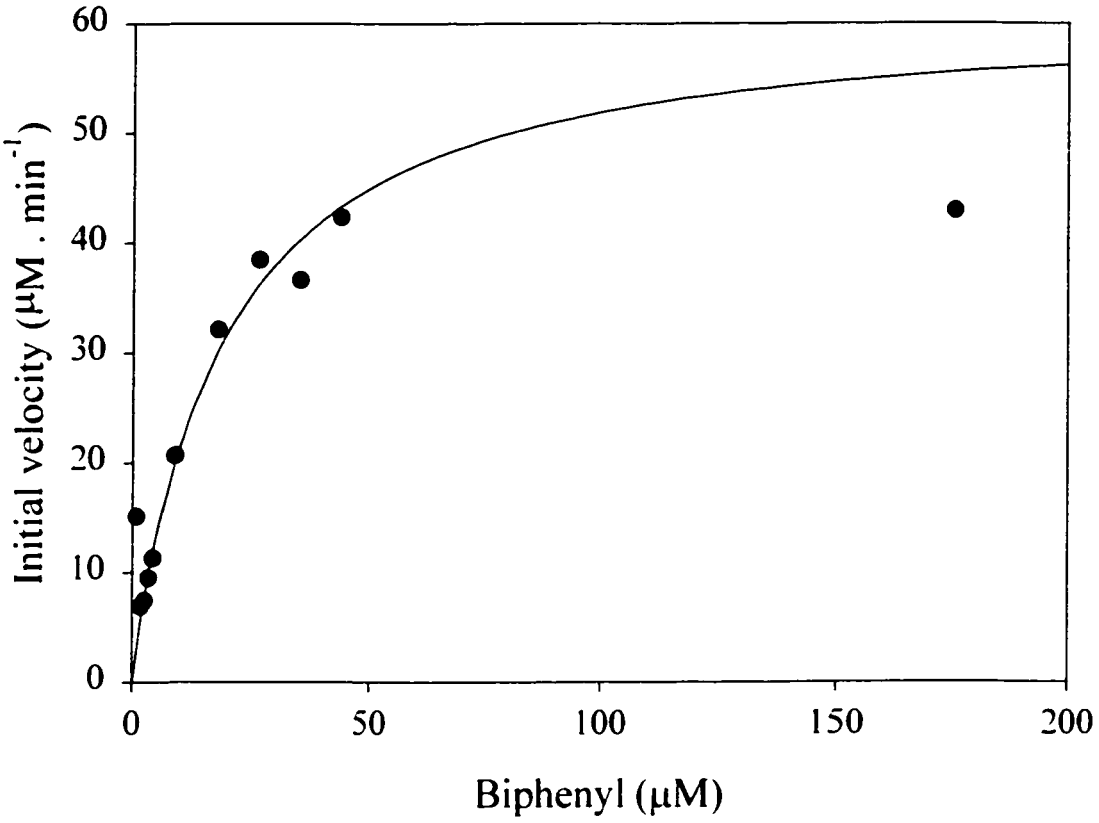
Initial velocity (μM . min-1)
60
50
40
30
20
10
0
0
50
100
150
200
Biphenyl (μM)

B.

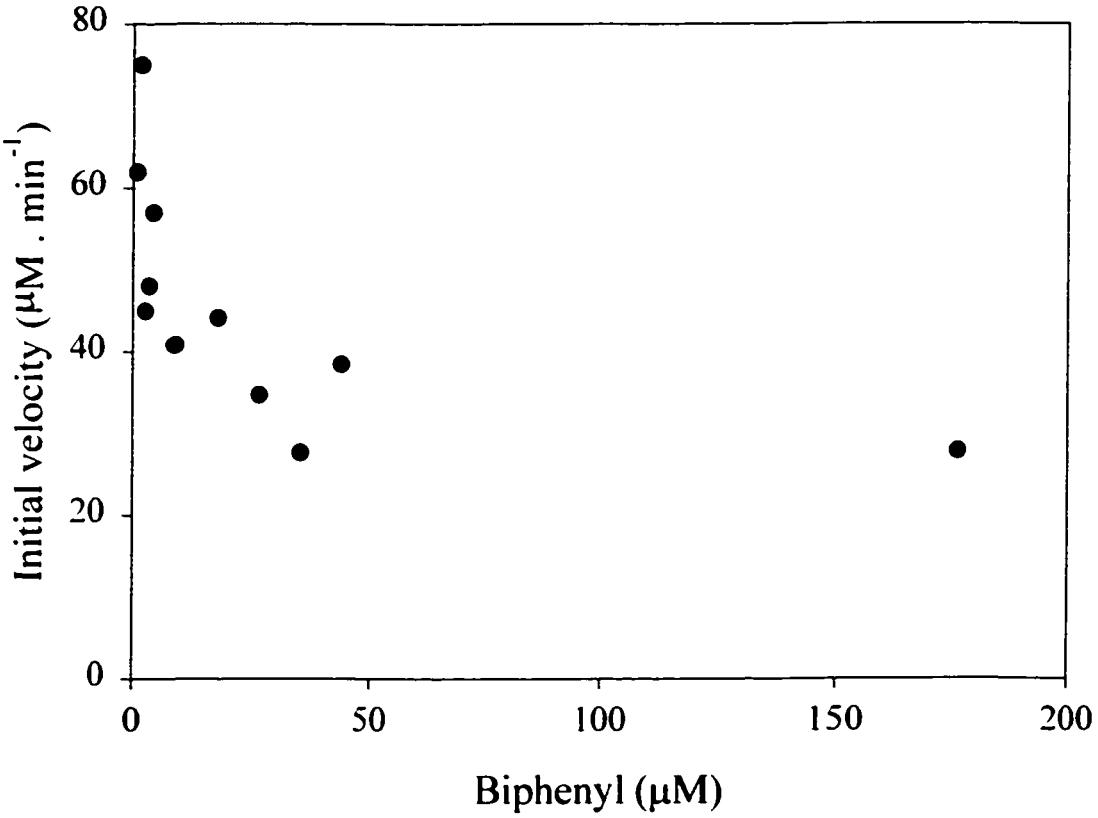
Initial velocity (μM . min-1)
80
60
40
20
0
0
50
100
150
200
Biphenyl (μM)

C.

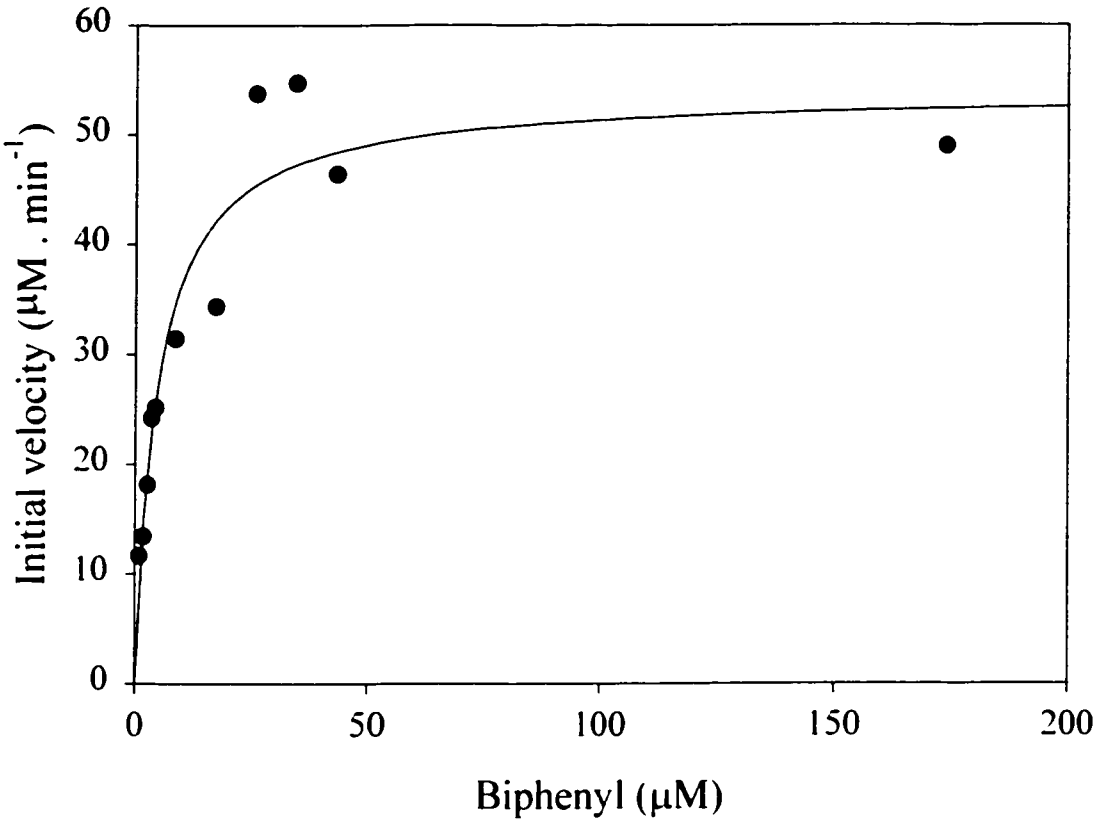
60
50
40
30
20
10
0
Initial velocity (μM . min-1)
0
50
100
150
200
Biphenyl (μM)

D.

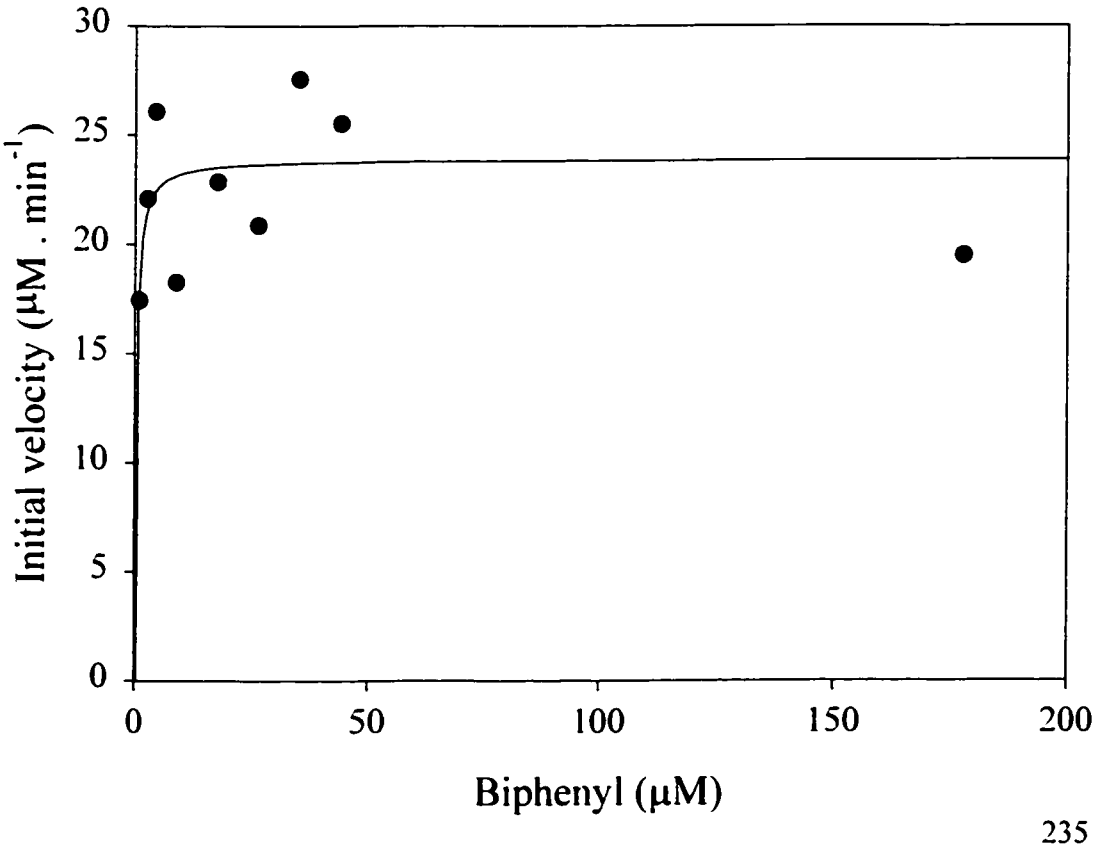
30
25
20
15
10
5
0
Initial velocity (μM . min-1)
0
50
100
150
200
Biphenyl (μM)

E.

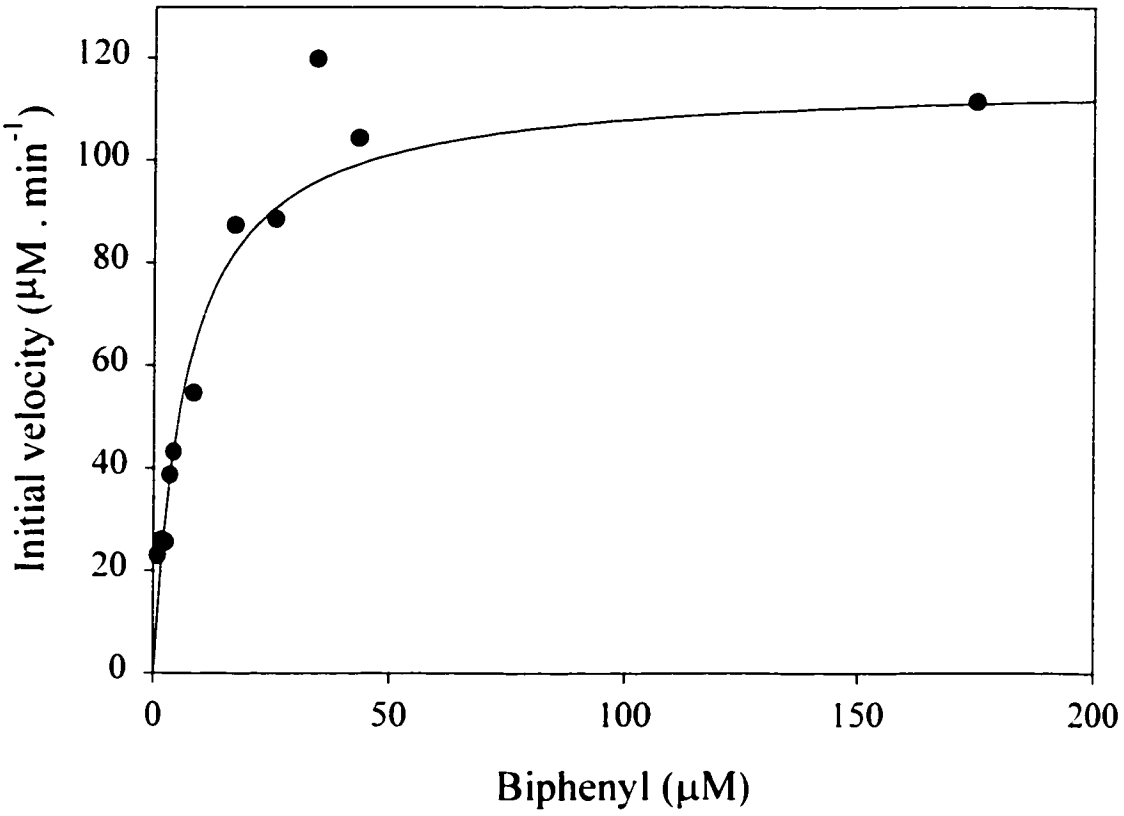
Initial velocity (μM . min-1)
120
100
80
60
40
20
0
0
50
100
150
200
Biphenyl (μM)

F.

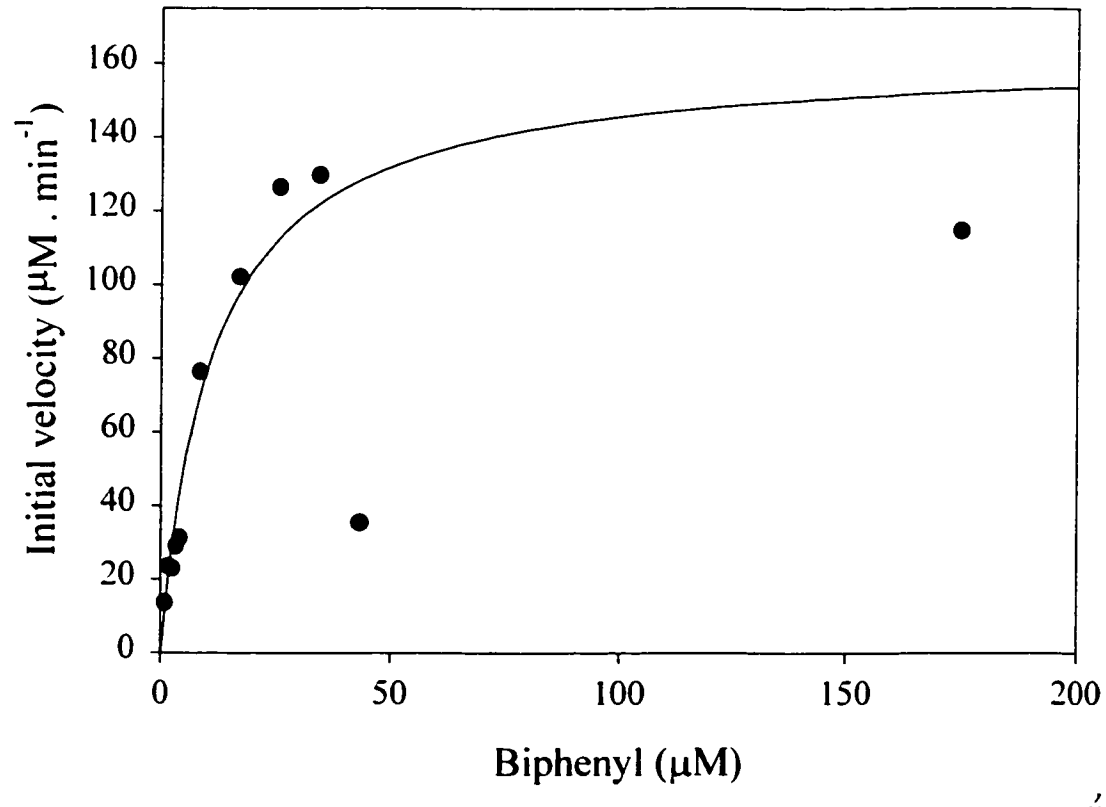
Initial velocity (μM . min-1)
160
140
120
100
80
60
40
20
0
0
50
100
150
200
Biphenyl (μM)

Table 4.4

Apparent steady-state kinetic and coupling parameters of BPDO variants for 2,2'-dichlorobiphenyl

BPDO	K_m (μM)	k_{cat} (s^{-1})	k_{cat} / K_m (x 10^6 $M^{-1}s^{-1}$)*	$H_2O_2 : O_2$
Wild Type	1.1 (0.2)	1.8 (0.1)	1.7 (0.3)	0.61 (0.03)
M231A	5.7 (0.9)	4.2 (0.2)	0.7 (0.1)	0.42 (0.06)
M231T	6.4 (1.1)	3.4 (0.2)	0.5 (0.1)	0.36 (0.03)